NASA Technical Paper 1291

Subsonic Dynamic Stability Characteristics of Two Close-Coupled Canard-Wing Configurations

Richmond P. Boyden

OCTOBER 1978

NASA Technical Paper 1291

Subsonic Dynamic Stability Characteristics of Two Close-Coupled Canard-Wing Configurations

Richmond P. Boyden
Langley Research Center
Hampton, Virginia

National Aeronautics
and Space Administration

**Scientific and Technical
Information Office**

1978

SUMMARY

The pitch, yaw, and roll damping as well as the oscillatory stability in pitch and in yaw were measured for two canard-wing configurations with wing sweeps of 44° and 60°. Other parameters measured during the test were the normal force due to pitch rate and the cross derivatives, yawing moment due to roll rate, and rolling moment due to yaw rate. The tests were made at free-stream Mach numbers of 0.3, 0.4, and 0.7 and for angles of attack from about -4° to 20°. The effects of various components such as the canard, nose strakes, wings, vertical tail, and horizontal tail were determined. The basic canard-wing vertical-tail configurations generally had positive damping in pitch, yaw, and roll. The effect of the canard was usually beneficial except for a tendency to decrease the oscillatory directional stability. Theoretical estimates were made using a vortex-lattice computer program; they were then compared with the experimental results.

INTRODUCTION

Airplanes with canard surfaces have been studied and flown since the beginning of powered flight. Over the years, however, the use of a horizontal stabilizer to the rear of the main lifting surface has become dominant world-wide for airplanes of all types. More recently, the advantages of canards on maneuvering fighter airplanes have been reexamined in detail as part of a study by the National Aeronautics and Space Administration. References 1, 2, and 3 form a part of this study and show that it is possible for a canard-wing configuration to have increased trimmed lift, reduced trim drag, and reduced wave drag. The present study was conducted to determine the pitch, yaw, and roll damping at subsonic speeds of two close-coupled canard-wing configurations of fighter-type airplanes. The tests were made at free-stream Mach numbers from 0.3 to 0.7 and at angles of attack from approximately -4° to 20°.

SYMBOLS

The aerodynamic parameters in this report are referred to the body system of axes as shown in figure 1 in which the coefficients, angles, and angular velocities are shown in the positive sense. These axes originate at the moment reference center which was located according to the model drawings in figure 2.

b reference span, 54.36 centimeters

C_l rolling-moment coefficient, $\dfrac{\text{Rolling moment}}{q_\infty Sb}$

C_{l_p} $= \dfrac{\partial C_l}{\partial\left(\dfrac{pb}{2V}\right)}$, per radian

$C_{l_{\dot{p}}}$ $= \dfrac{\partial C_l}{\partial\left(\dfrac{\dot{p}b^2}{4V^2}\right)}$, per radian

$C_{l_p} + C_{l_{\dot{\beta}}} \sin \alpha$ damping-in-roll parameter, per radian

C_{l_r} $= \dfrac{\partial C_l}{\partial\left(\dfrac{rb}{2V}\right)}$, per radian

$C_{l_{\dot{r}}}$ $= \dfrac{\partial C_l}{\partial\left(\dfrac{\dot{r}b^2}{4V^2}\right)}$, per radian

$C_{l_r} - C_{l_{\dot{\beta}}} \cos \alpha$ rolling moment due to yaw rate parameter, per radian

C_{l_β} $= \dfrac{\partial C_l}{\partial \beta}$, per radian

$C_{l_{\dot{\beta}}}$ $= \dfrac{\partial C_l}{\partial\left(\dfrac{\dot{\beta}b}{2V}\right)}$, per radian

$C_{l_\beta} \cos \alpha + k^2 C_{l_{\dot{r}}}$ effective dihedral parameter, per radian

$C_{l_\beta} \sin \alpha - k^2 C_{l_{\dot{p}}}$ rolling moment due to roll displacement parameter, per radian

C_m pitching-moment coefficient, $\dfrac{\text{Pitching moment}}{q_\infty S \bar{c}}$

$C_{m_q} = \dfrac{\partial C_m}{\partial\left(\dfrac{q\bar{c}}{2V}\right)}$, per radian

$C_{m_{\dot{q}}} = \dfrac{\partial C_m}{\partial\left(\dfrac{\dot{q}\bar{c}^2}{4V^2}\right)}$, per radian

$C_{m_q} + C_{m_{\dot{\alpha}}}$ damping-in-pitch parameter, per radian

$C_{m_\alpha} = \dfrac{\partial C_m}{\partial \alpha}$, per radian

$C_{m_{\dot{\alpha}}} = \dfrac{\partial C_m}{\partial\left(\dfrac{\dot{\alpha}\bar{c}}{2V}\right)}$, per radian

$C_{m_\alpha} - k^2 C_{m_{\dot{q}}}$ oscillatory longitudinal-stability parameter, per radian

C_N normal-force coefficient, $\dfrac{\text{Normal force}}{q_\infty S}$

$C_{N_q} = \dfrac{\partial C_N}{\partial\left(\dfrac{q\bar{c}}{2V}\right)}$, per radian

$C_{N_{\dot{q}}} = \dfrac{\partial C_N}{\partial\left(\dfrac{\dot{q}\bar{c}^2}{4V^2}\right)}$, per radian

$C_{N_q} + C_{N_{\dot{\alpha}}}$ normal force due to pitch rate parameter, per radian

$C_{N_\alpha} = \dfrac{\partial C_N}{\partial \alpha}$, per radian

$C_{N_{\dot{\alpha}}}$ $= \dfrac{\partial C_N}{\partial\left(\dfrac{\dot{\alpha}\bar{c}}{2V}\right)}$, per radian

$C_{N_\alpha} - k^2 C_{N_{\dot{q}}}$ normal force due to pitch displacement parameter, per radian

C_n yawing-moment coefficient, $\dfrac{\text{Yawing moment}}{q_\infty Sb}$

C_{n_p} $= \dfrac{\partial C_n}{\partial\left(\dfrac{pb}{2V}\right)}$, per radian

$C_{n_{\dot{p}}}$ $= \dfrac{\partial C_n}{\partial\left(\dfrac{\dot{p}b^2}{4V^2}\right)}$, per radian

$C_{n_p} + C_{n_{\dot{\beta}}} \sin\alpha$ yawing moment due to roll rate parameter, per radian

C_{n_r} $= \dfrac{\partial C_n}{\partial\left(\dfrac{rb}{2V}\right)}$, per radian

$C_{n_{\dot{r}}}$ $= \dfrac{\partial C_n}{\partial\left(\dfrac{\dot{r}b^2}{4V^2}\right)}$, per radian

$C_{n_r} - C_{n_{\dot{\beta}}} \cos\alpha$ damping-in-yaw parameter, per radian

C_{n_β} $= \dfrac{\partial C_n}{\partial\beta}$, per radian

$C_{n_{\dot{\beta}}}$ $= \dfrac{\partial C_n}{\partial\left(\dfrac{\dot{\beta}b}{2V}\right)}$, per radian

$C_{n_\beta} \cos \alpha + k^2 C_{n_{\dot{r}}}$ oscillatory directional-stability parameter, per radian

$C_{n_\beta} \sin \alpha - k^2 C_{n_{\dot{p}}}$ yawing moment due to roll displacement parameter, per radian

$\bar{c}$ mean geometric chord, 24.56 centimeters

f frequency of oscillation, hertz

k reduced frequency parameter, $\omega\bar{c}/2V$ in pitch and $\omega b/2V$ in roll and yaw, radians

M free-stream Mach number

p angular velocity of model about X-axis, radians per second

q angular velocity of model about Y-axis, radians per second

q_∞ free-stream dynamic pressure, pascals

R Reynolds number based on $\bar{c}$

r angular velocity of model about Z-axis, radians per second

S reference area, 1156 centimeters^2

V free-stream velocity, meters per second

X,Y,Z body reference axes

α angle of attack, degrees or radians

β angle of sideslip, radians

ω angular velocity, $2\pi f$, radians per second

Dot over quantity indicates first derivative with respect to time.

Model component designations:

B body

C canard

H horizontal tail

S strake

V vertical tail

W wing

MODEL AND TEST APPARATUS

Three-view drawings of the model with both the 44° and 60° swept wing configurations are shown in figure 2. The horizontal tail and the strakes on the fuselage forebody were tested with the 44° sweep wing only. The canard, horizontal tail, and vertical tail surfaces had a leading-edge sweep of 51.70° and each of the exposed panels had the same dimensions. Detailed geometric characteristics of the model are listed in table I. The characteristics of all the aerodynamic surfaces are based on the planform formed by extending the leading and trailing edges to the model center line.

A photograph of the 60° swept wing configuration mounted on the sting for the forced-oscillation dynamic stability tests in the Langley high-speed 7- by 10-foot tunnel is shown in two views in figure 3. A description and the operating characteristics of this wind tunnel can be found in reference 4. Photographs of the small-amplitude forced-oscillation dynamic stability balances are in figure 4. Reference 5 contains a detailed description of the dynamic stability balances and the associated data reduction equations.

TESTS

The dynamic stability parameters were measured primarily at Mach numbers of 0.4 and 0.7 for all configurations. In addition, the damping-in-roll and the associated parameters were measured at a Mach number of 0.3 for the 44° swept wing configuration in order to obtain data over the available angle-of-attack range. The parameters were measured at this Mach number because an extraneous model-sting vibration had limited the BVW configuration in angle of attack at the higher Mach numbers. The range of angle of attack available with the dynamic stability sting was from about -4° to 20°. The nominal values of the wind-tunnel test conditions are listed in table II while the amplitude of the forced oscillation and the range of reduced frequency parameters for the various axes of oscillation are listed in table III.

To insure a turbulent boundary layer over the models, carborundum grains were applied as three-dimensional roughness to the model nose and along the leading edges of the canard, wing, and tail surfaces. The size and location of the grit were chosen based on the work in reference 6. The transition strips consisted of No. 120 carborundum grit applied in bands 0.16 cm wide. These bands were located 2.54 cm aft of the model nose and 1.27 cm streamwise aft of the leading edges of the canard, wing, and tail surfaces.

RESULTS AND DISCUSSION

The results for the component breakdown of the 44° swept wing configuration are shown in figure 5 for damping in pitch and oscillatory longitudinal stability. The BVWC configuration is seen to have positive damping in pitch $\left(\text{negative values of } C_{m_q} + C_{m_{\dot{\alpha}}}\right)$ and positive oscillatory longitudinal stability $\left(\text{negative values of } C_{m_\alpha} - k^2 C_{m_{\dot{q}}}\right)$ for Mach numbers of 0.4 and 0.7. The model moment center location was chosen prior to the test to give positive longitudinal stability by using the vortex-lattice computer program discussed in a subsequent section of this paper. The destabilizing influence of the canard is evident in figure 5 except for angles of attack above 16° at a Mach number of 0.4. The effect of the addition of a low aft-mounted horizontal tail to the canard-wing configuration (BVWC) is seen in figure 6 and shows the expected increase in positive damping and in stability. Nose strakes (see fig. 2(a)) were added to the 44° swept wing configuration in an effort to maintain the directional stability to higher angles of attack. The strakes were modeled after one version of those tested in reference 7. For the BVWC configuration of figure 7 and the BV configuration of figure 8, the addition of the nose strakes is seen to increase the damping in pitch and to decrease the oscillatory longitudinal stability at the higher angles of attack. The 60° swept wing configuration BVWC in figure 9 has positive stability and has positive damping in pitch except for almost zero damping at $M = 0.4$ and 18° angle of attack.

The normal force due to pitch rate and the normal force due to pitch displacement parameters are plotted in figure 10 for the 44° swept wing configuration. The BVWC configuration has either positive or negative values of the normal force due to pitch rate parameter depending on Mach number and angle of attack. The effects of the addition of the horizontal tail and the nose strakes on the normal force parameters are shown in figures 11, 12, and 13. The results for the component breakdown of the 60° swept wing configuration are shown in figure 14. Like the 44° swept wing BVWC configuration, at a Mach number of 0.4 the normal force due to pitch rate results for the 60° swept wing BVWC configuration are positive, but both positive and negative values are found at $M = 0.7$.

The results for the component breakdown of the 44° swept wing configuration are presented in figure 15 for damping in yaw and oscillatory directional stability. The BVWC configuration has positive damping in yaw over the angle-of-attack range but the oscillatory stability changes sign and the configuration becomes unstable at angles of attack between 14° and 17°. The canard tends to destabilize the configuration. The use of the nose strakes with the canard on (fig. 16) showed a small decrease in oscillatory directional stability at a Mach number of 0.4 and only resulted in a small increase in directional stability for angles of attack above 16° at a Mach number of 0.7. At a Mach number of 0.7, there was no increase in angle of attack where the model retained positive oscillatory directional stability as a result of adding the nose strakes. Figure 17 shows the limited and sometimes adverse effect of adding the nose strakes to the BVW configuration. The 60° swept wing BVWC configuration in figure 18 had positive yaw damping and satisfactory values of the oscillatory directional stability up to angles of attack of 17° to 19° where

this parameter changed signs. Adding the canard resulted in a less directionally stable BVWC configuration for the 60° swept wing just as it did for the 44° swept wing.

The results for the component breakdown of the various configurations are presented in figures 19 to 22 for the rolling moment due to yaw rate and the effective dihedral parameter. Generally, at the positive angles of attack the winged configurations had positive values of the rolling moment due to yaw rate and negative values of the effective dihedral parameter.

The component breakdown of the 44° swept wing configuration for the roll oscillation tests in figure 23 was made at a Mach number of 0.3 because of an extraneous model-sting vibration which precluded testing over the full angle-of-attack range for the BVW configuration at the higher Mach numbers. Both the BVW and the BVWC configurations maintained a high level of roll damping over the complete angle-of-attack range. In figure 23 the roll damping contribution of the canard and its favorable interference with the 44° swept wing (the difference between the BVWC and the BVW configurations) generally increased with angle of attack. On the other hand, the canard and body alone (configuration BC) has almost a constant level of roll damping up to an angle of attack of about 16°. There is a large negative peak in the damping-in-roll parameter evident at an angle of attack of about 18° for the BVWC configuration in figures 23 and 24. As expected, the nose strakes in figure 25 influenced the roll damping only slightly. In figure 26 the canards did not affect the damping in roll of the 60° swept wing configuration as much as the 44° swept wing configuration except at isolated angles of attack.

Results for the yawing moment due to roll rate parameter and the yawing moment due to roll displacement parameter for the various configurations are in figures 27 to 30. Removing the canard surfaces from the complete BVWC configuration resulted in a positive increment to the yawing moment due to roll rate.

COMPARISON OF EXPERIMENTAL RESULTS WITH VORTEX-LATTICE ESTIMATES

Theoretical estimates of some of the aerodynamic stability derivatives were made using the vortex-lattice computer program described in reference 8. This program has the capability to accommodate multiple lifting surfaces such as the canard-wing horizontal-tail configuration. The program utilizes a vortex-lattice representation of a zero-thickness lifting planform, but the vertical separation of the various lifting surfaces, such as occurs between the canard and the wing, can be modeled in the program as one of the inputs. The theoretical estimates do not include any vortex lift contributions. The estimates are based on the assumption of an attached-flow condition and are therefore only valid near an angle of attack of 0°. The experimental results for comparison purposes are for an angle of attack of 0°; the multiple experimental data points for each configuration have been averaged for clarity.

Figure 31(a) compares the experimentally determined pitching-moment parameters with the theoretical estimates for the 44° swept wing configurations. The significant differences for the damping-in-pitch comparison are considered to be a result of omitting the $C_{m_{\dot{\alpha}}}$ term from the theoretical estimates.

Therefore, the estimates have smaller negative values than the experimental values. The agreement of the oscillatory longitudinal-stability parameters in the lower part of figure 31(a) is considered good because each of the configurations shows close agreement with the experimental results and the estimates. In addition, the $k^2C_{m_{\dot{q}}}$ term in the oscillatory longitudinal-stability parameter should be insignificant for this aircraft configuration. The normal-force-parameter comparison is shown in figure 31(b). For the winged configurations, the experimental results for $C_{N_q} + C_{N_{\dot{q}}}$ decrease in magnitude from $M = 0.4$ to $M = 0.7$ while the theoretical estimates for C_{N_q} alone have a positive slope with Mach number. The theoretical estimates for the winged configurations for C_{N_α} are seen to be higher, but in reasonable agreement with the experimental values of the normal force due to pitch displacement. The damping-in-roll comparisons for the 44° swept wing configurations are in figure 31(c). The second term of the experimental damping-in-roll parameter should be zero because the data are for 0° angle of attack. The theoretical estimates for the damping in roll do not include the effect of the vertical tail in the presence of the lifting surfaces because this was not within the capabilities of the computer program. The experimental damping-in-roll values for the winged configurations are higher than the estimated values. Also, for the configurations with the wings removed, the theoretical estimates are higher at the single Mach number for which experimental values were measured.

The comparisons of the theoretical estimates with the experimental values of the stability parameters for the 60° swept wing configurations are contained in figure 32. Except for differences in magnitude of the parameters, the same trends exist in the comparisons for the 44° and the 60° swept wing configurations and the statements made concerning the 44° swept wing configurations are equally applicable to the 60° swept wing configurations.

SUMMARY OF RESULTS

An investigation has been conducted to determine the dynamic stability characteristics of two close-coupled canard-wing models at subsonic speeds. The two wing planforms tested had leading-edge wing sweeps of 44° and 60°. The basic canard-wing vertical-tail configurations (BVWC) had positive oscillatory longitudinal stability and positive damping in pitch except for a loss in damping at a Mach number of 0.4 and an angle of attack of 18° with the 60° swept wing. In yaw the canard tends to decrease the oscillatory directional stability of the basic configuration, and the oscillatory directional stability became unstable at angles of attack between 14° and 19° depending on wing sweep and Mach number. The use of a particular set of nose strakes did not significantly improve this loss in stability. Both the 44° and the 60° swept wings with the canards on had positive damping in yaw. The addition of the canard surfaces to the 44° swept wing resulted in an increase in the damping in roll as the angle of attack was increased. The canard with the 60° swept wing did not show this higher level of roll damping with increasing angle of attack.

Theoretical estimates made for the various configurations showed reasonable agreement with the experimental results for the oscillatory longitudinal stability and the normal force due to pitch displacement. Only fair agreement was obtained for the damping-in-pitch and damping-in-roll parameters.

Langley Research Center
National Aeronautics and Space Administration
Hampton, VA 23665
August 17, 1978

REFERENCES

1. McKinney, Linwood W.; and Dollyhigh, Samuel M.: Some Trim Drag Considerations for Maneuvering Aircraft. J. Aircr., vol. 8, no. 8, Aug. 1971, pp. 623-629.

2. Dollyhigh, Samuel M.: Static Longitudinal Aerodynamic Characteristics of Close-Coupled Wing-Canard Configurations at Mach Numbers From 1.60 to 2.86. NASA TN D-6597, 1971.

3. Gloss, Blair B.; and McKinney, Linwood W.: Canard-Wing Lift Interference Related to Maneuvering Aircraft at Subsonic Speeds. NASA TM X-2897, 1973.

4. Fox, Charles H.; and Huffman, Jarrett K.: Calibration and Test Capabilities of the Langley 7- by 10-Foot High Speed Tunnel. NASA TM X-74027, 1977.

5. Freeman, Delma C., Jr.; Boyden, Richmond P.; and Davenport, E. E.: Supersonic Dynamic Stability Characteristics of a Space Shuttle Orbiter. NASA TN D-8043, 1976.

6. Braslow, Albert L.; Hicks, Raymond M.; and Harris, Roy V., Jr.: Use of Grit-Type Boundary-Layer-Transition Trips on Wind-Tunnel Models. NASA TN D-3579, 1966.

7. Polhamus, Edward C.; and Spreemann, Kenneth P.: Effect at High Subsonic Speeds of Fuselage Forebody Strakes on the Static Stability and Vertical-Tail-Load Characteristics of a Complete Model Having a Delta Wing. NASA TN D-903, 1961.

8. Luckring, James M.: Some Recent Applications of the Suction Analogy to Asymmetric Flow Situations. Vortex-Lattice Utilization. NASA SP-405, 1976, pp. 219-236.

TABLE I.- GEOMETRIC CHARACTERISTICS OF MODEL

Body length, cm	101.05
Body width, maximum, cm	11.18
Actual leading-edge sweep of nominal 44° swept wing, deg	44.03
Actual leading-edge sweep of nominal 60° swept wing, deg	59.45
Wings:	
Aspect ratio	2.56
Span, cm	54.36
Mean geometric chord, cm	24.56
Area, cm^2	1156
Root chord at fuselage juncture, cm	29.80
Tip chord, cm	6.77
Airfoil section	Circular arc
Maximum thickness, percent chord, at -	
Root at fuselage juncture	6
Tip	4
Canard and horizontal tail:	
Aspect ratio	2.77
Span, cm	38.06
Leading-edge sweep, deg	51.70
Mean geometric chord, cm	16.23
Area, cm^2	522.6
Root chord at fuselage juncture, cm	17.92
Tip chord, cm	3.59
Airfoil section	Circular arc
Maximum thickness, percent chord, at -	
Root at fuselage juncture	6
Tip	4
Vertical tail:	
Aspect ratio	1.39
Span, cm	19.03
Leading-edge sweep, deg	51.70
Mean geometric chord, cm	16.23
Area, cm^2	261.3
Root chord at fuselage juncture, cm	17.92
Tip chord, cm	3.59
Airfoil section	Circular arc
Maximum thickness, percent chord, at -	
Root at fuselage juncture	6
Tip	4

TABLE II.- NOMINAL TUNNEL TEST CONDITIONS

Free-stream Mach number, M	Dynamic pressure, q_∞, kPa	Velocity, V, m/sec	Stagnation temperature, T, K	Reynolds number, R
0.3	6.00	102	292	1.62×10^6
.4	10.17	137	301	2.02
.7	25.05	233	303	3.05

TABLE III.- OSCILLATION TEST PARAMETERS

Axis	Amplitude, deg	Reduced frequency parameter, k, rad
Pitch	1.0	0.0097 to 0.0268
Yaw	1.0	0.0188 to 0.0407
Roll	2.5	0.0341 to 0.1307

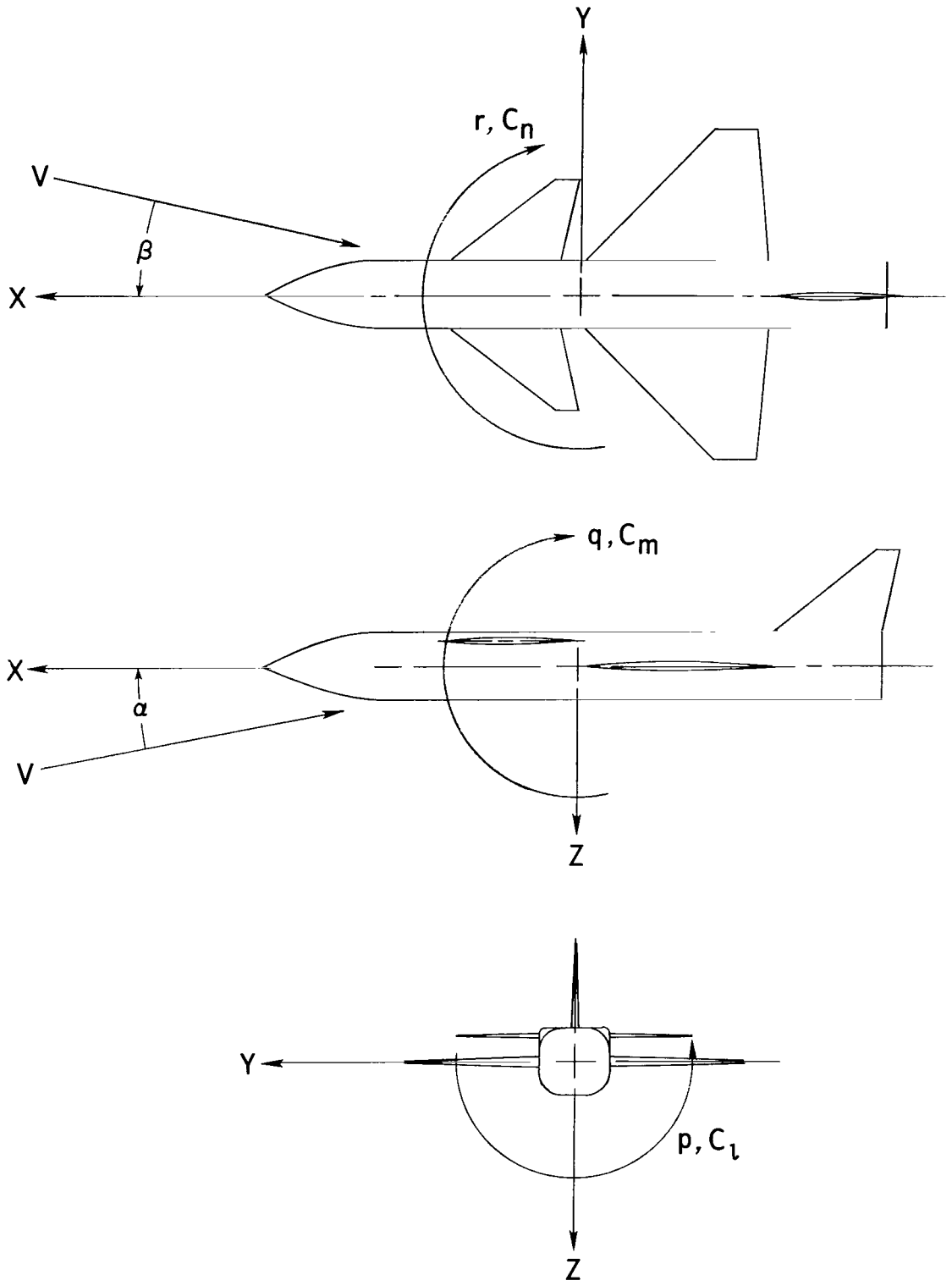

Figure 1.- Body reference axes with coefficients, angles, and angular velocities shown in positive sense.

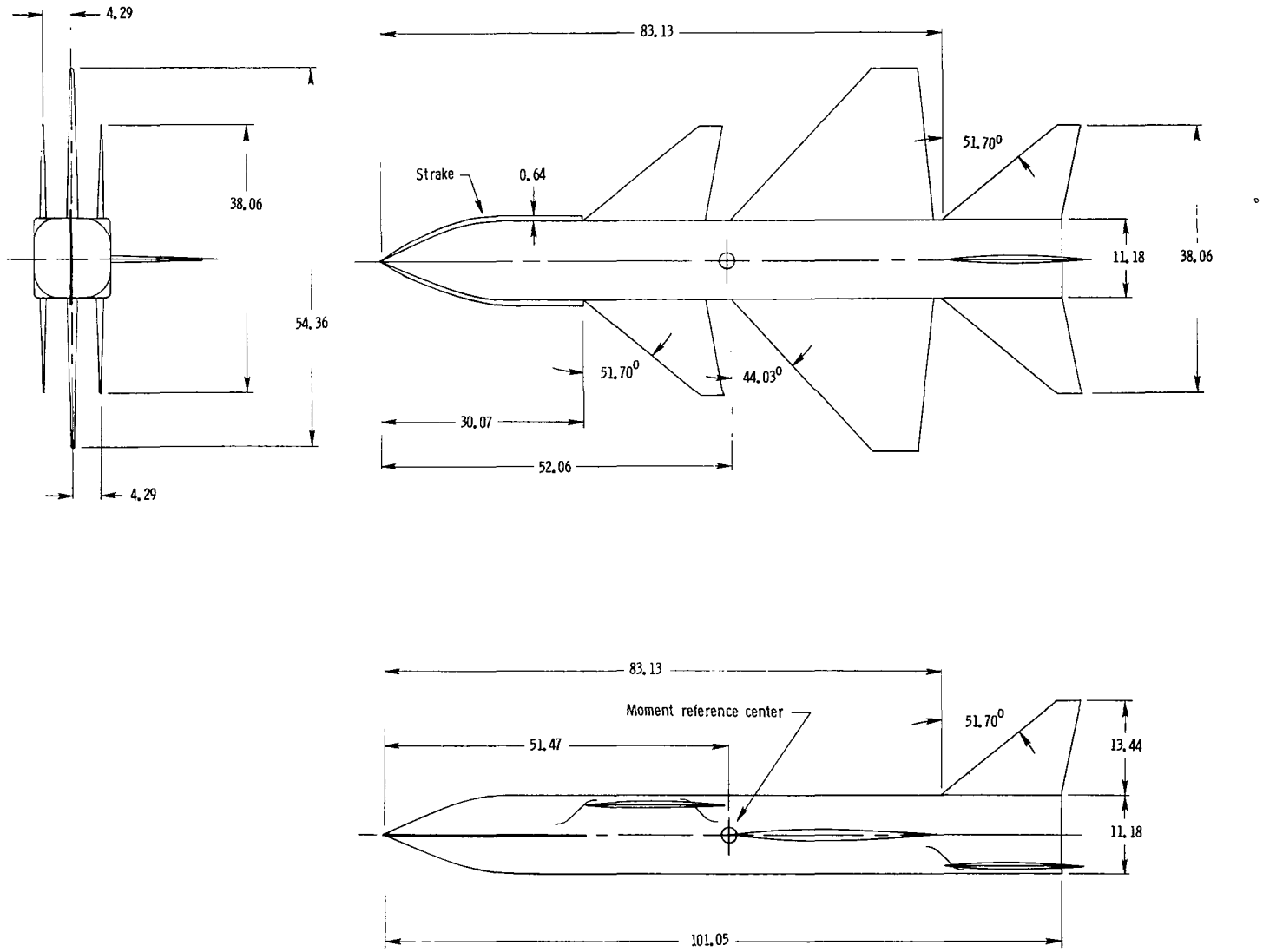

(a) Configuration with 44° swept wing.

Figure 2.- General arrangement of models. All linear dimensions are in centimeters.

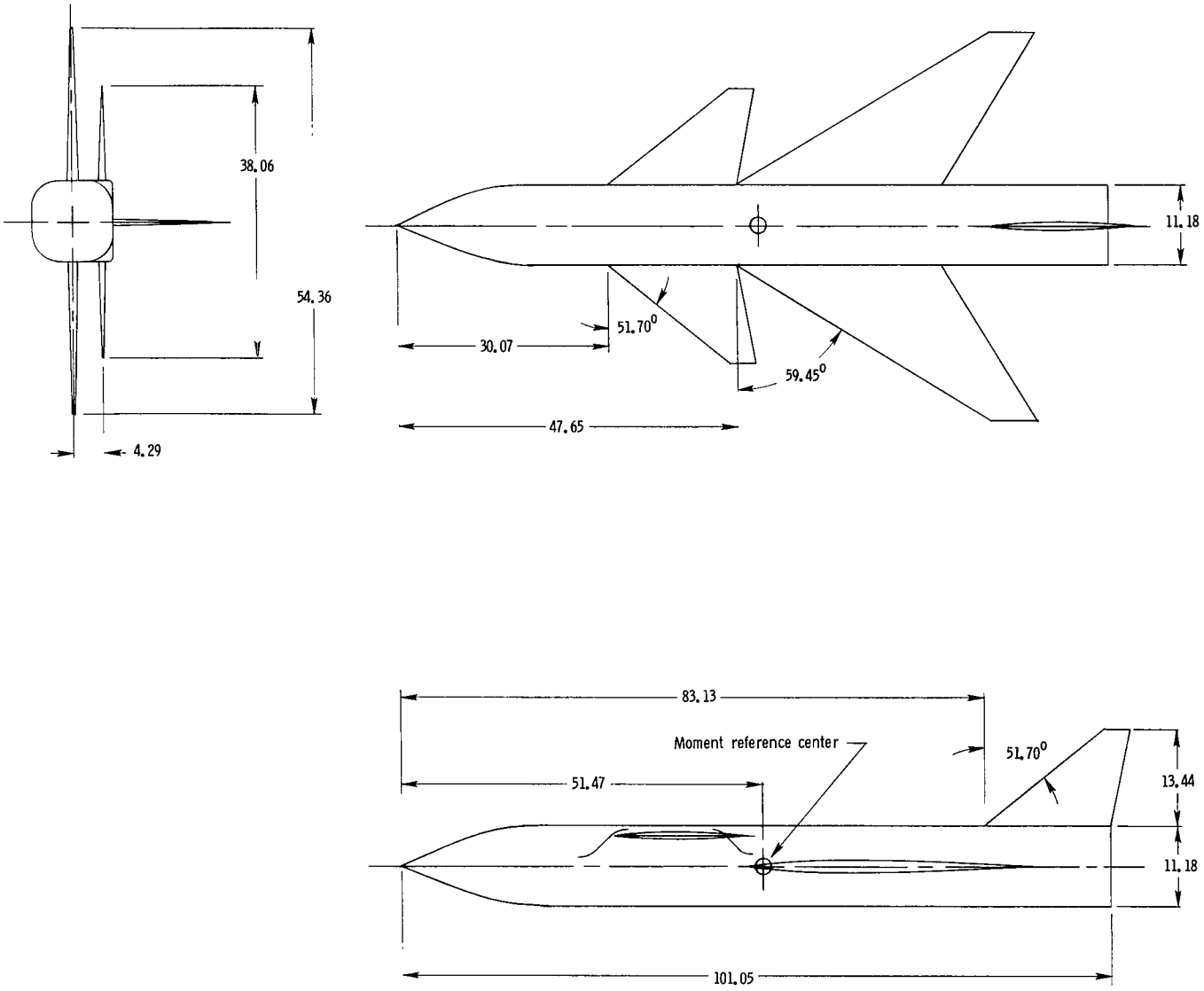

(b) Configuration with 60° swept wing.

Figure 2.- Concluded.

L-77-721

(a) View looking upstream toward model.

Figure 3.- Photographs of 60° swept wing model on forced-oscillation dynamic stability sting in Langley high-speed 7- by 10-foot tunnel.

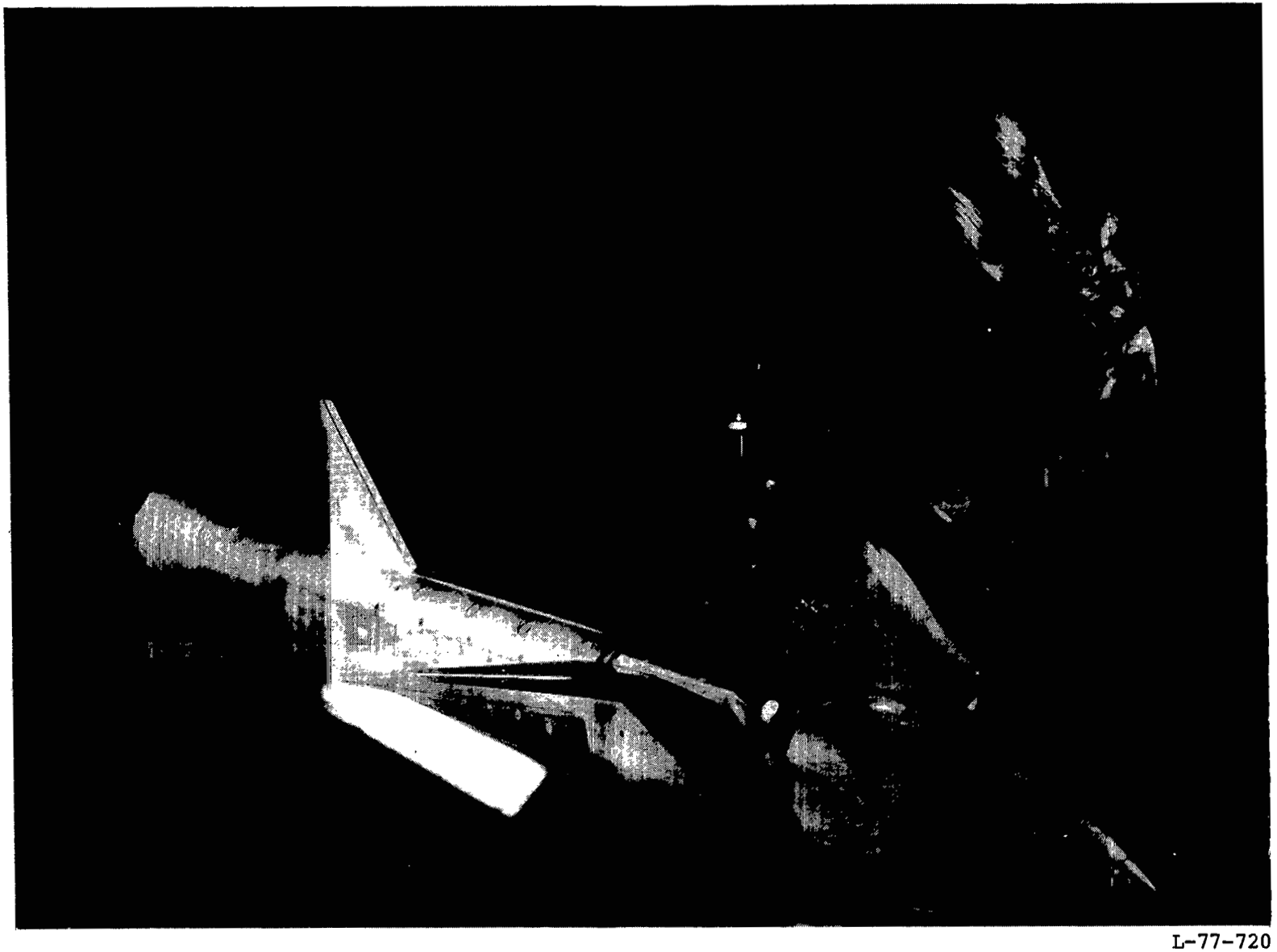

L-77-720

(b) One-quarter front view of model.

Figure 3.- Concluded.

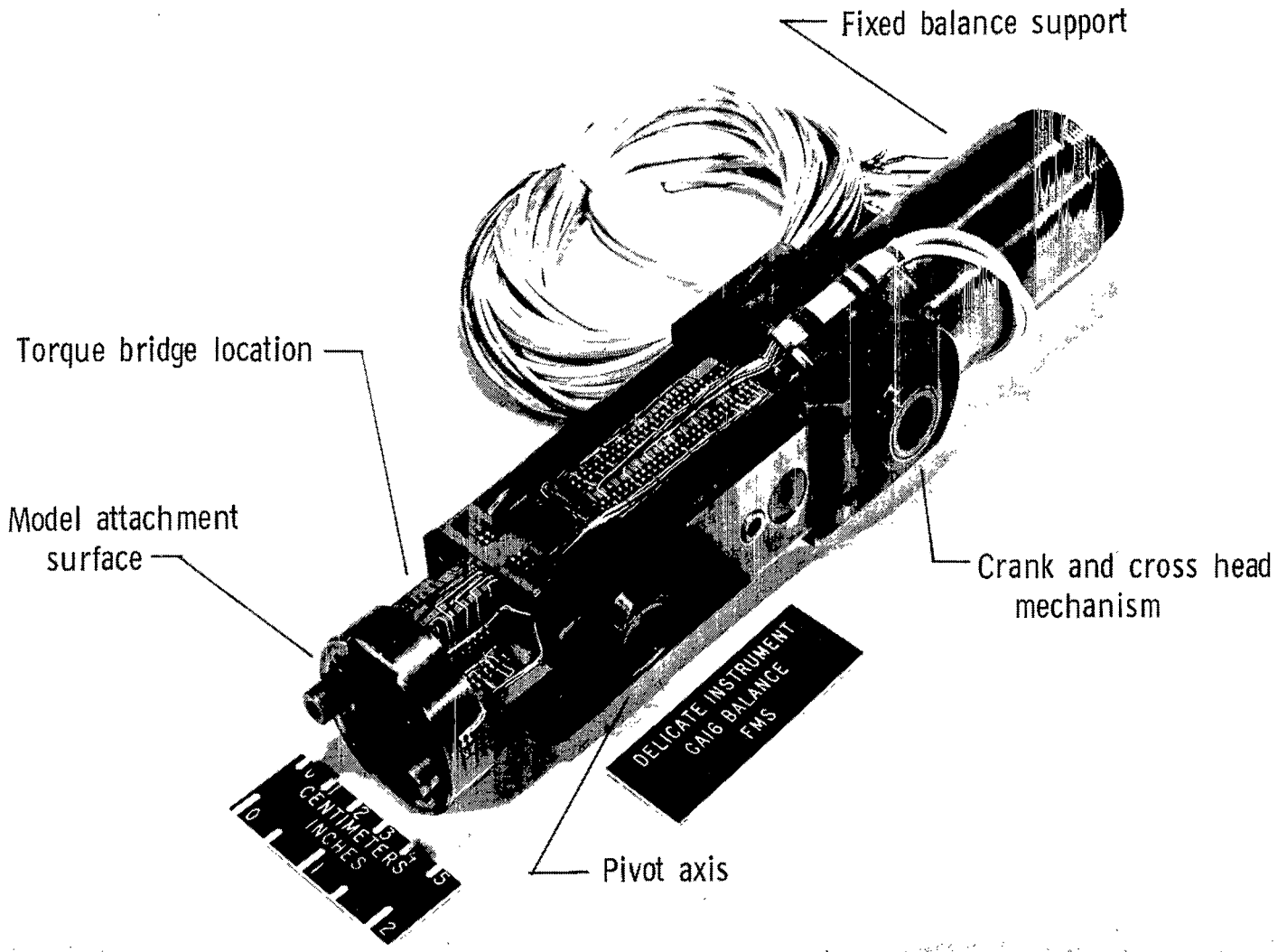

L-68-10 690.2

(a) Pitch or yaw balance.

Figure 4.- Photographs of small-amplitude forced-oscillation dynamic stability balances.

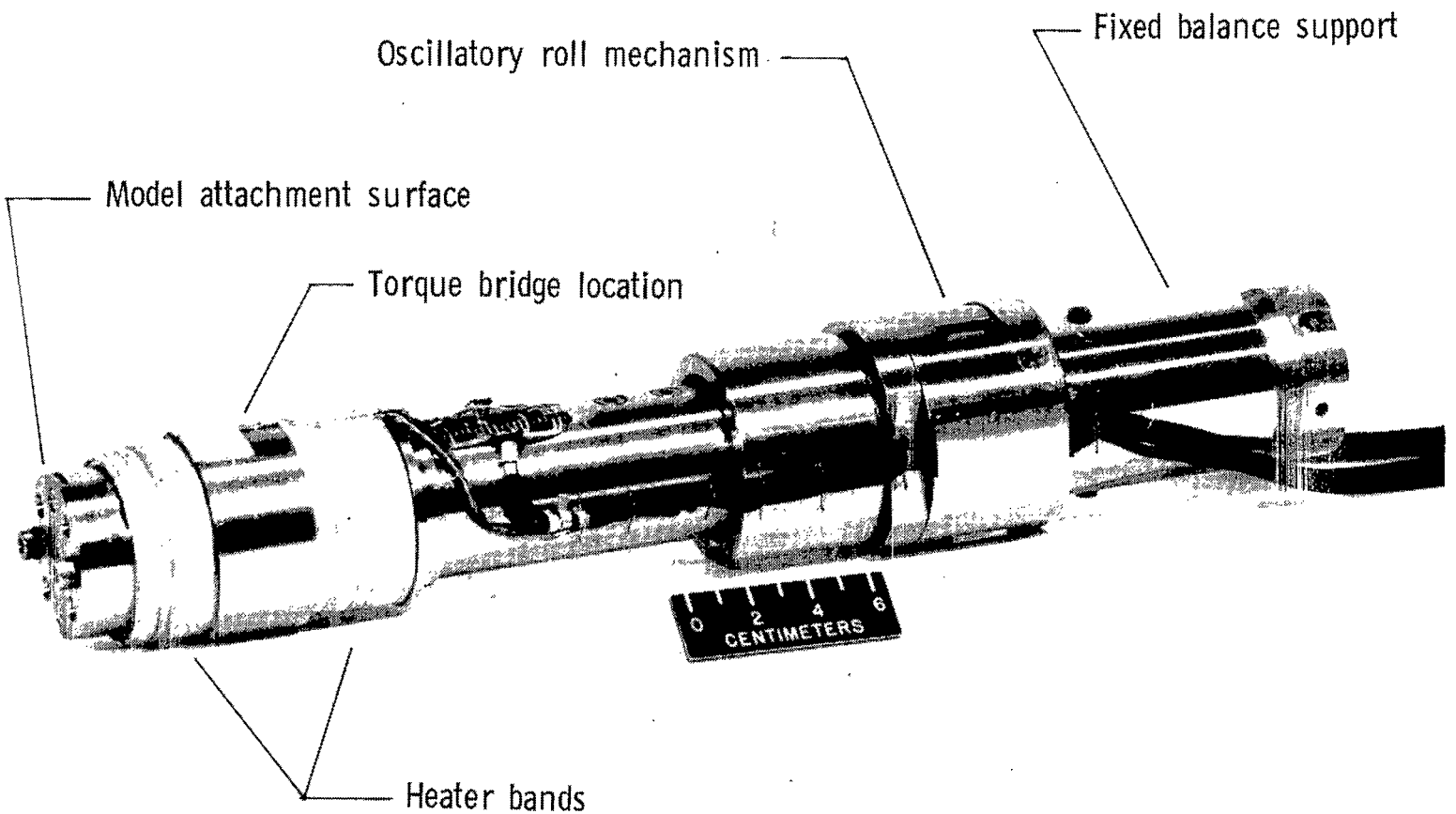

L-74-7051.2

(b) Roll balance.

Figure 4.- Concluded.

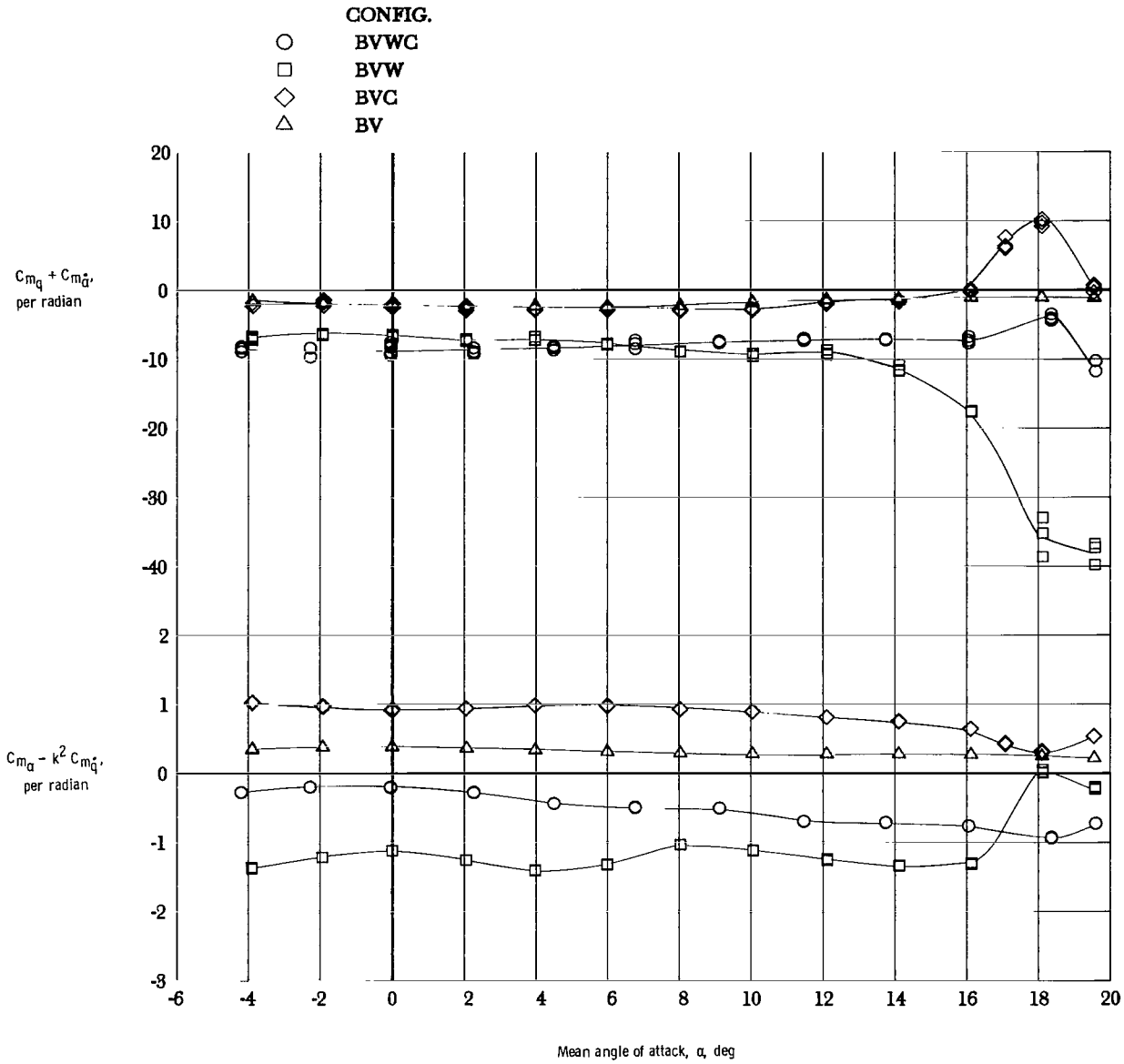

(a) M = 0.4.

Figure 5.- Results for component breakdown of 44° swept wing configuration for damping-in-pitch parameter and oscillatory longitudinal-stability parameter.

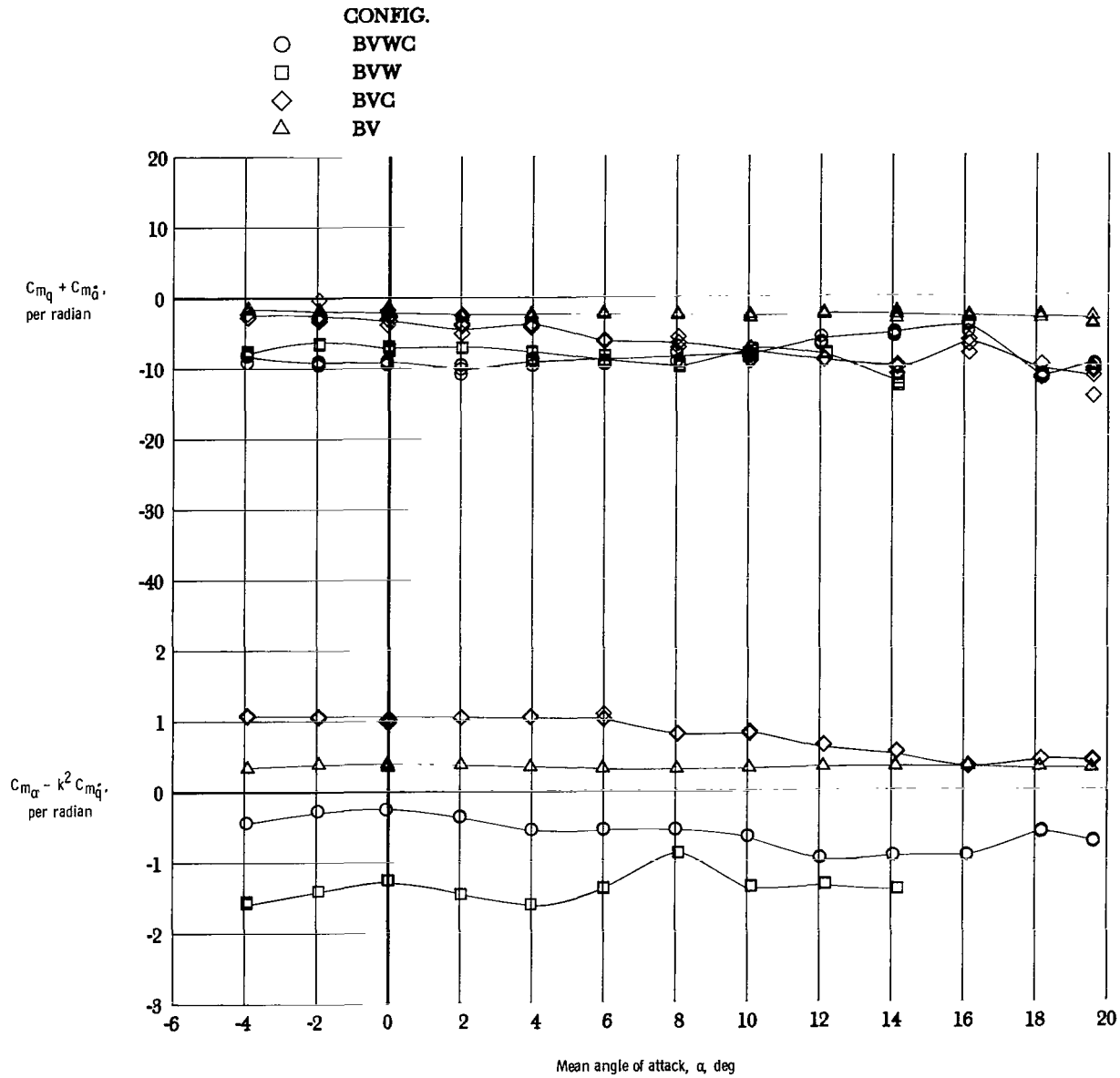

(b) M = 0.7.

Figure 5.- Concluded.

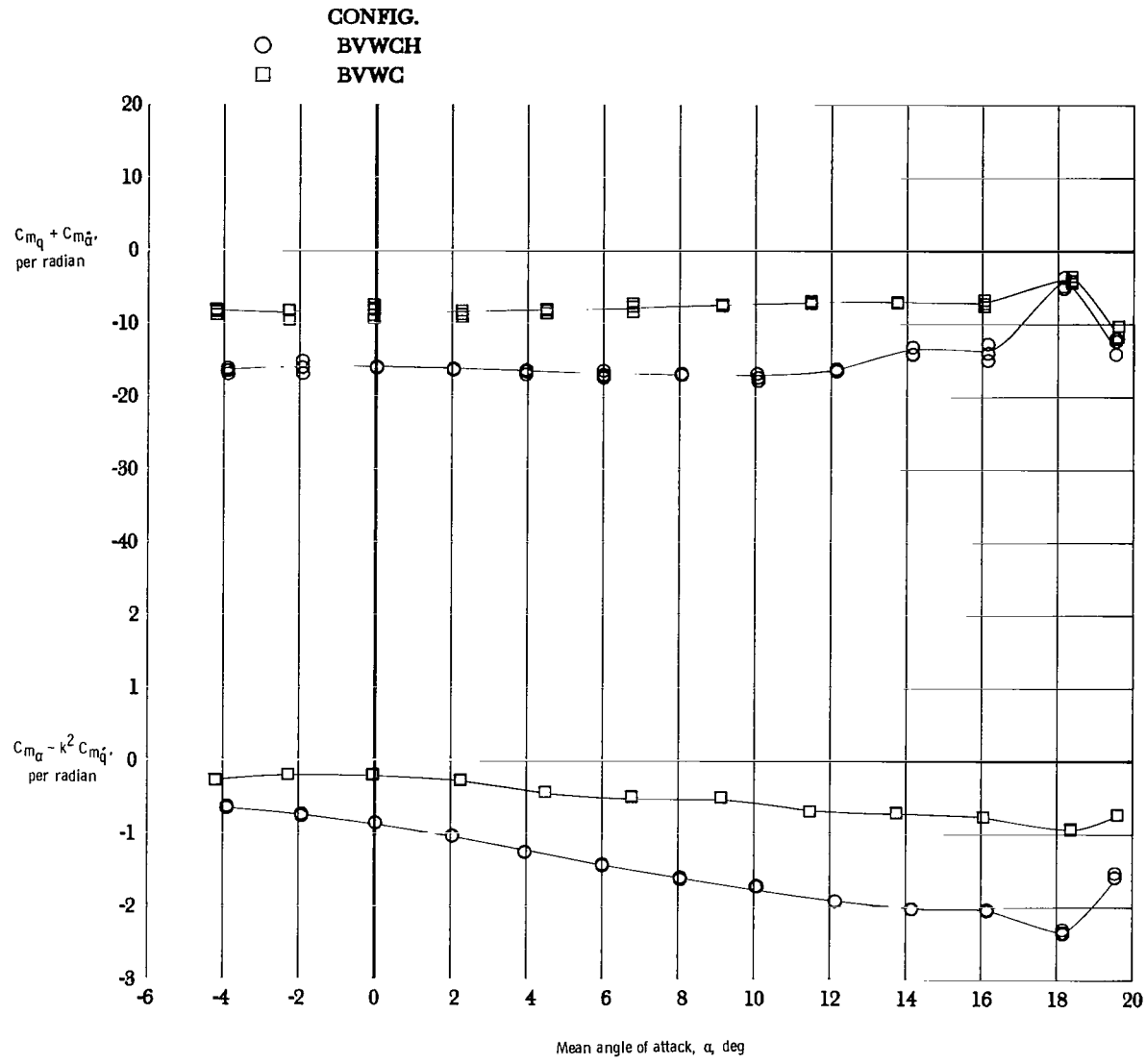

(a) M = 0.4.

Figure 6.- Effect of horizontal tail with 44° swept wing configuration on damping-in-pitch parameter and on oscillatory longitudinal-stability parameter.

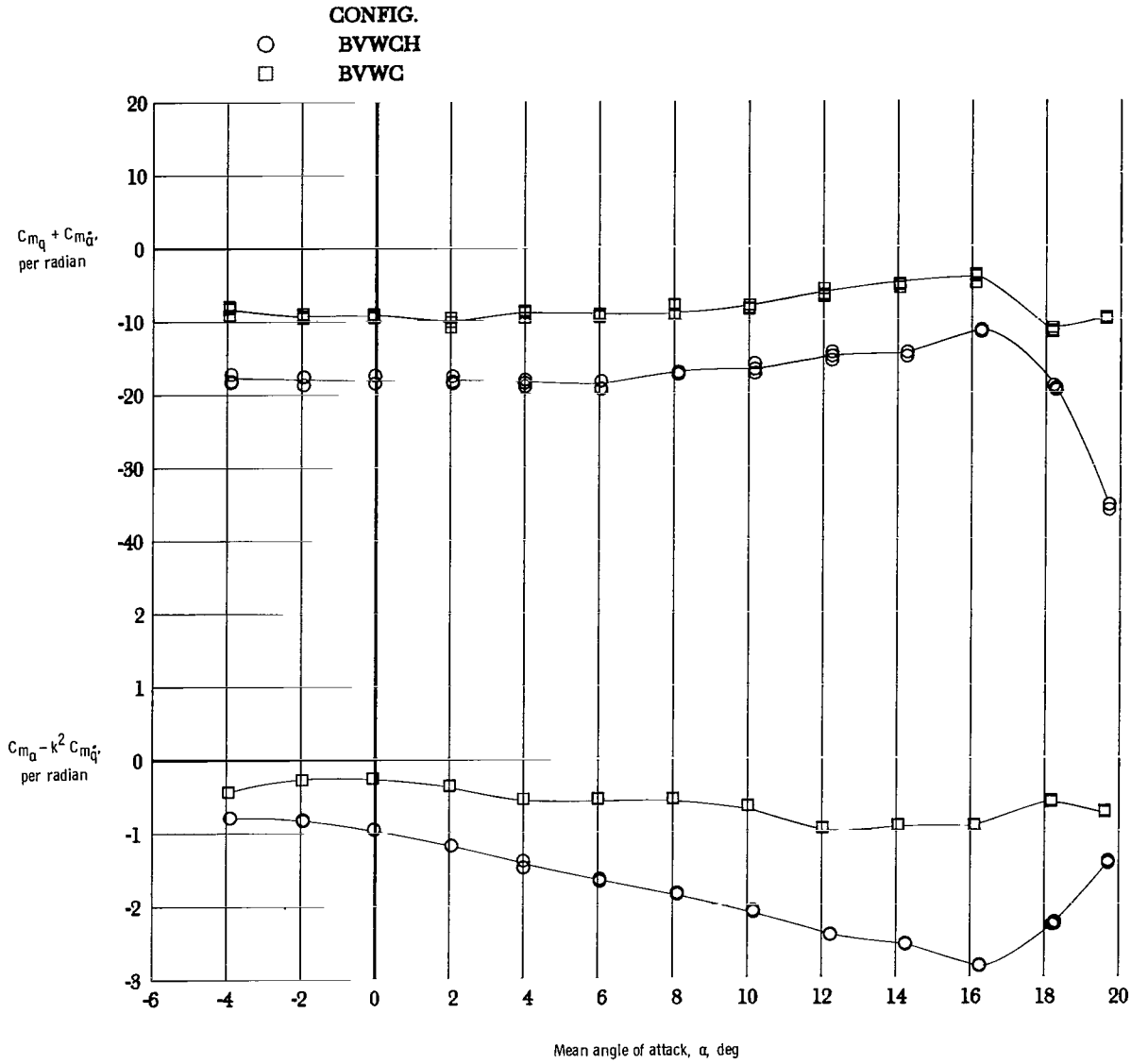

(b) M = 0.7.

Figure 6.- Concluded.

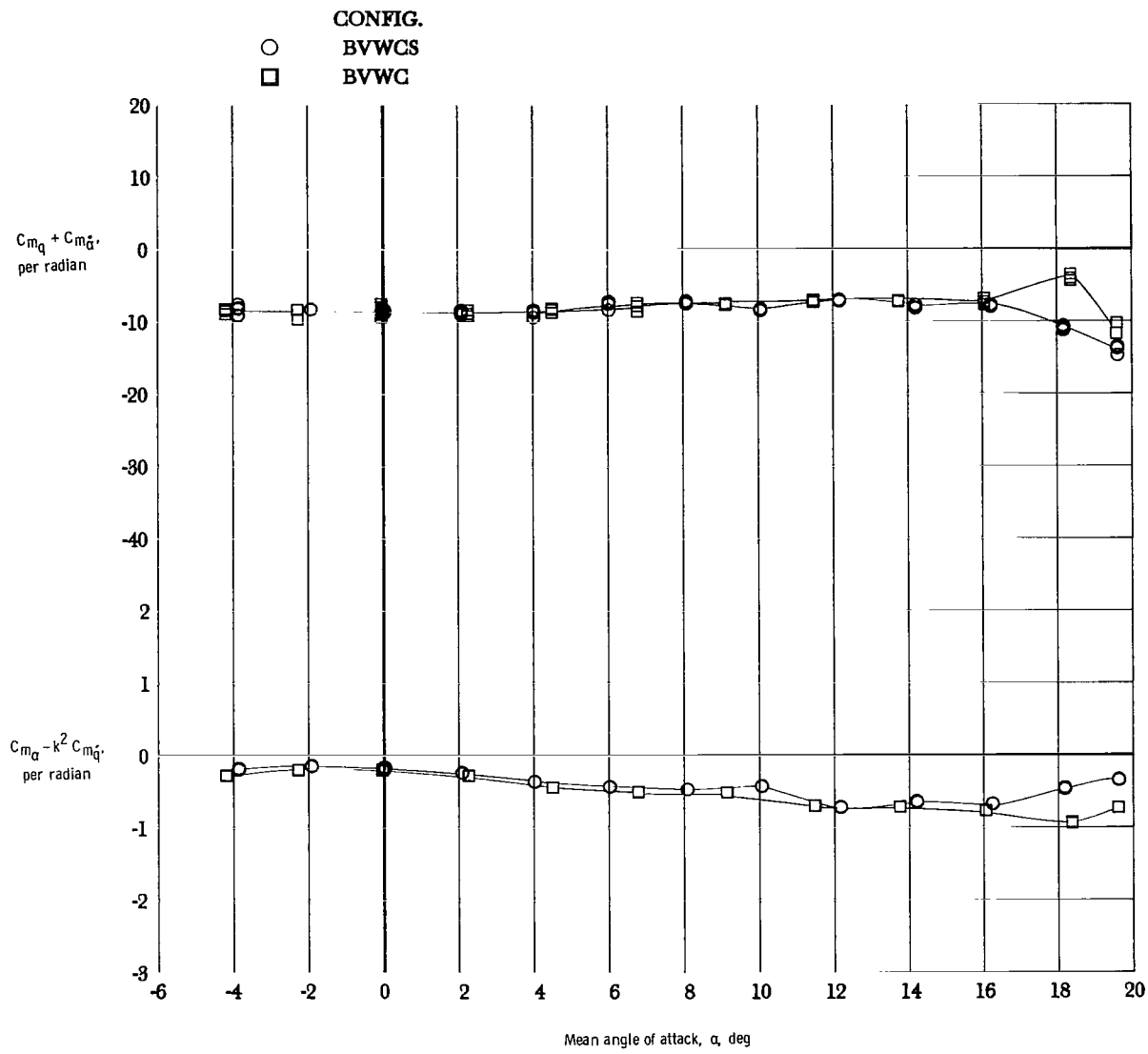

(a) M = 0.4.

Figure 7.- Effect of strake with 44° swept wing configuration on damping-in-pitch parameter and on oscillatory longitudinal-stability parameter.

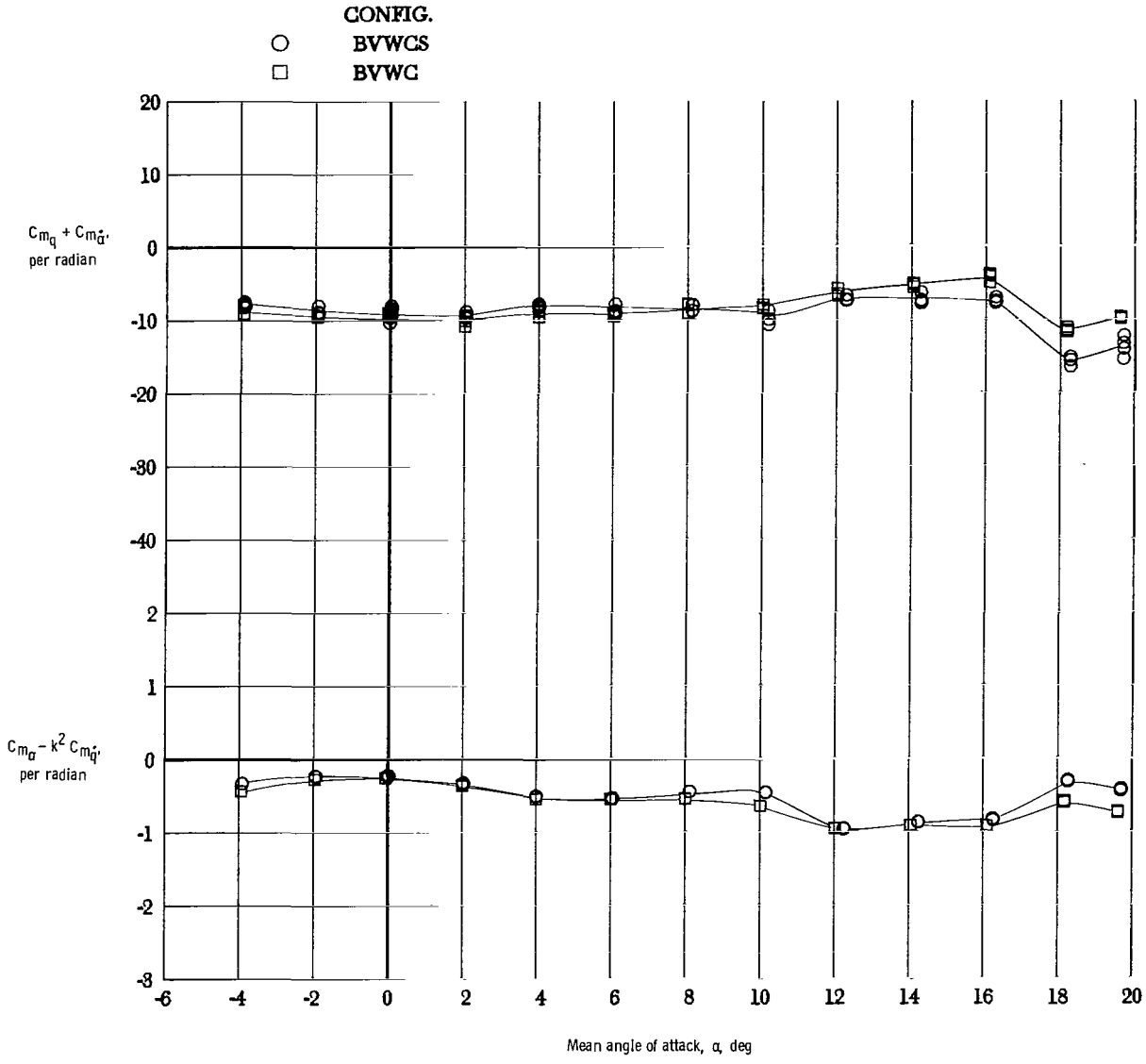

(b) M = 0.7.

Figure 7.- Concluded.

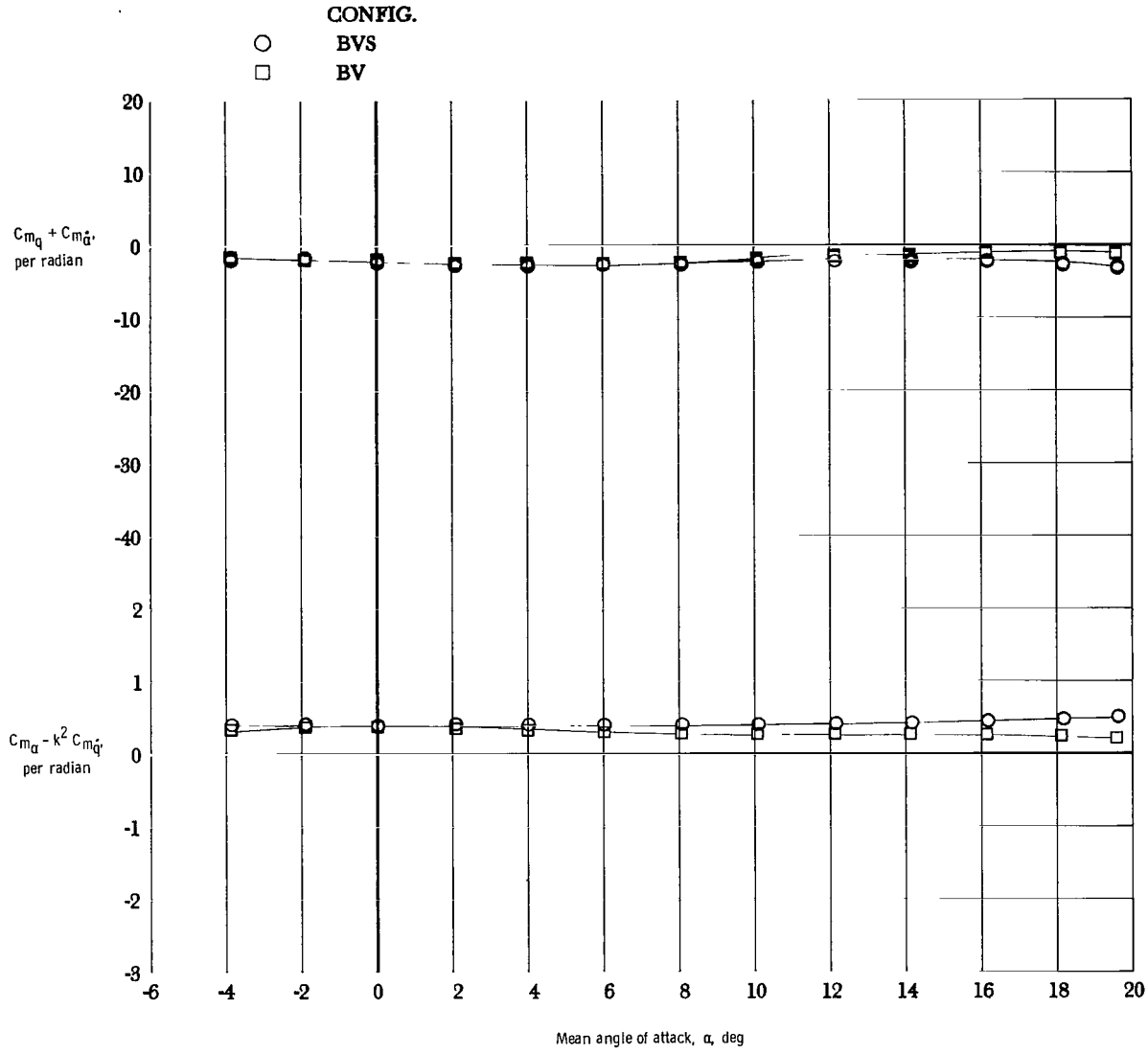

(a) M = 0.4.

Figure 8.- Effect of strake with BV configuration on damping-in-pitch parameter and on oscillatory longitudinal-stability parameter.

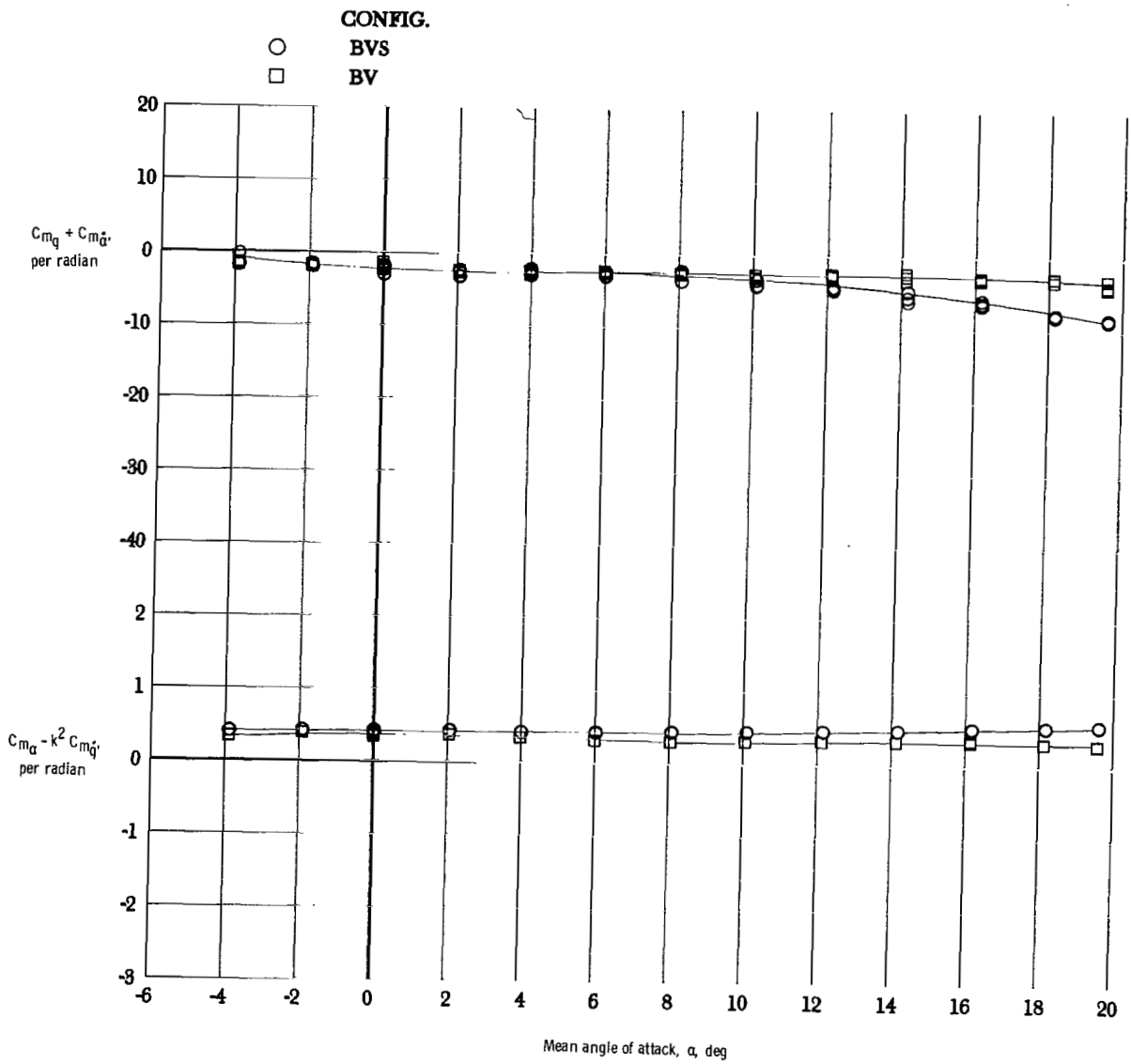

(b) M = 0.7.

Figure 8.- Concluded.

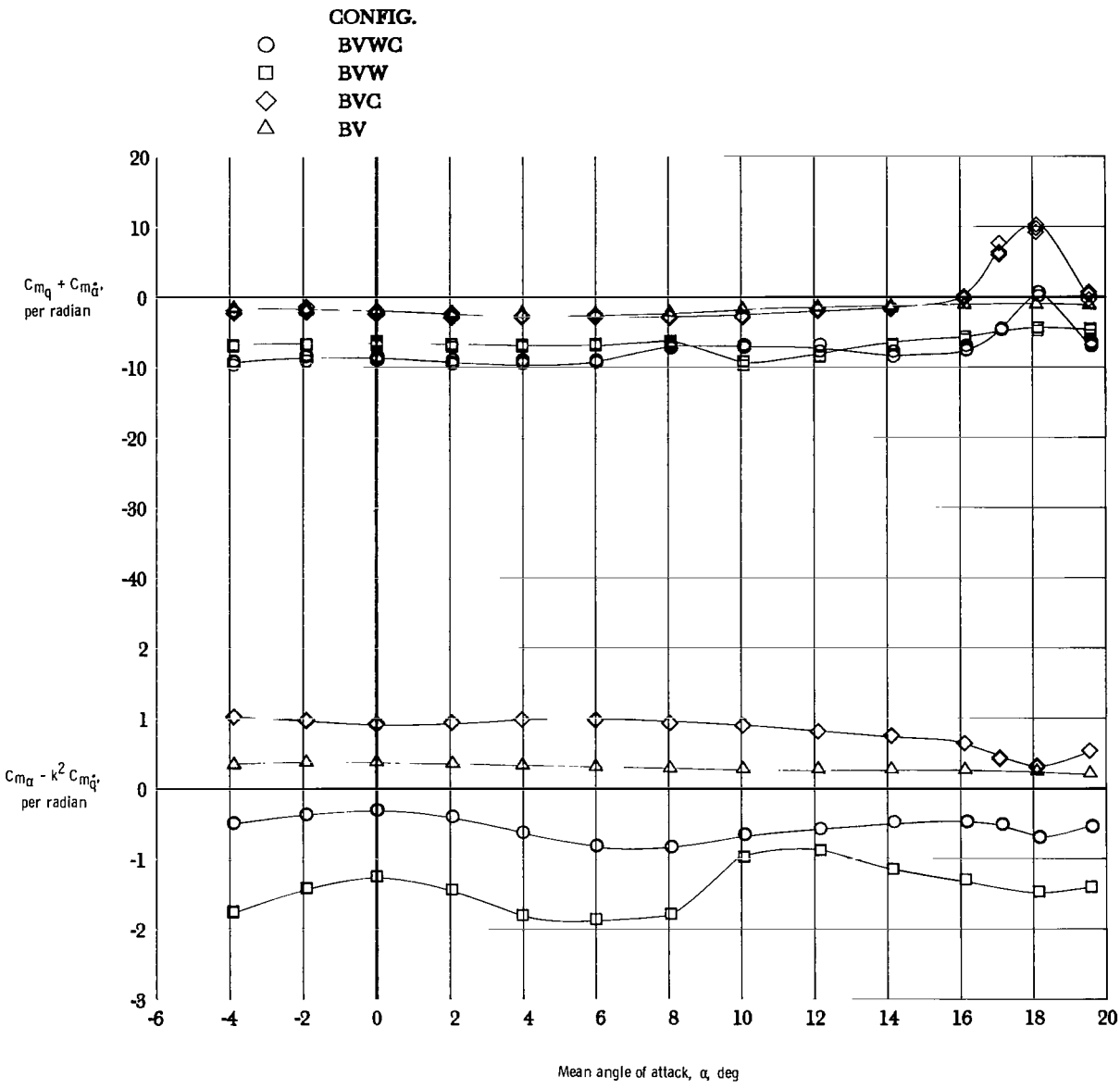

(a) M = 0.4.

Figure 9.- Results for component breakdown of 60° swept wing configuration for damping-in-pitch parameter and oscillatory longitudinal-stability parameter.

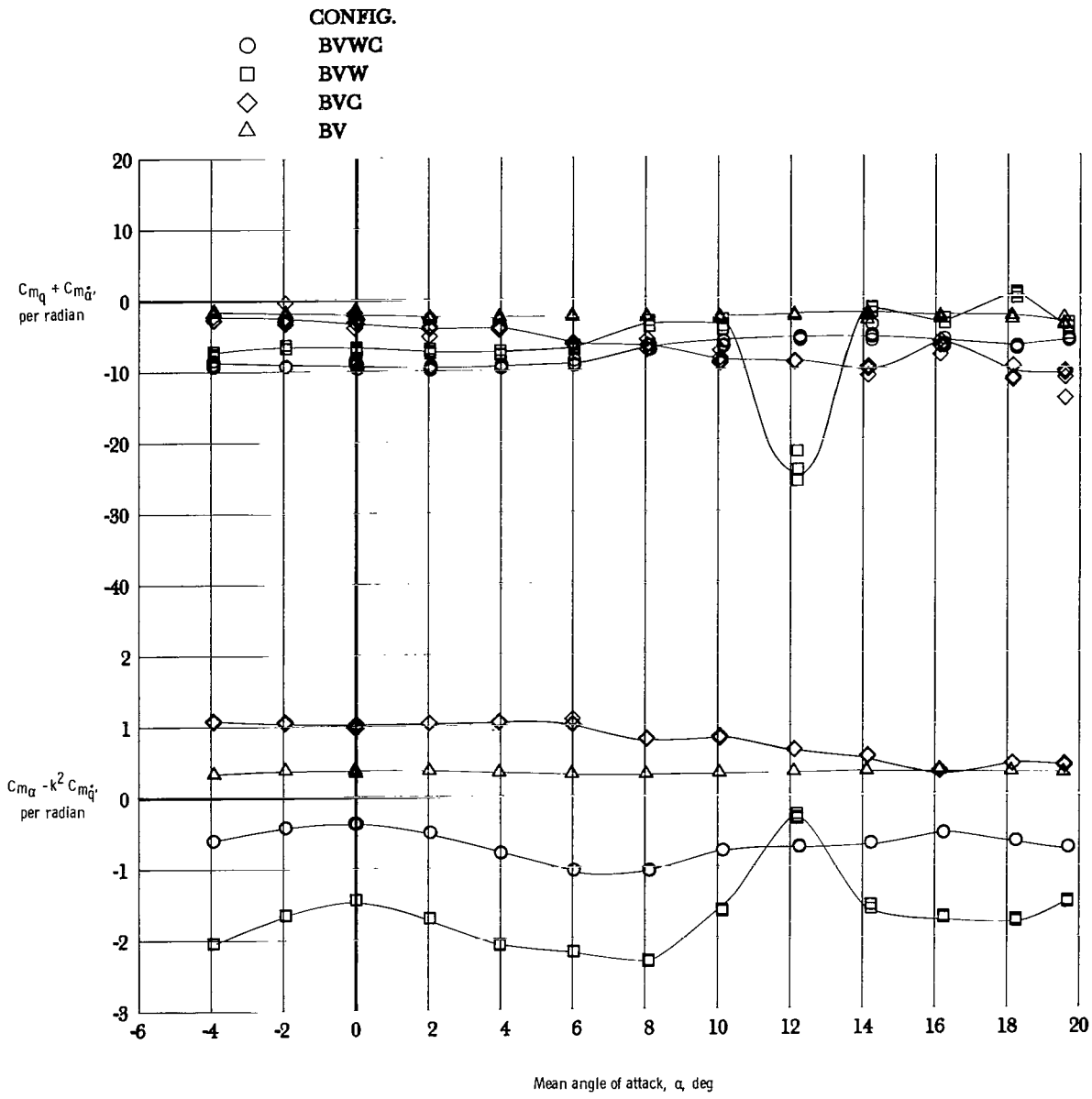

(b) M = 0.7.

Figure 9.- Concluded.

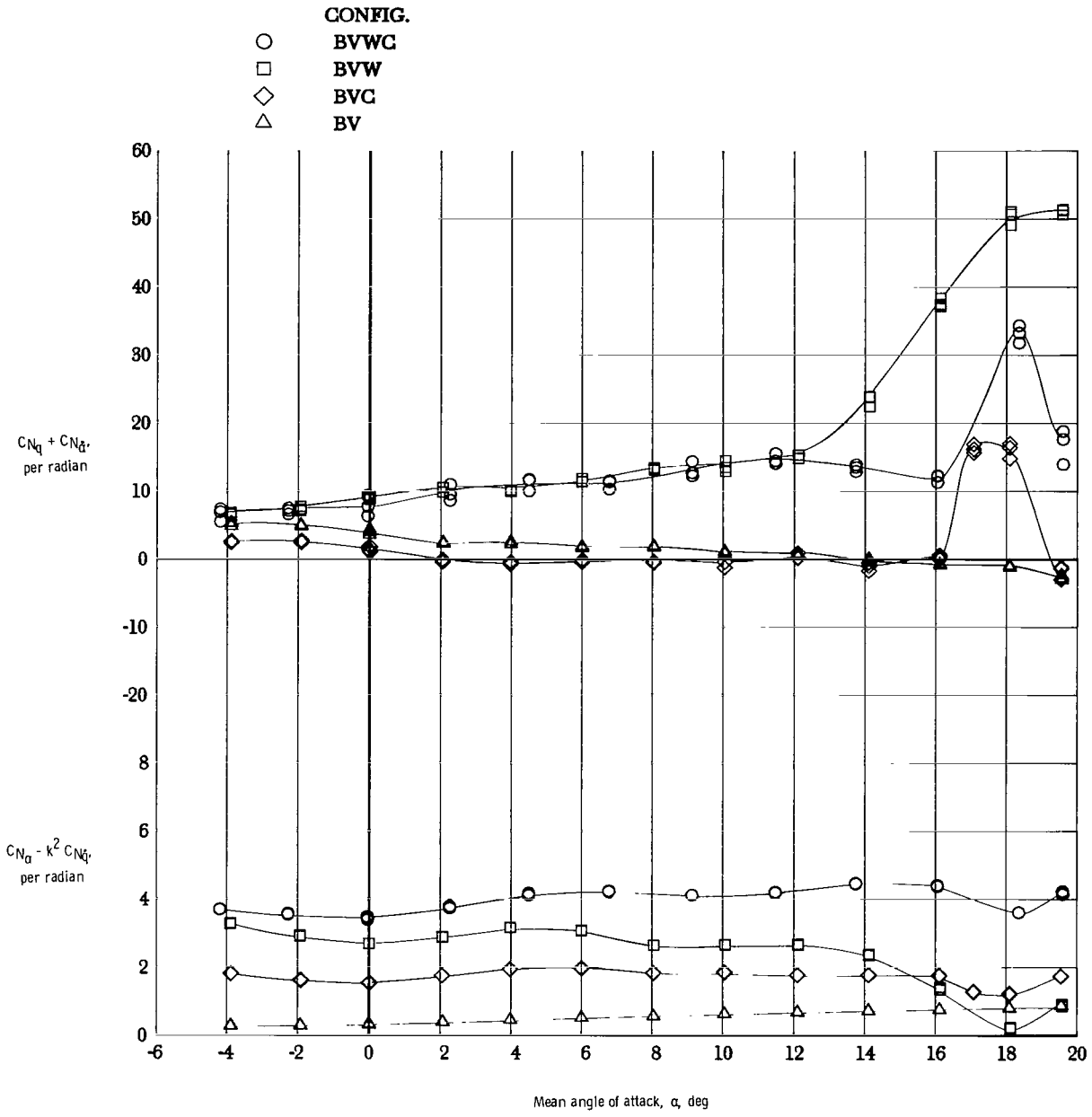

(a) M = 0.4.

Figure 10.- Results for component breakdown of 44° swept wing configuration for normal force due to pitch rate parameter and normal force due to pitch displacement parameter.

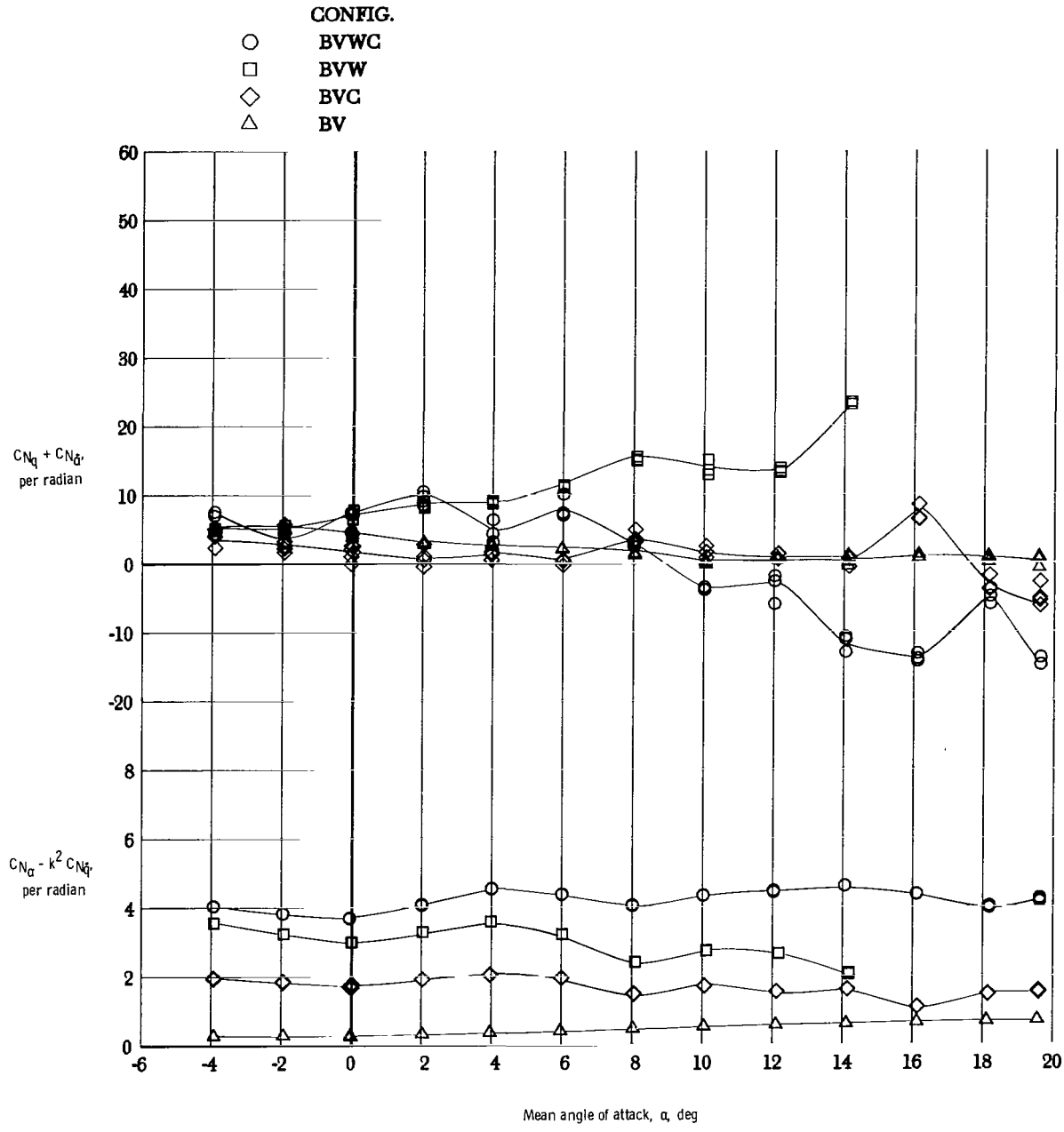

(b) M = 0.7.

Figure 10.- Concluded.

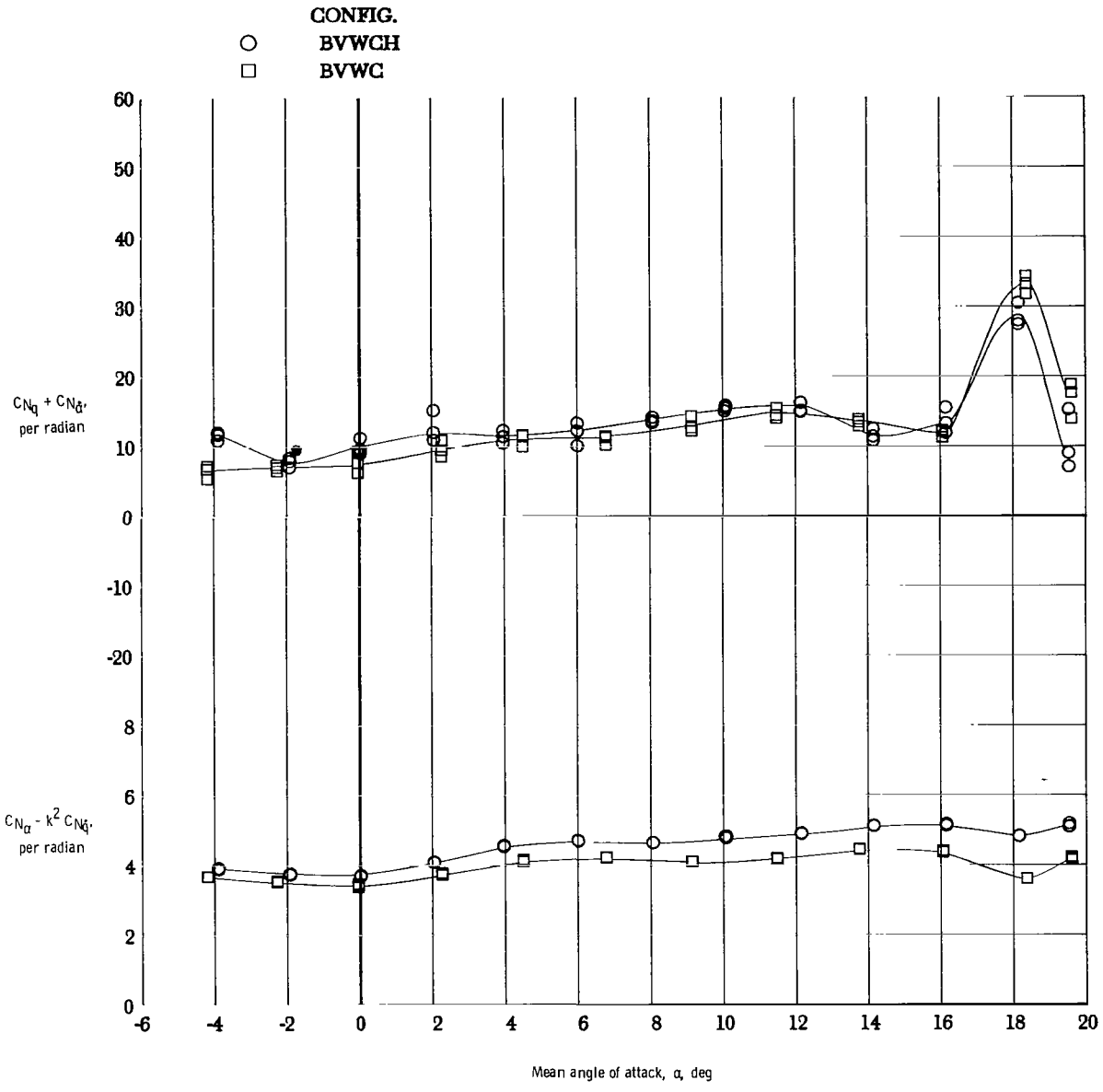

(a) M = 0.4.

Figure 11.- Effect of horizontal tail with 44° swept wing configuration on normal force due to pitch rate parameter and on normal force due to pitch displacement parameter.

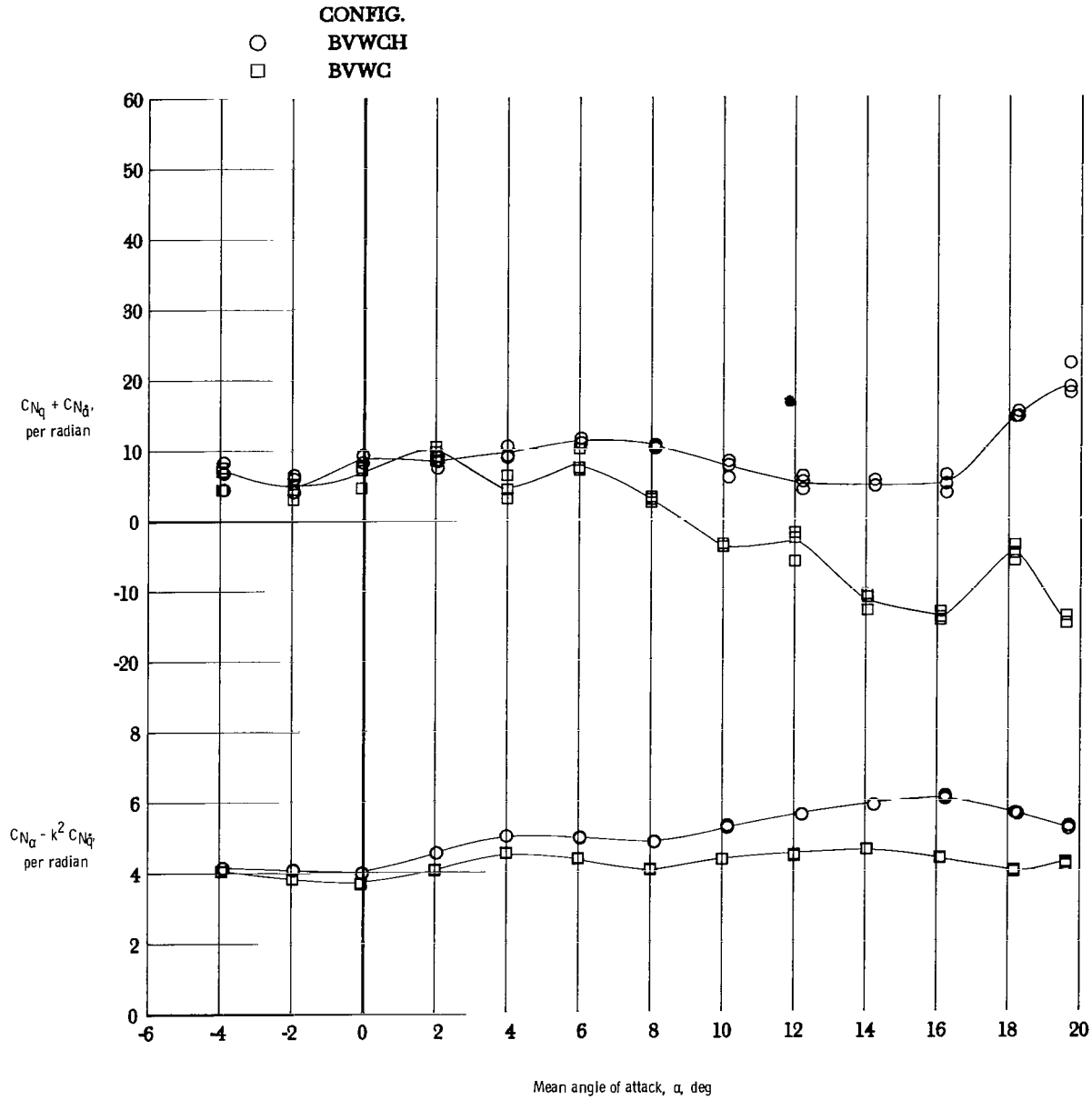

(b) M = 0.7.

Figure 11.- Concluded.

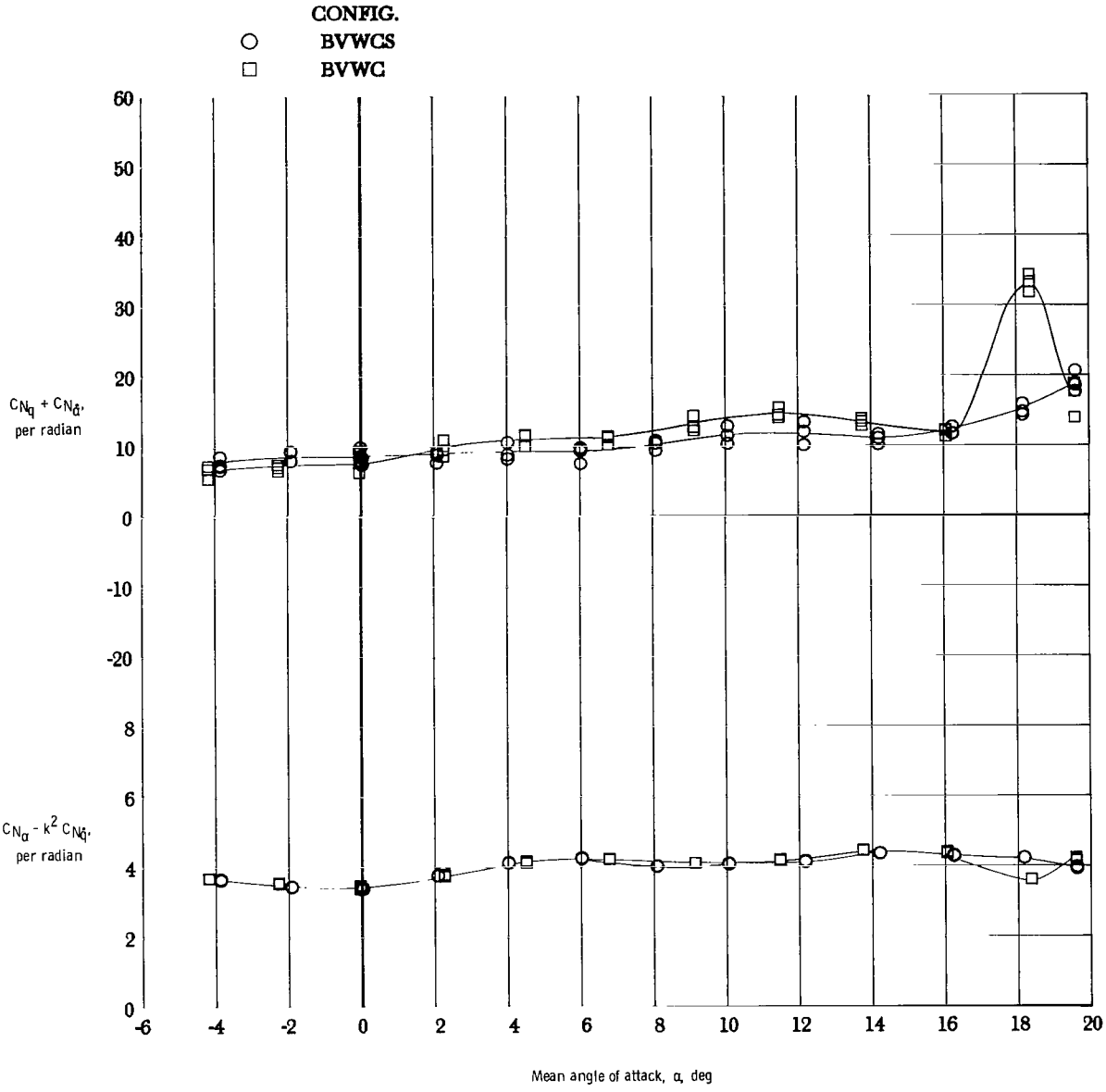

(a) M = 0.4.

Figure 12.- Effect of strake with 44° swept wing configuration on normal force due to pitch rate parameter and on normal force due to pitch displacement parameter.

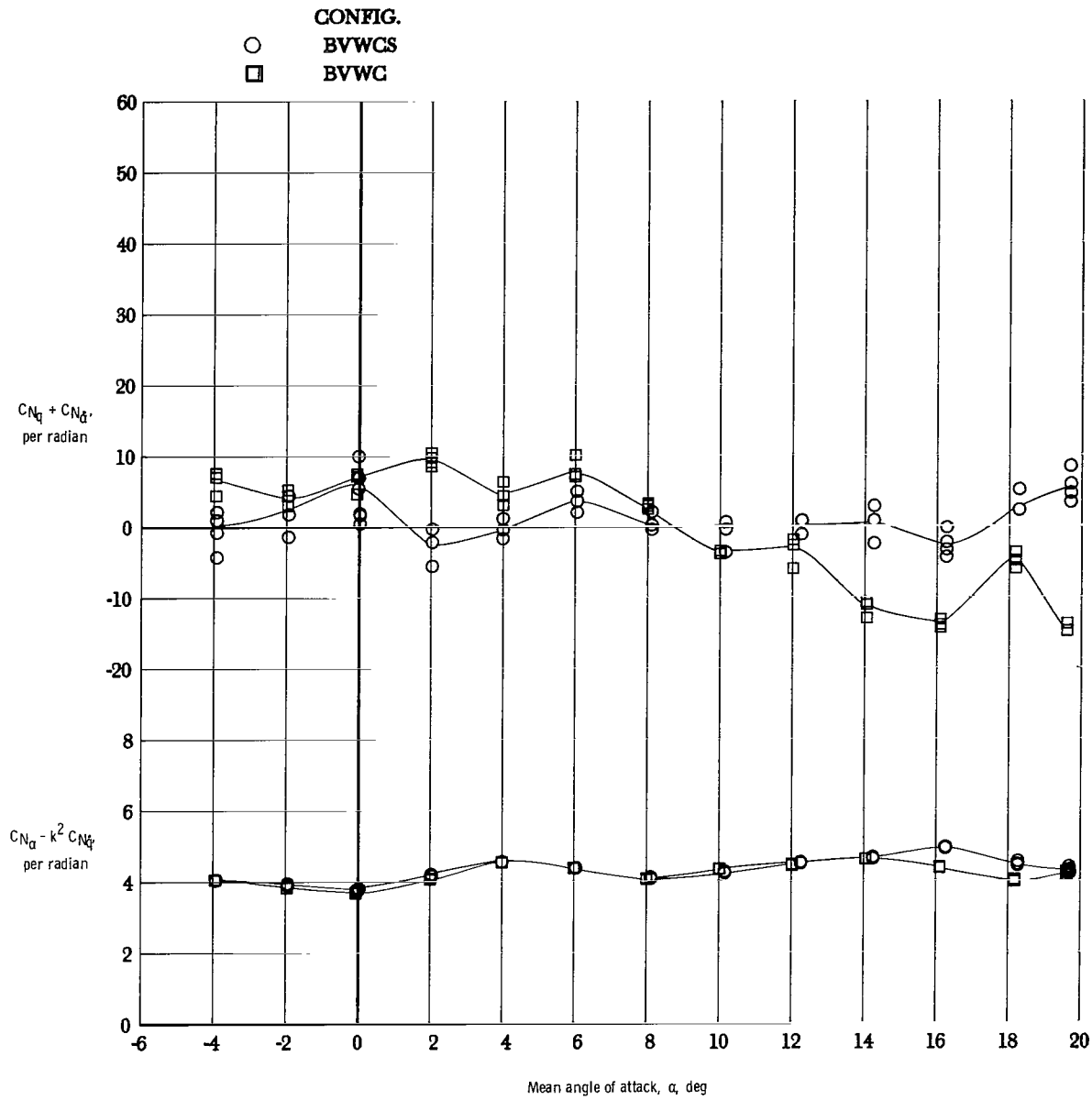

(b) M = 0.7.

Figure 12.- Concluded.

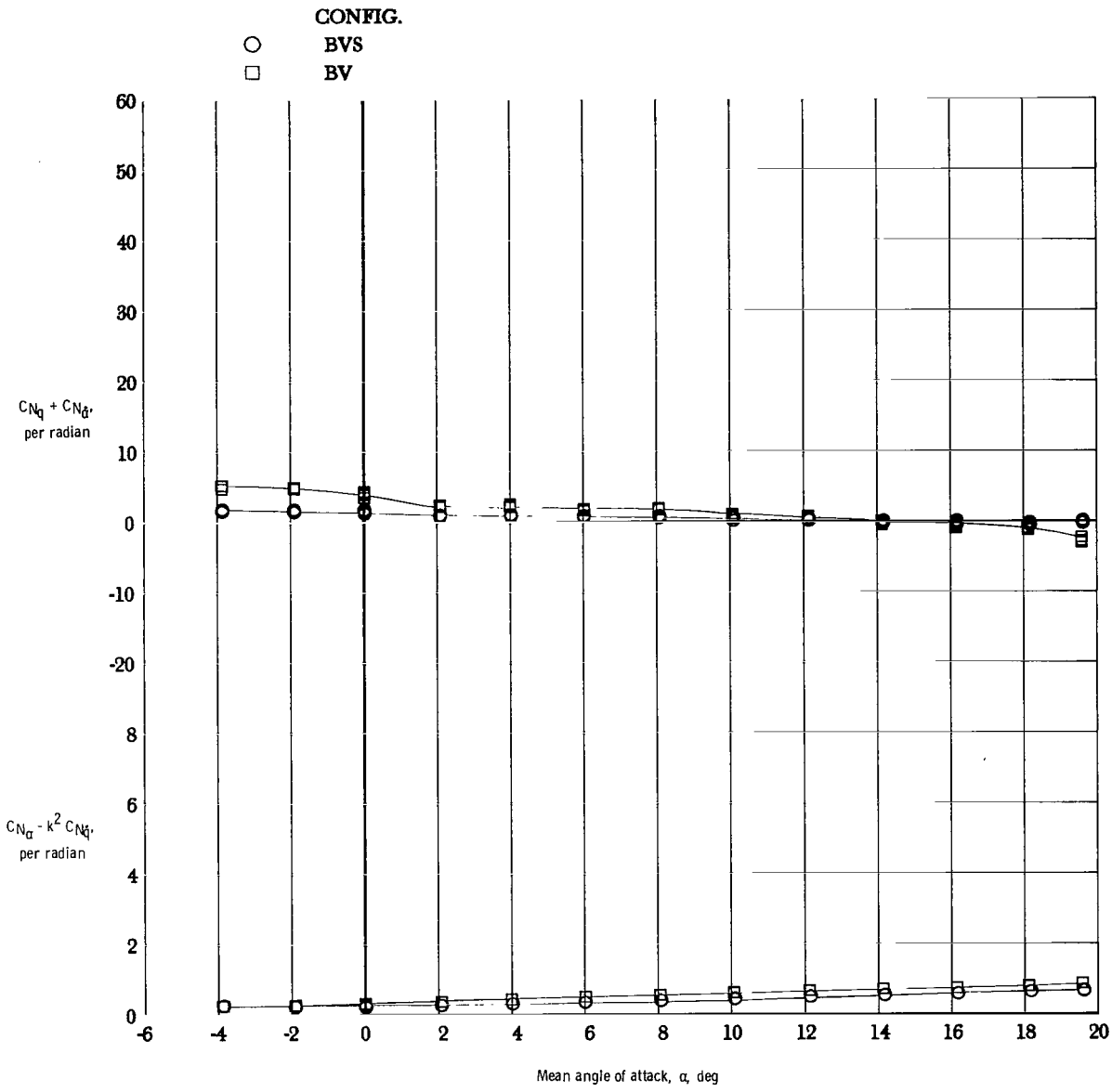

(a) M = 0.4.

Figure 13.- Effect of strake with BV configuration on normal force due to pitch rate parameter and on normal force due to pitch displacement parameter.

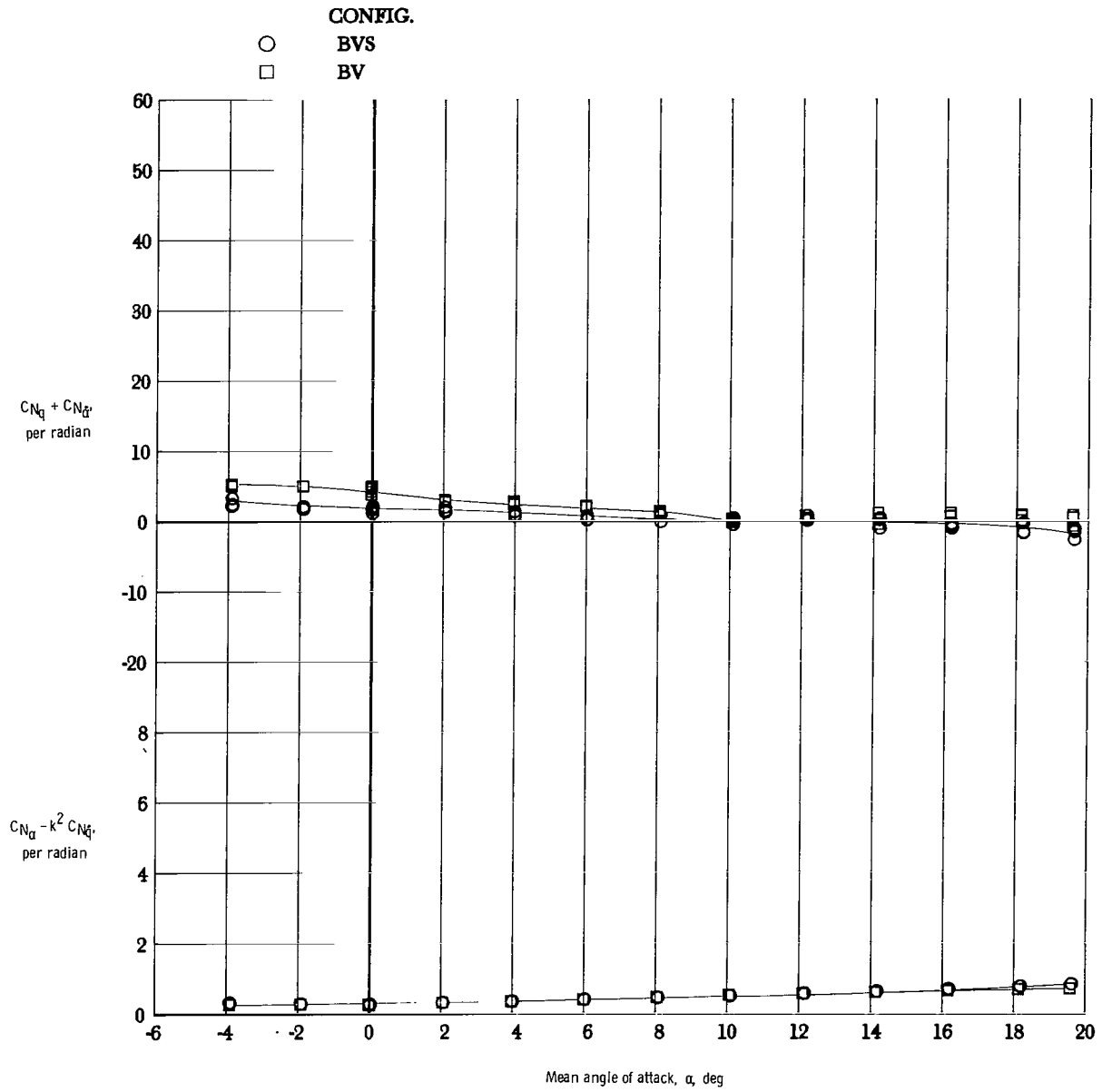

(b) M = 0.7.

Figure 13.- Concluded.

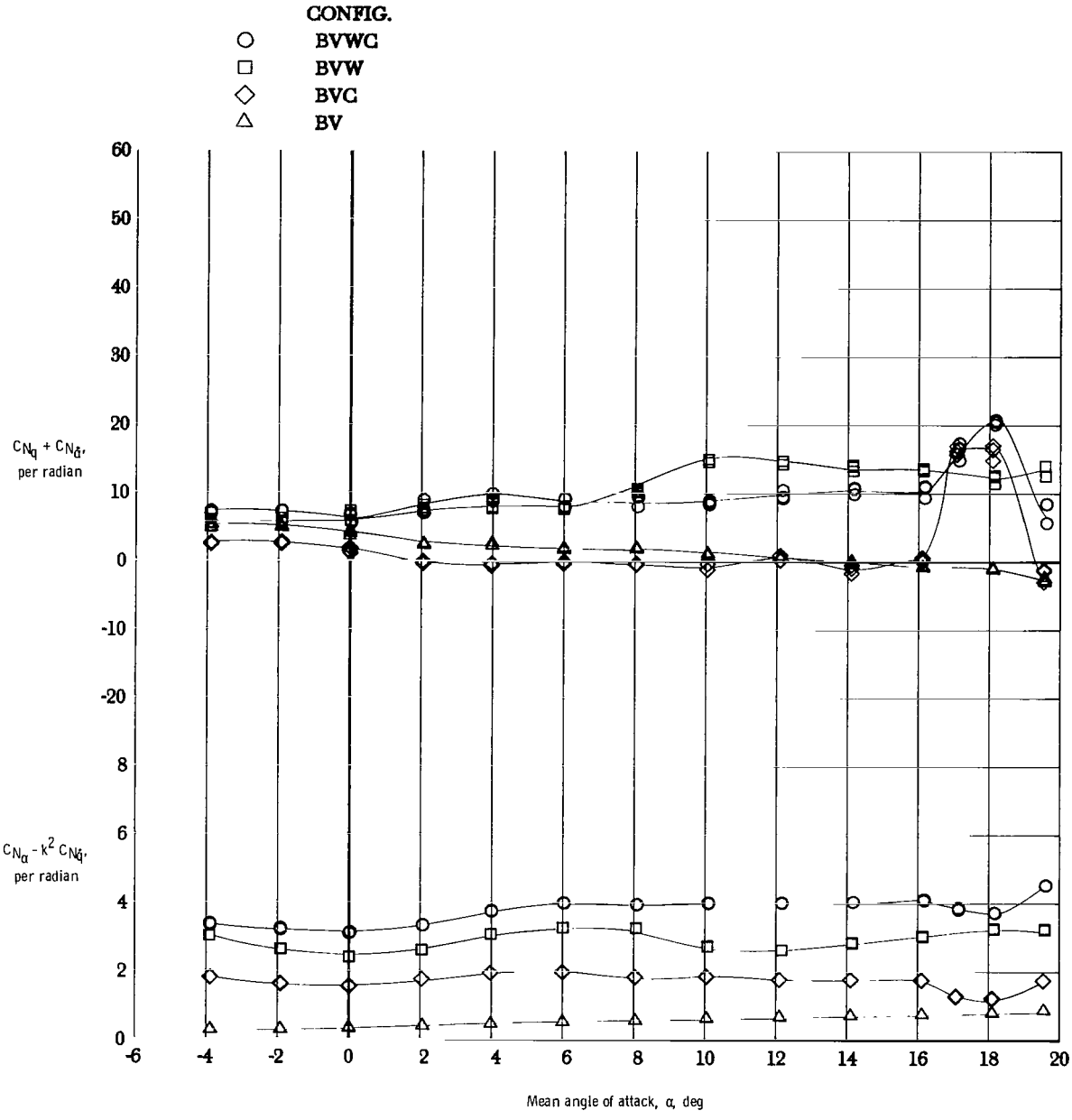

(a) M = 0.4.

Figure 14.- Results for component breakdown of 60° swept wing configuration for normal force due to pitch rate parameter and normal force due to pitch displacement parameter.

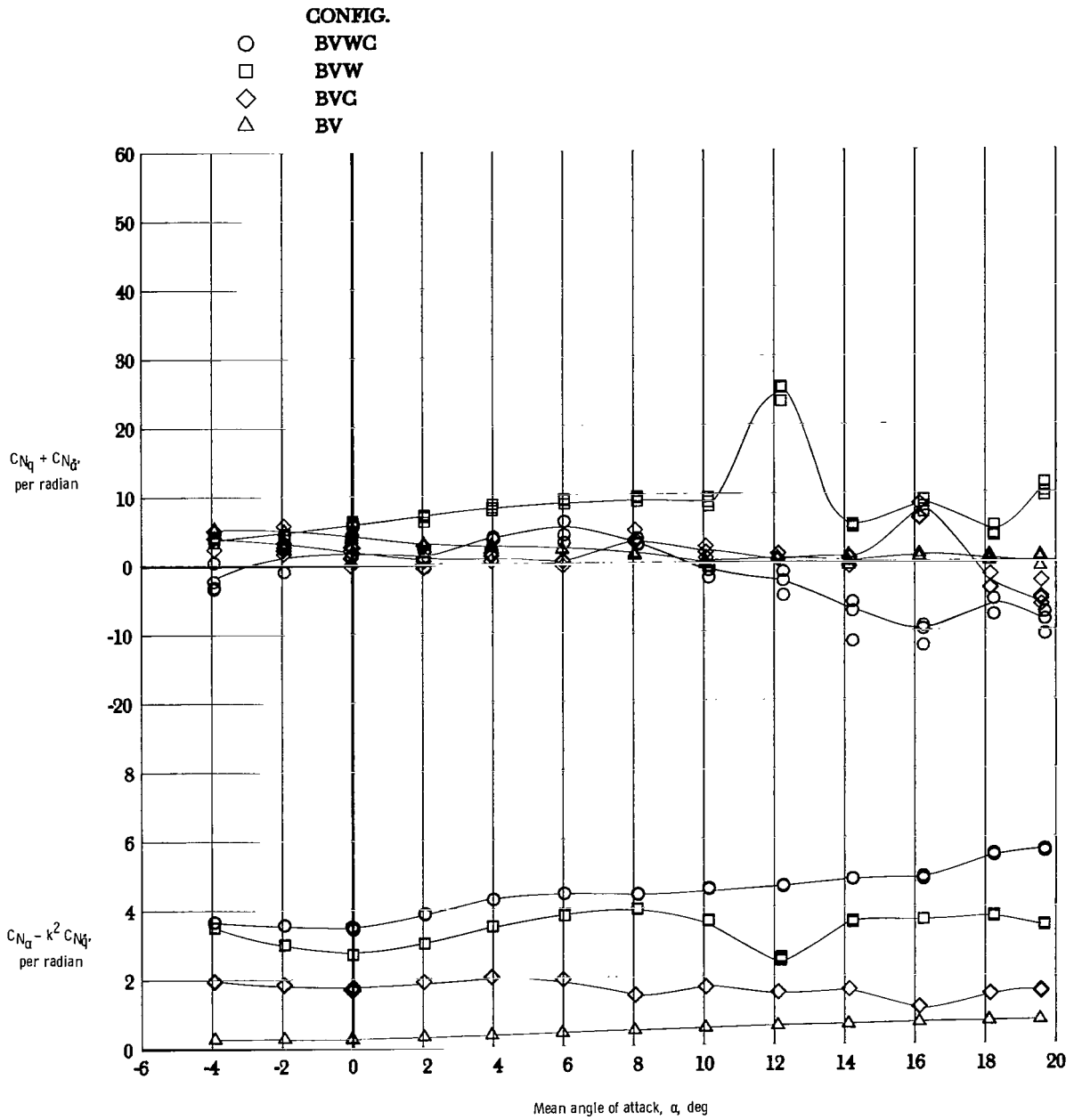

(b) M = 0.7.

Figure 14.- Concluded.

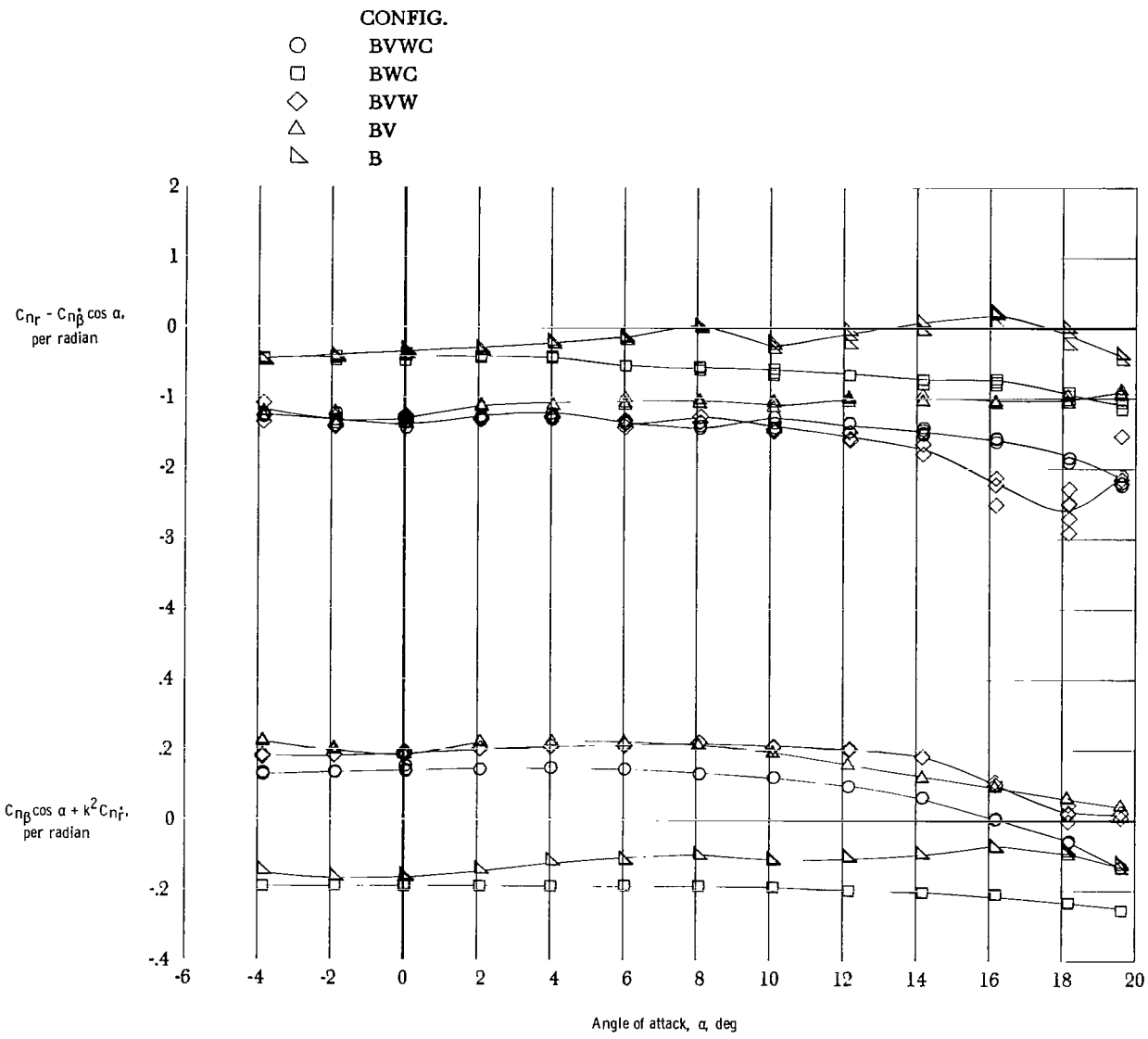

(a) M = 0.4.

Figure 15.- Results for component breakdown of 44° swept wing configuration for damping-in-yaw parameter and oscillatory directional-stability parameter.

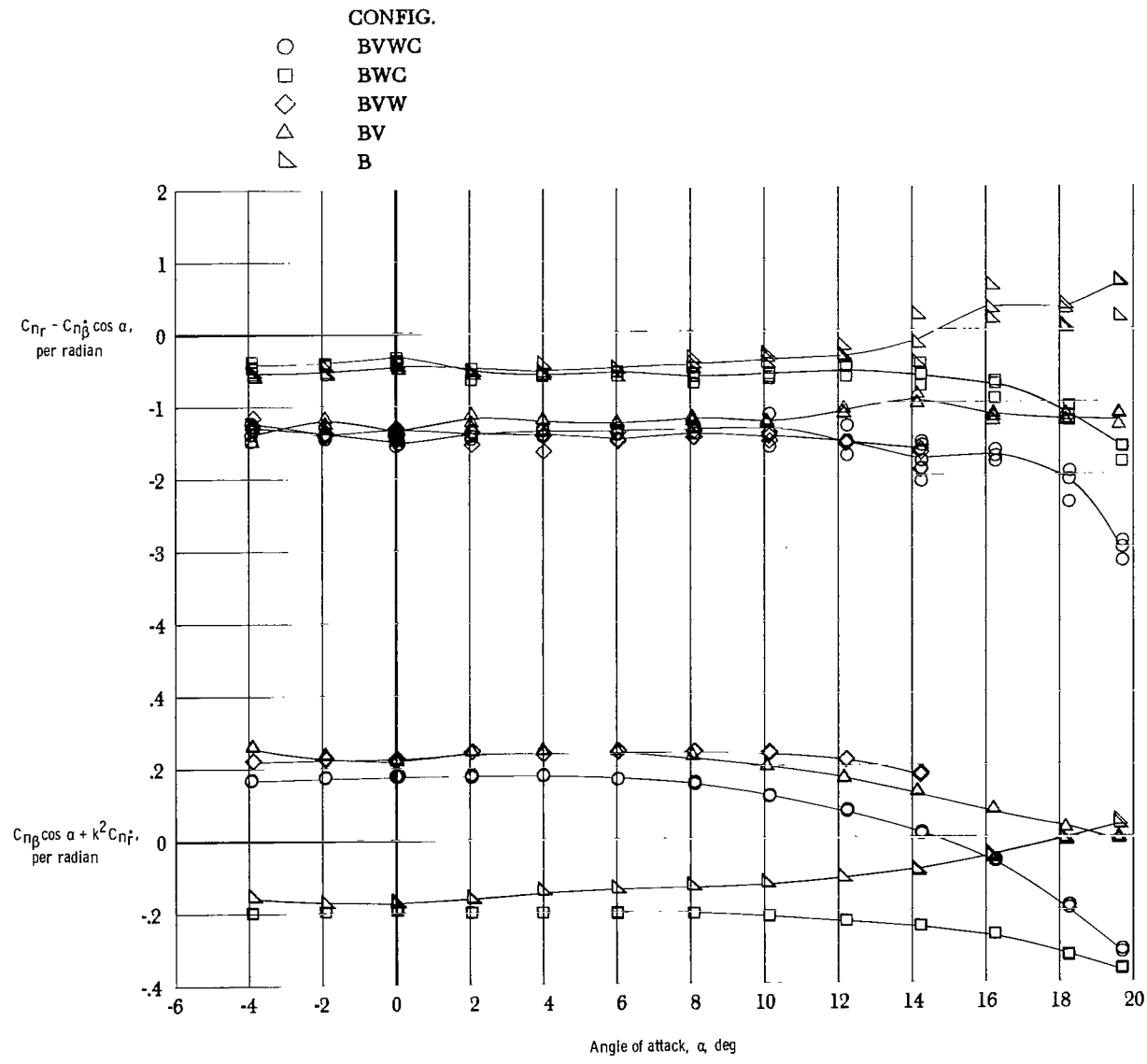

(b) M = 0.7.

Figure 15.- Concluded.

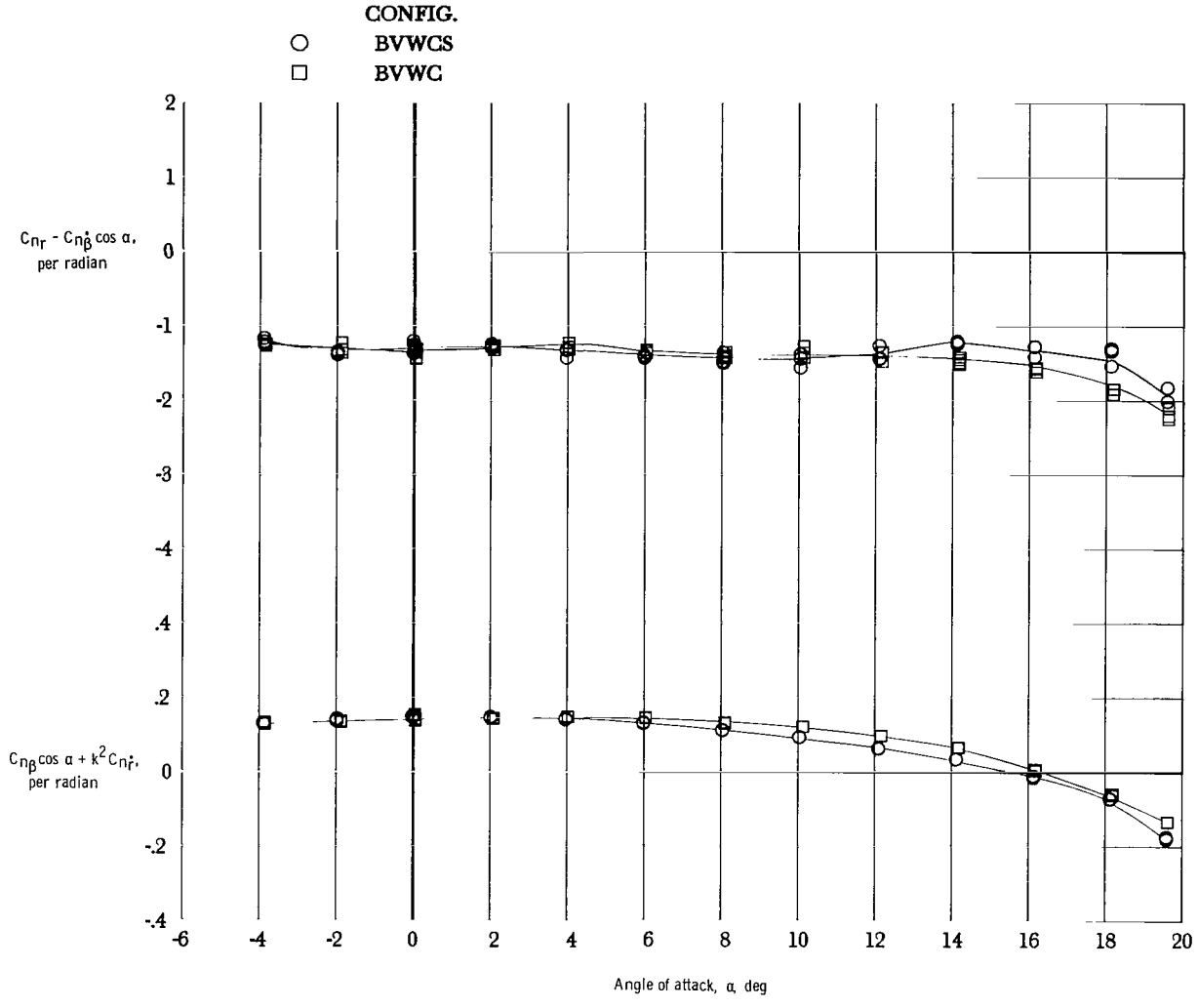

(a) M = 0.4.

Figure 16.- Effect of strake with 44° swept wing configuration on damping-in-yaw parameter and on oscillatory directional-stability parameter.

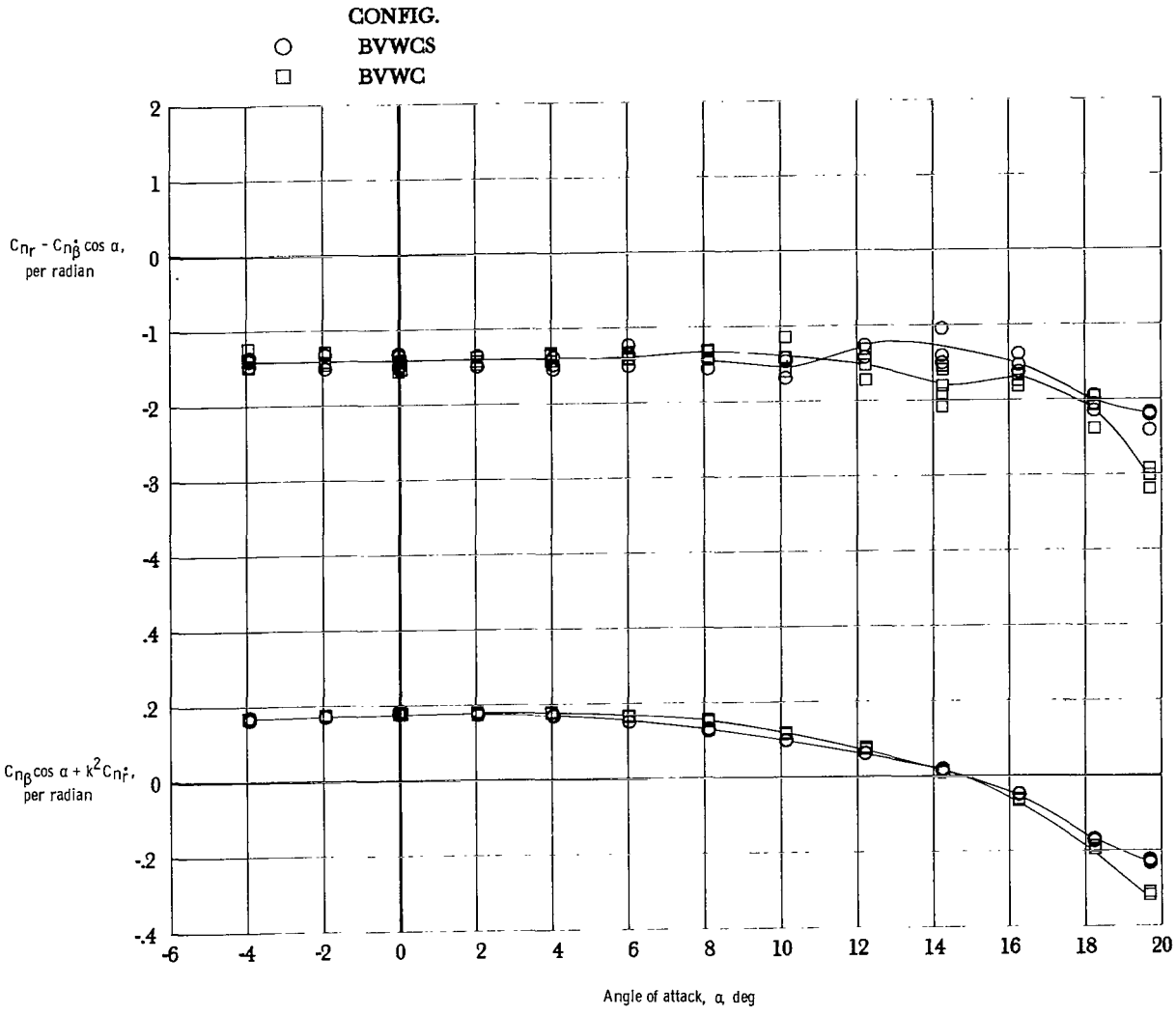

(b) M = 0.7.

Figure 16.- Concluded.

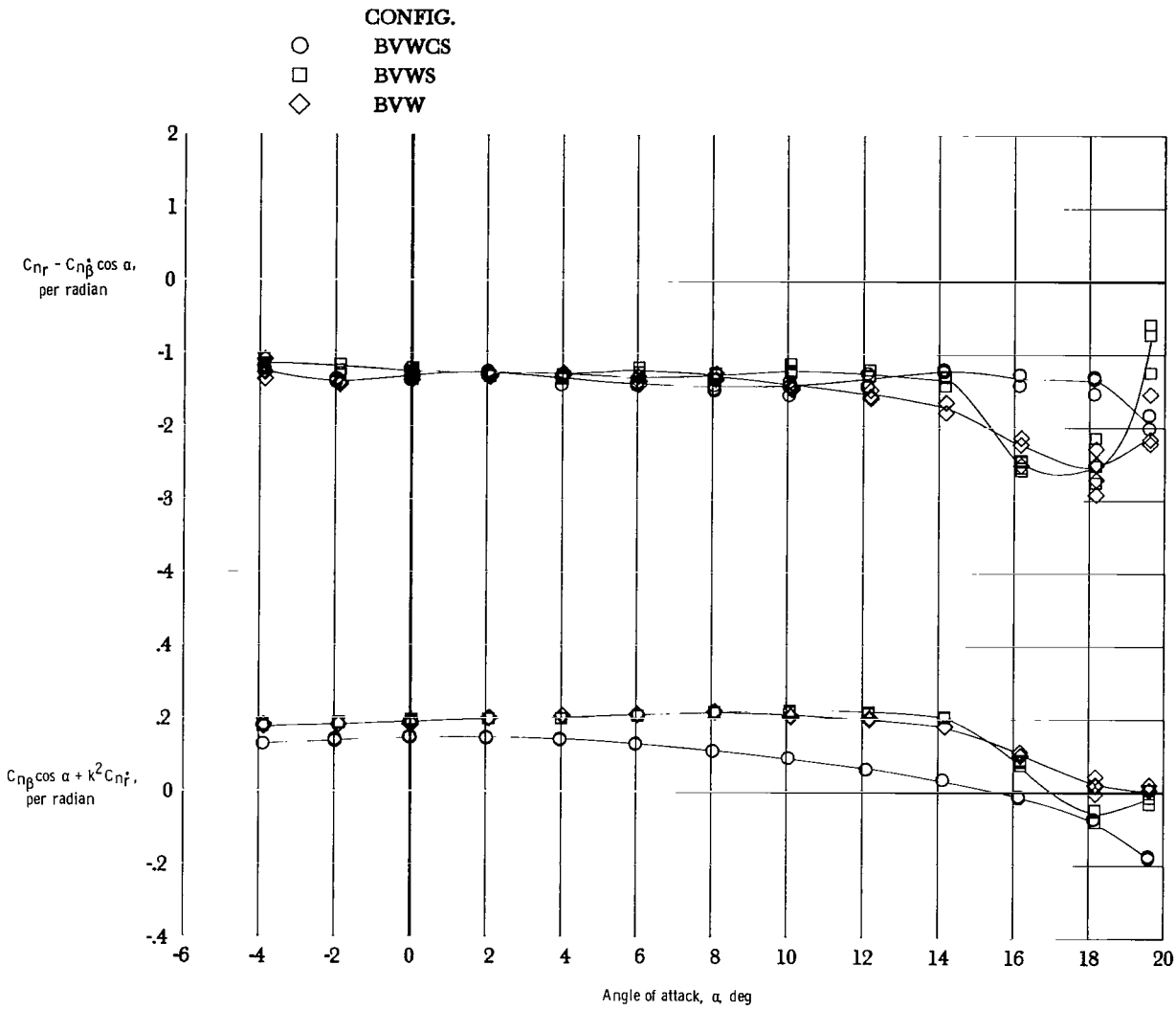

(a) M = 0.4.

Figure 17.- Effect of strake and canard with 44° swept wing configuration on damping-in-yaw parameter and on oscillatory directional-stability parameter.

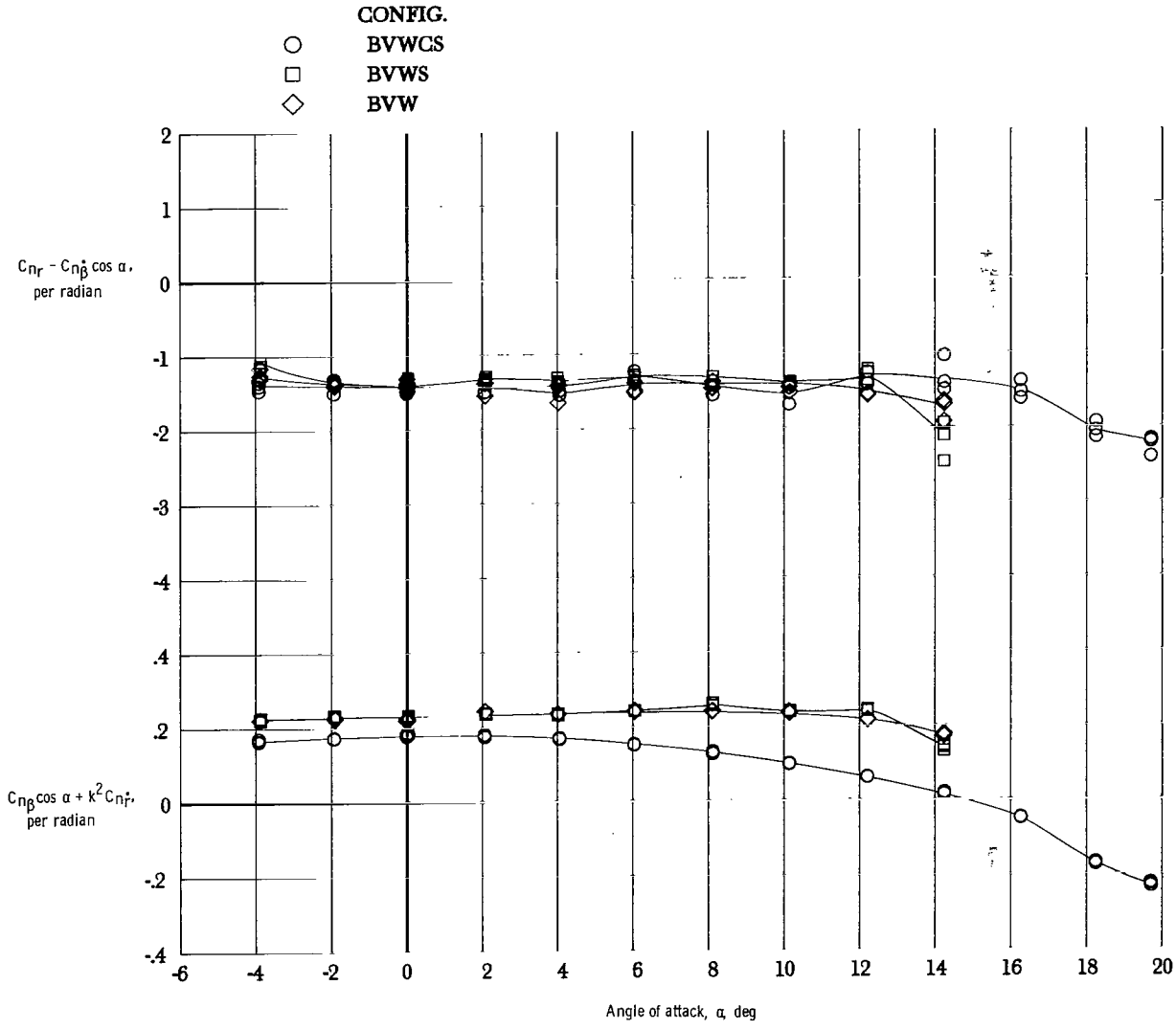

(b) M = 0.7.

Figure 17.- Concluded.

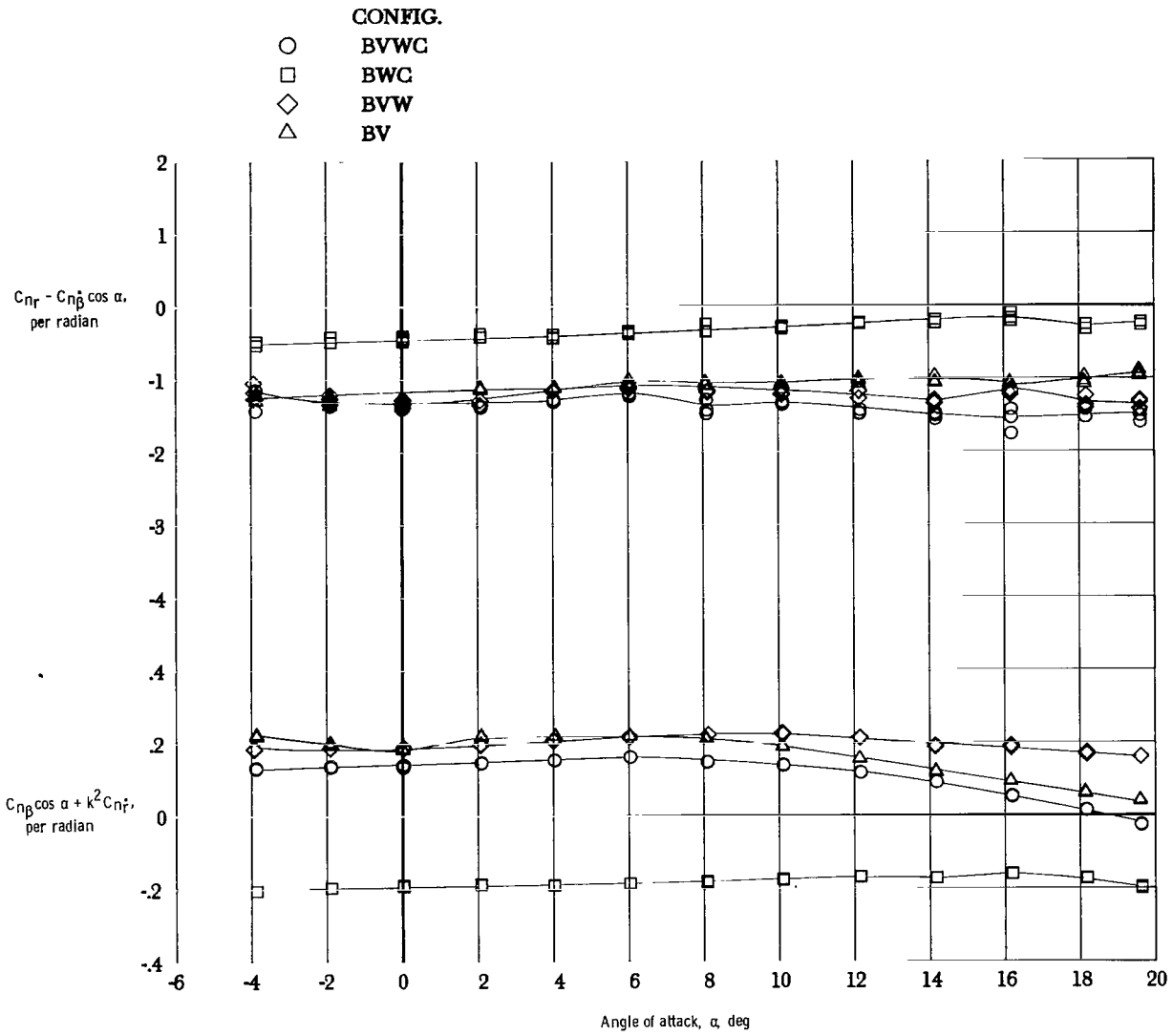

(a) M = 0.4.

Figure 18.- Results for component breakdown of 60° swept wing configuration for damping-in-yaw parameter and oscillatory directional-stability parameter.

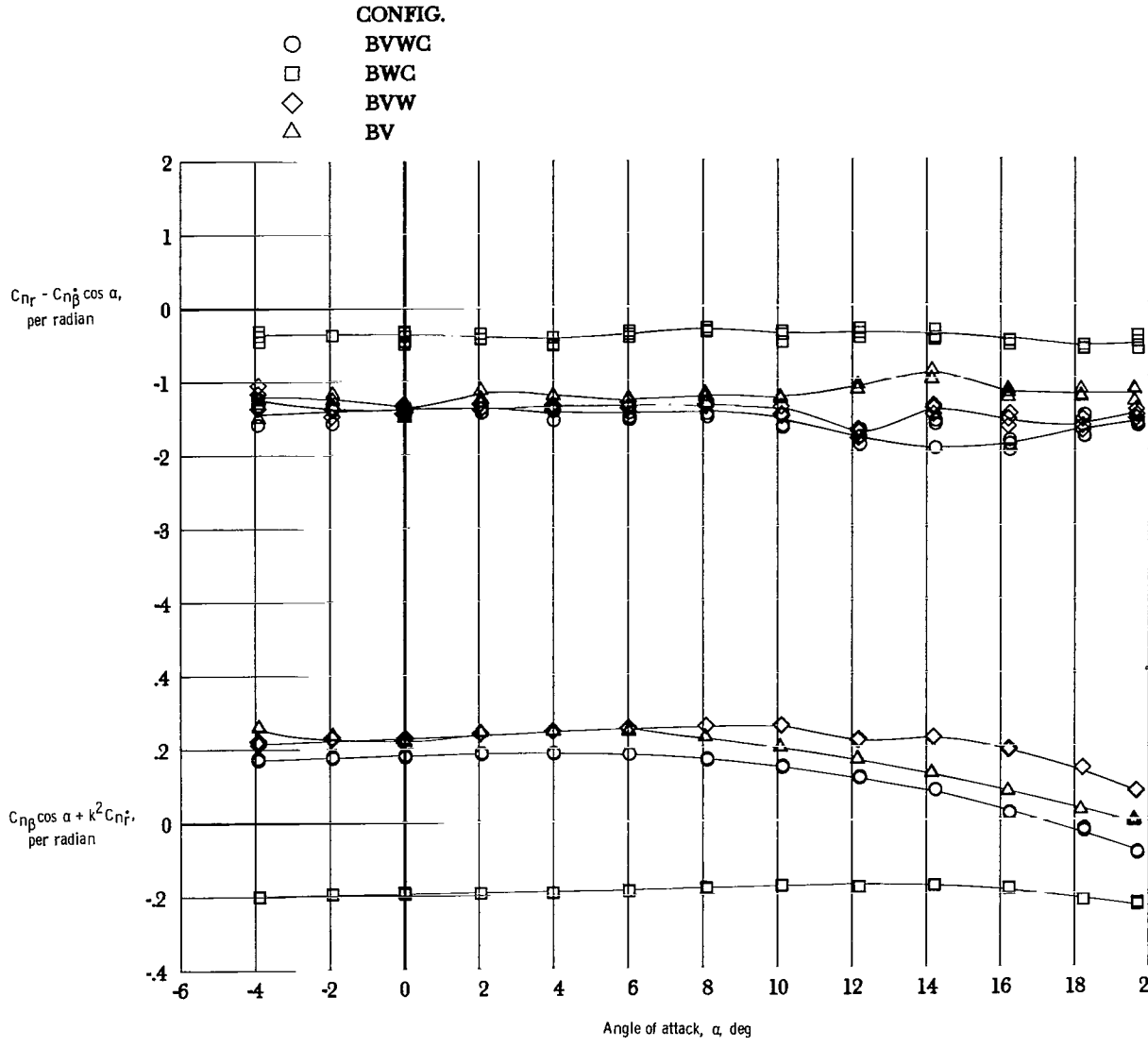

(b) M = 0.7.

Figure 18.- Concluded.

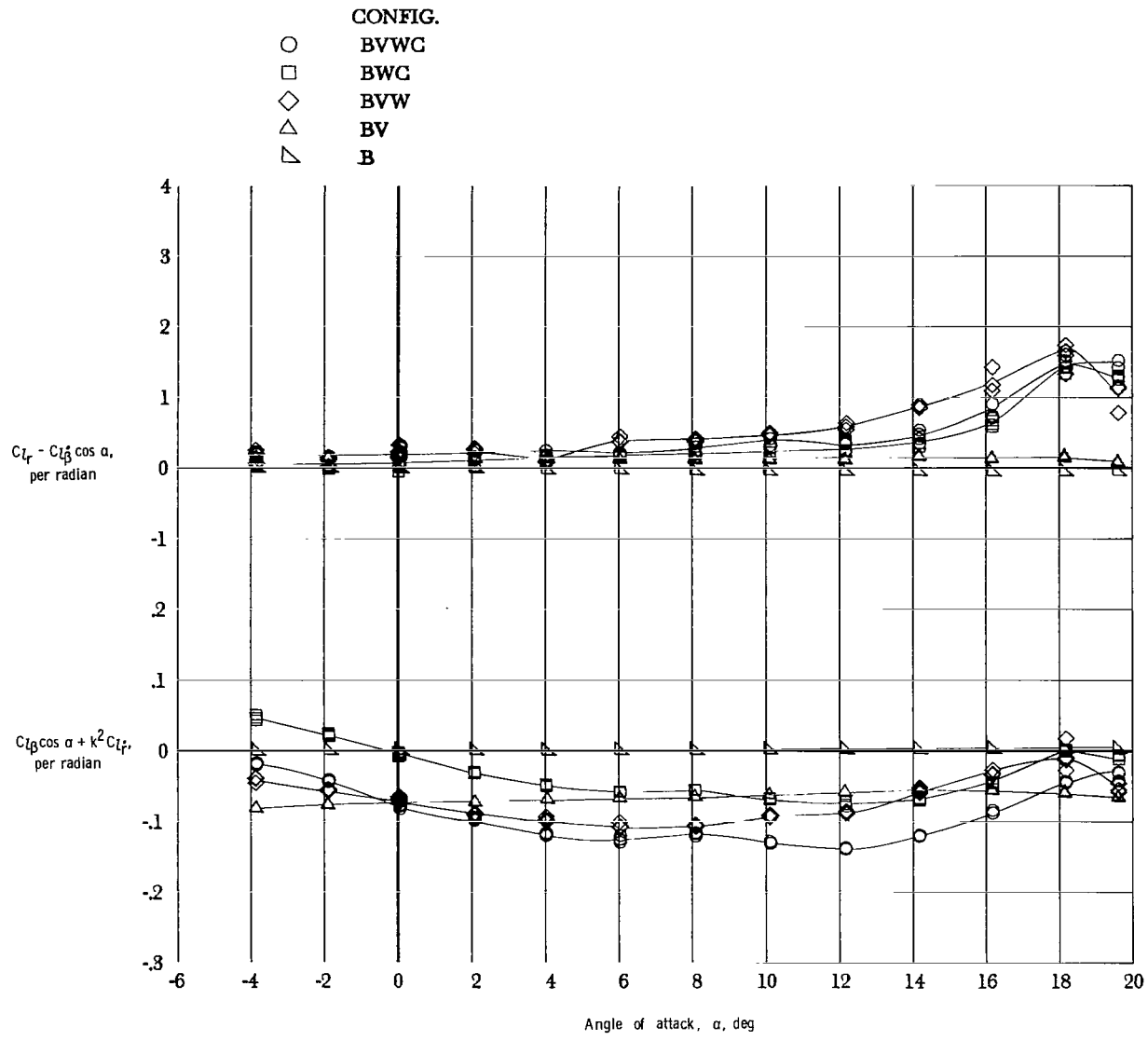

(a) M = 0.4.

Figure 19.- Results for component breakdown of 44° swept wing configuration for rolling moment due to yaw rate parameter and effective dihedral parameter.

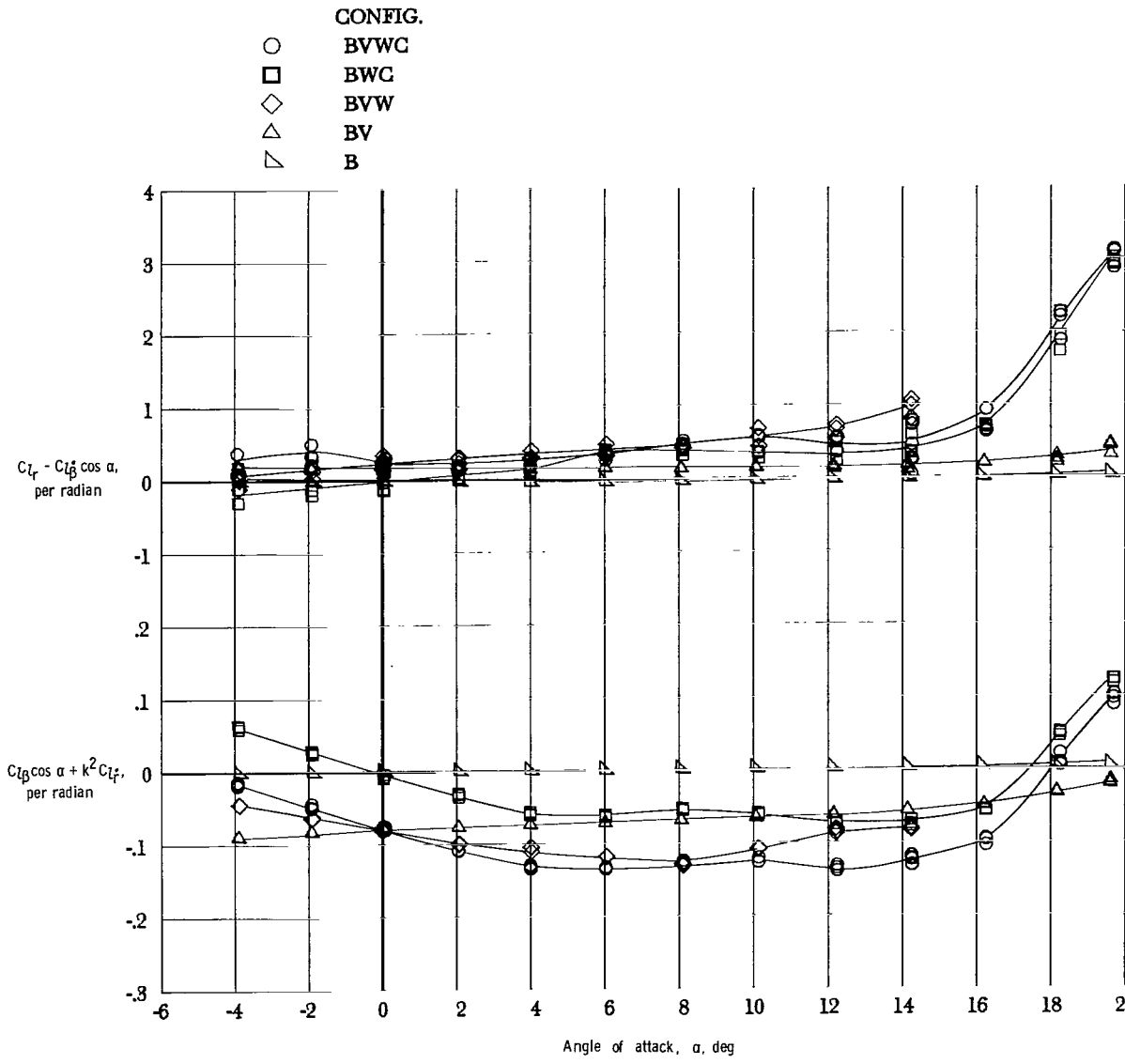

(b) M = 0.7.

Figure 19.- Concluded.

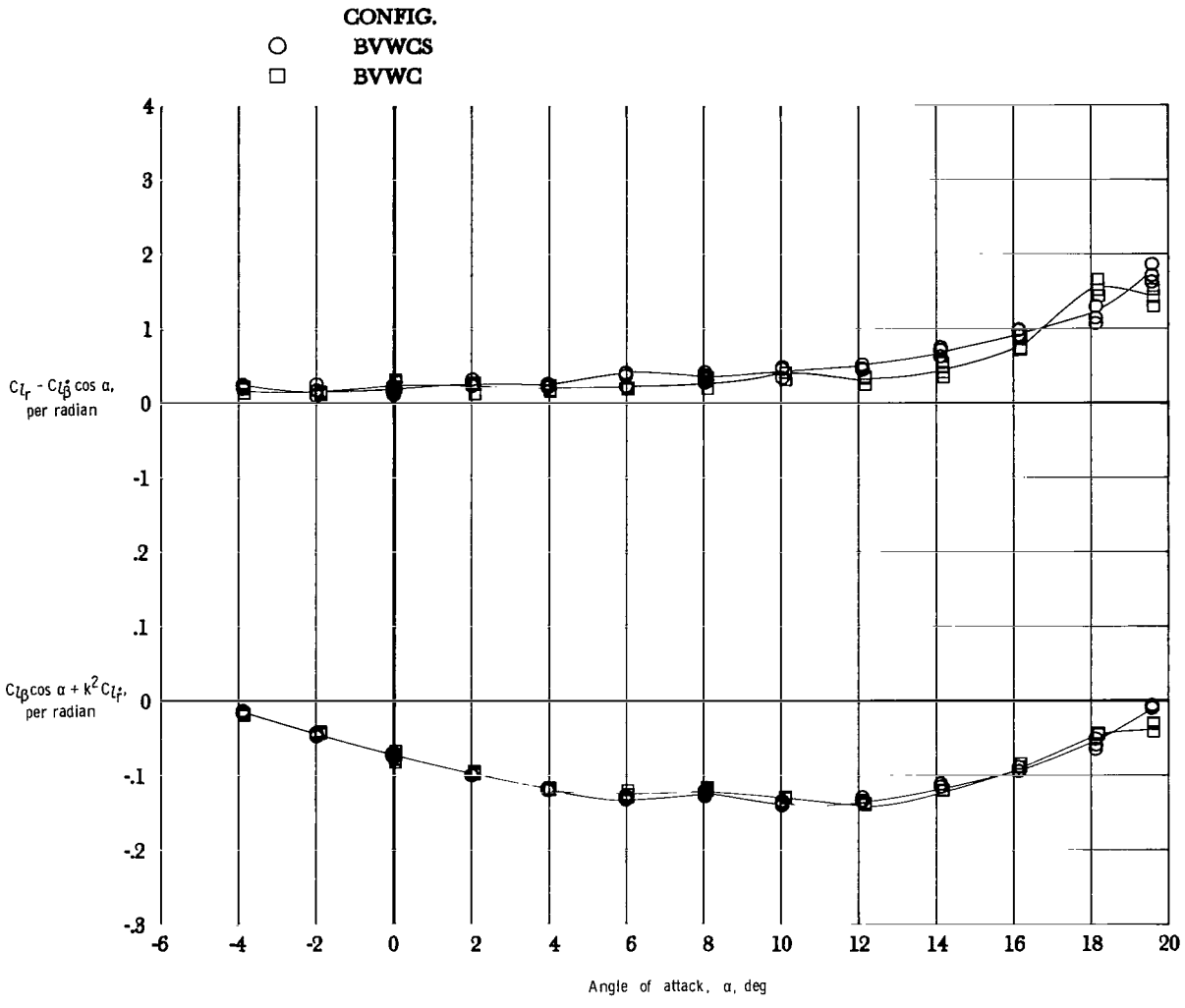

(a) M = 0.4.

Figure 20.- Effect of strake with 44° swept wing configuration on rolling moment due to yaw rate parameter and on effective dihedral parameter.

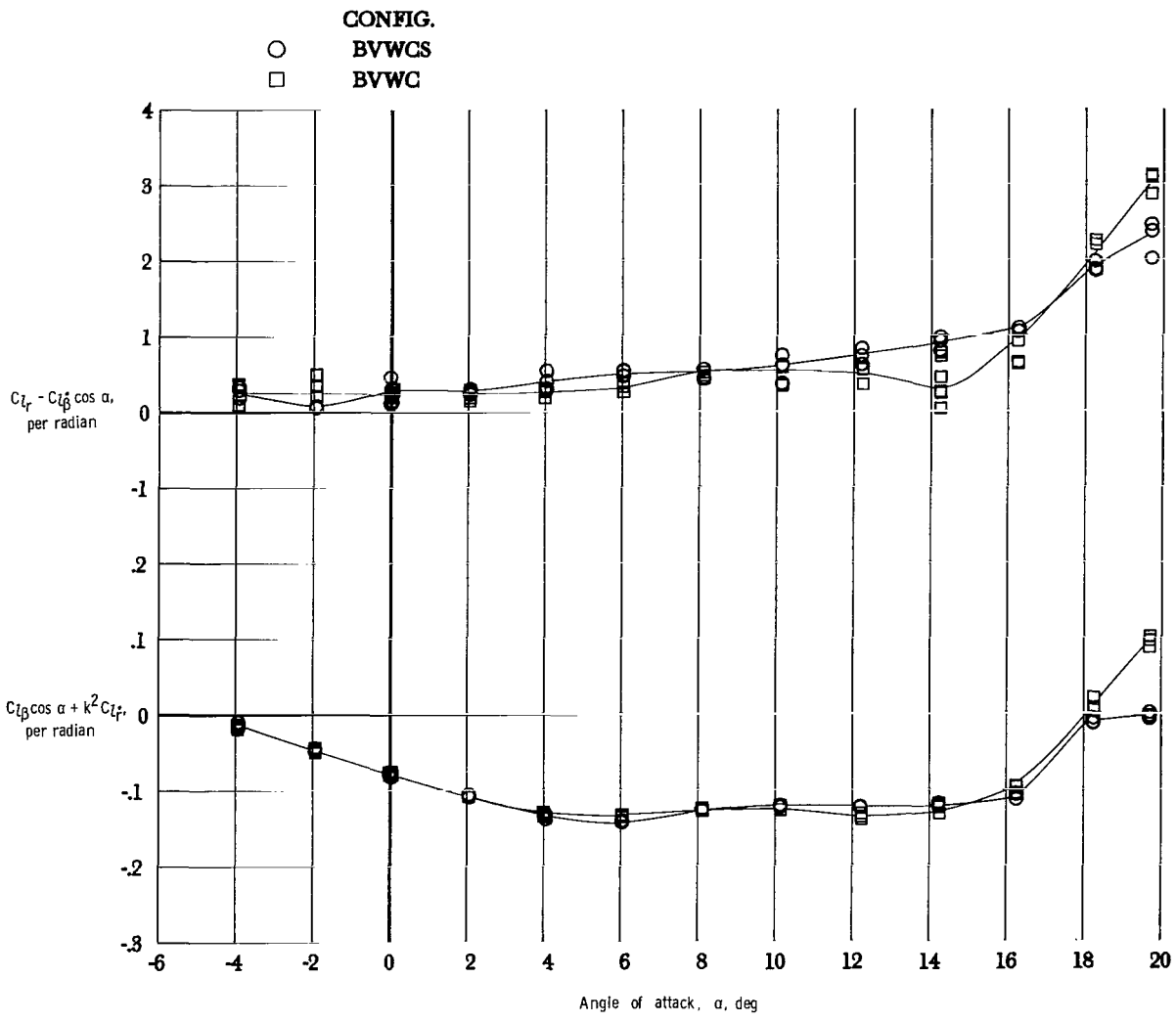

(b) M = 0.7.

Figure 20.- Concluded.

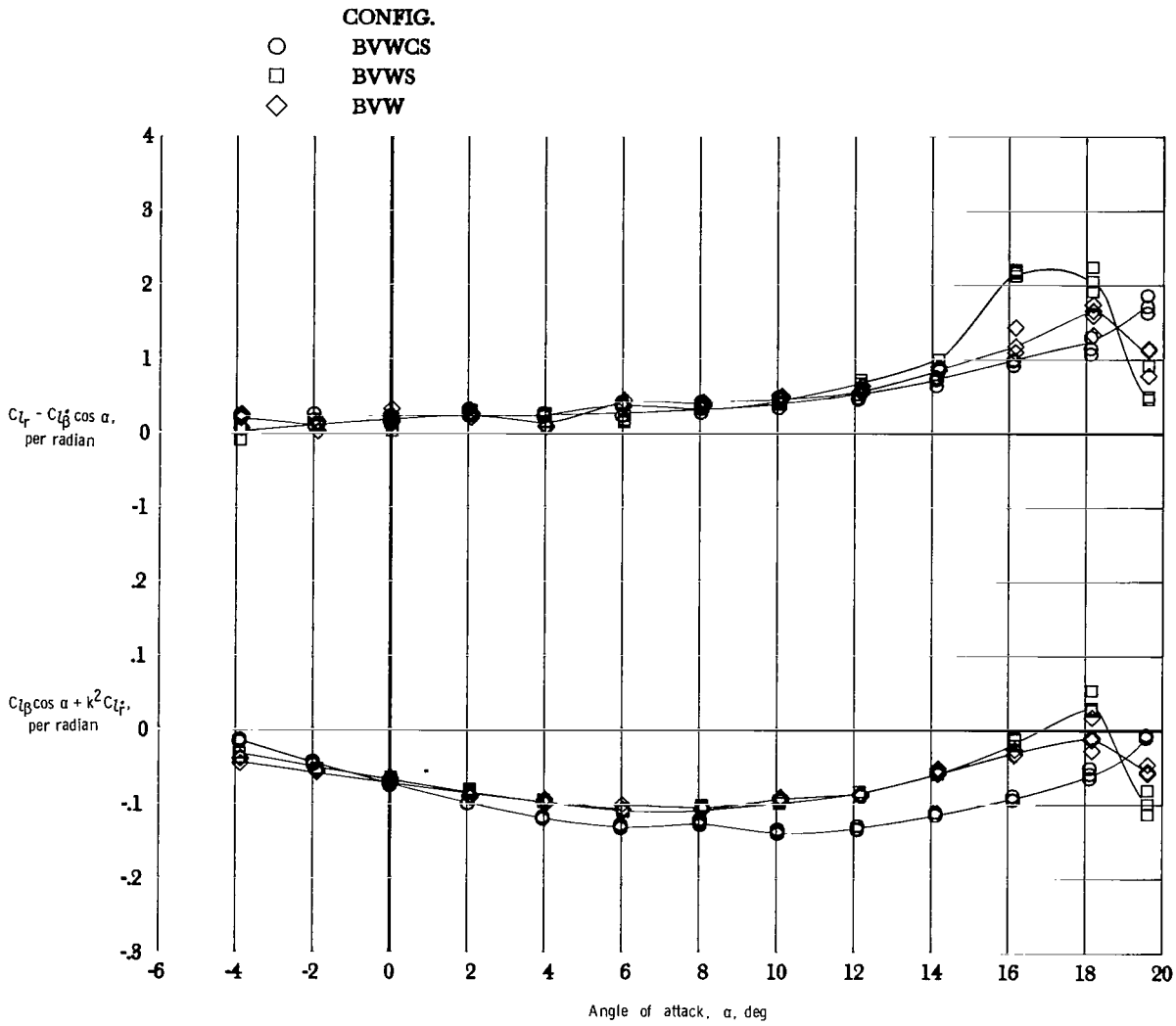

(a) M = 0.4.

Figure 21.- Effect of strake and canard with 44° swept wing configuration on rolling moment due to yaw rate parameter and on effective dihedral parameter.

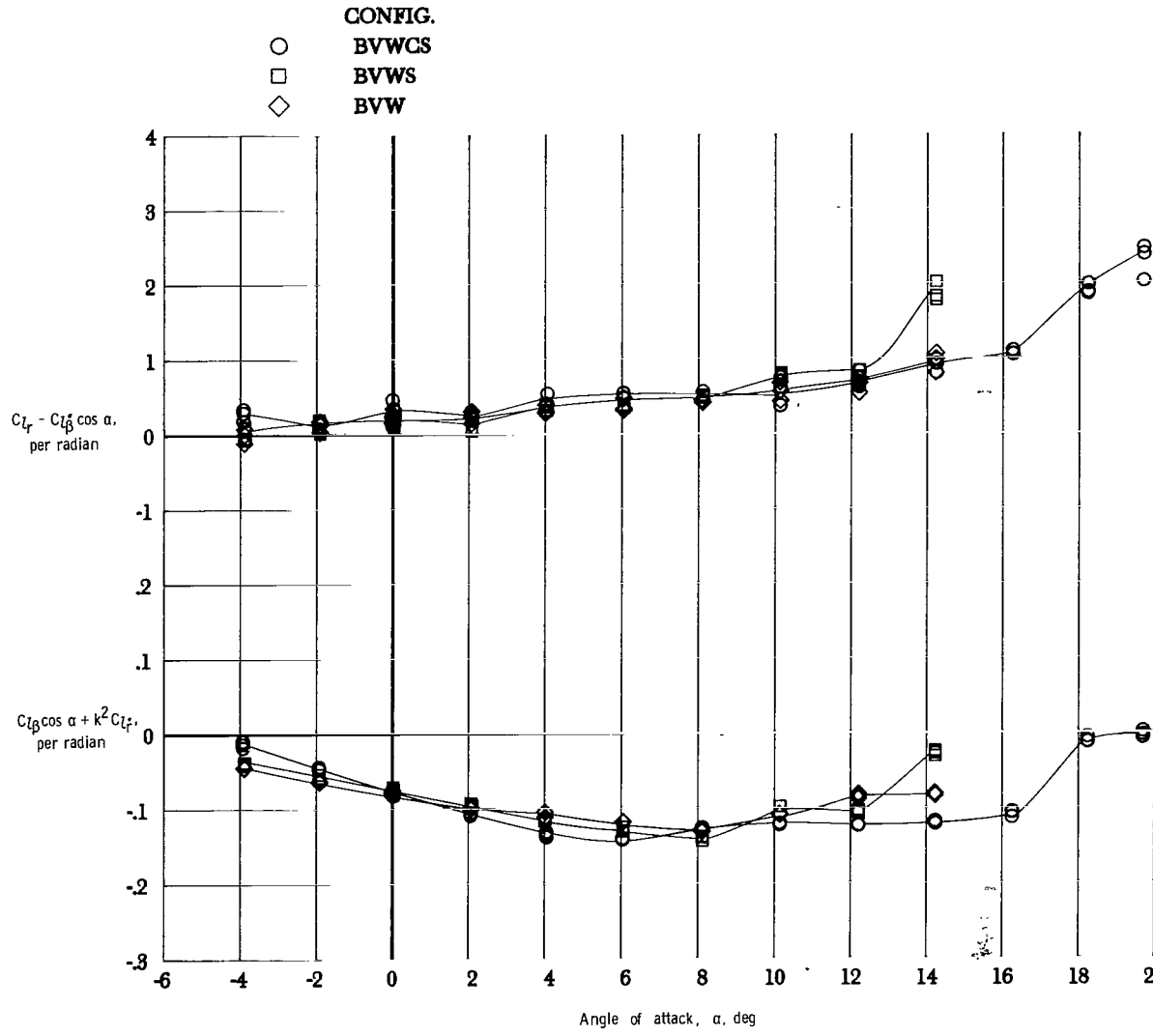

(b) M = 0.7.

Figure 21.- Concluded.

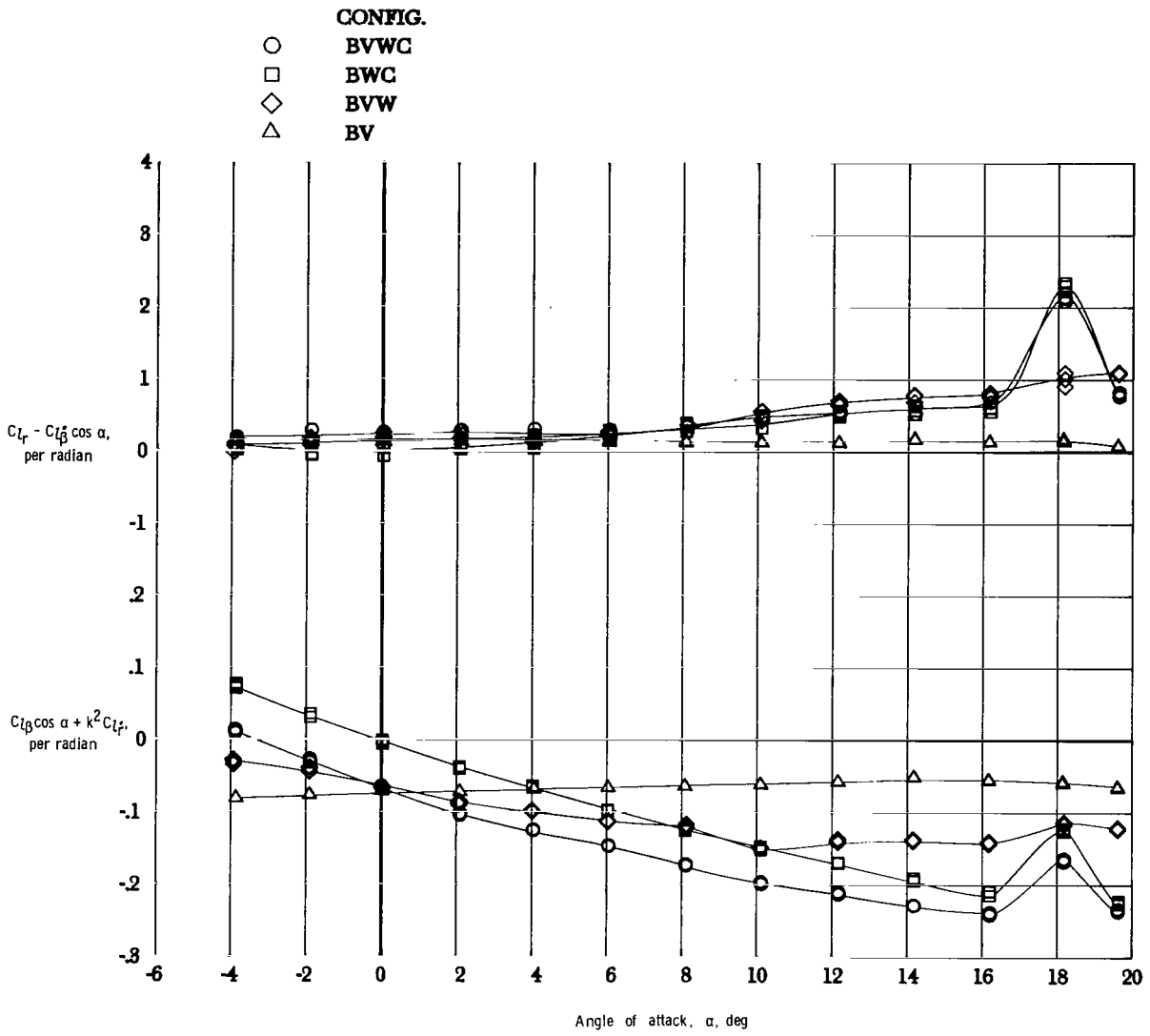

(a) M = 0.4.

Figure 22.- Results for component breakdown of 60° swept wing configuration for rolling moment due to yaw rate parameter and effective dihedral parameter.

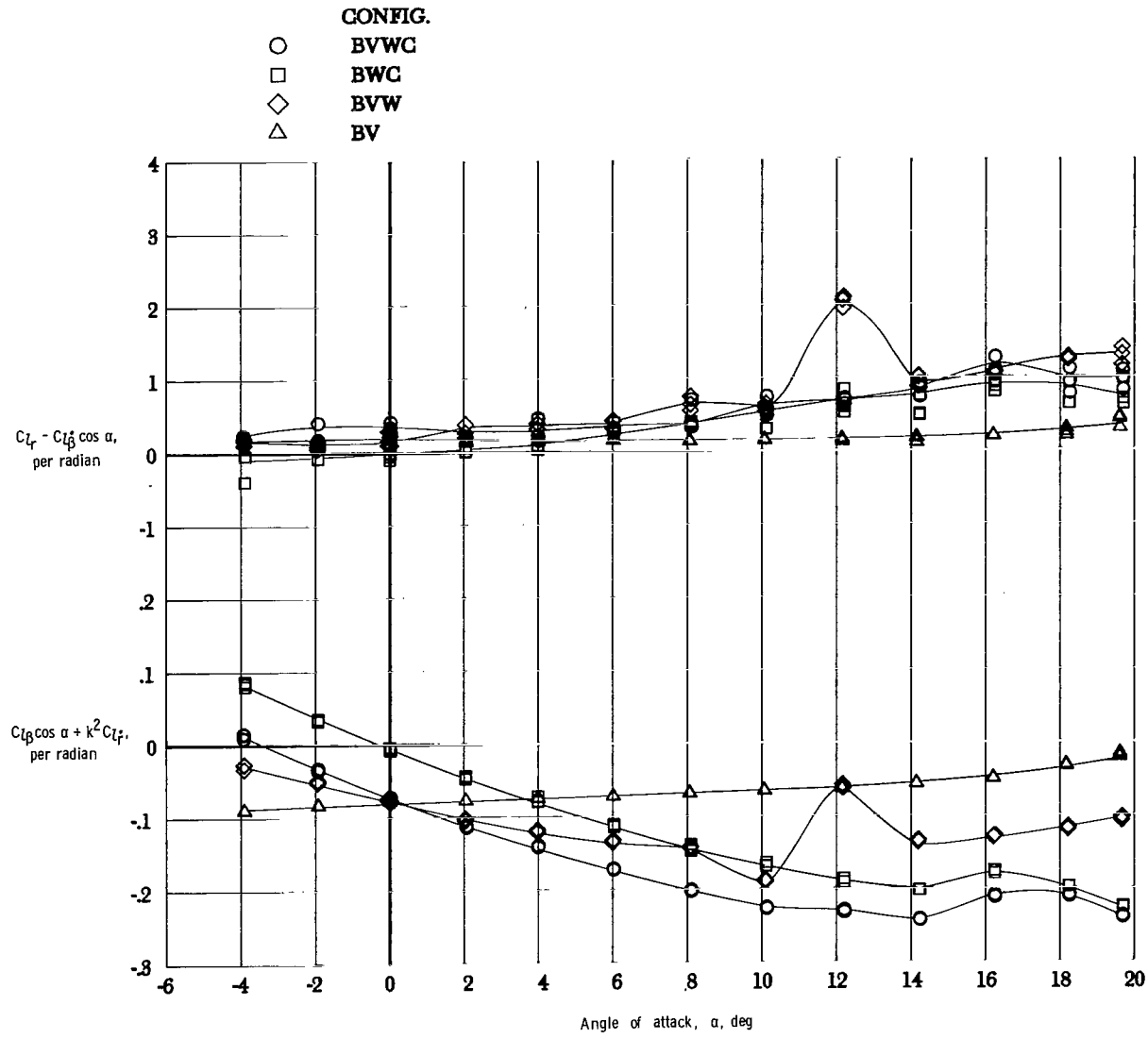

(b) M = 0.7.

Figure 22.- Concluded.

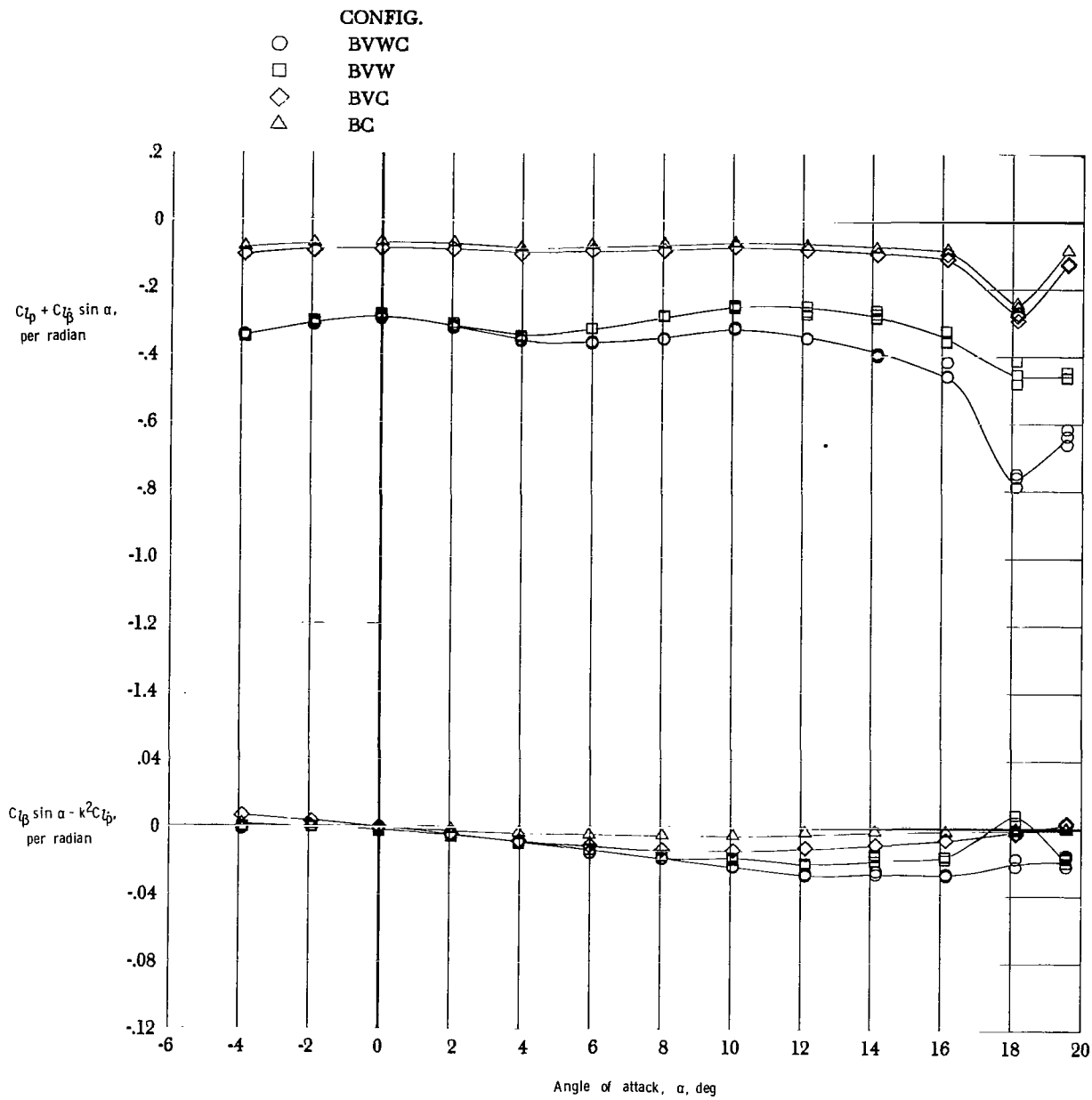

Figure 23.- Results for component breakdown of 44° swept wing configuration for damping-in-roll parameter and rolling moment due to roll displacement parameter. M = 0.3.

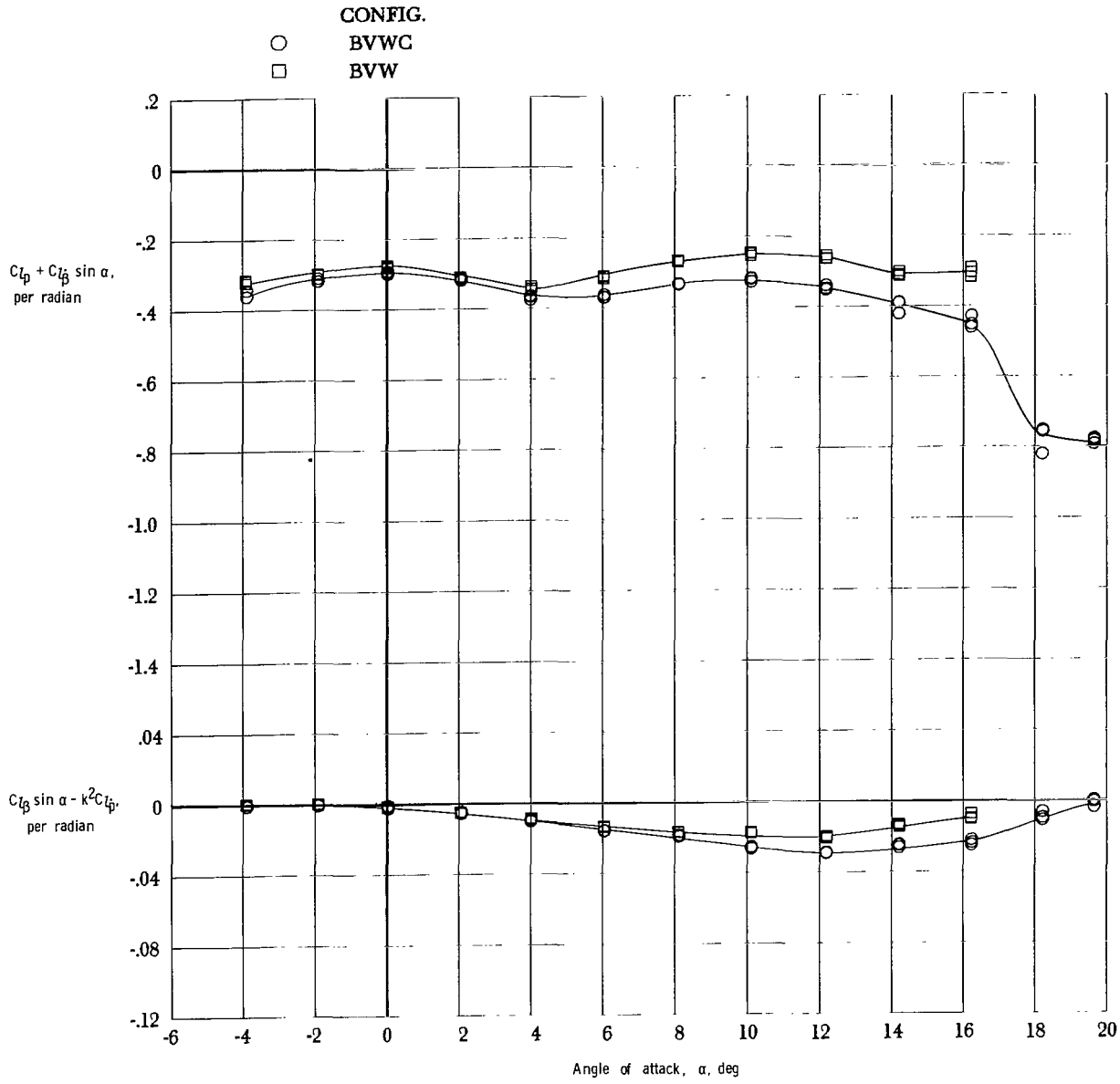

(a) M = 0.4.

Figure 24.- Effect of canard with 44° swept wing configuration on damping-in-roll parameter and on rolling moment due to roll displacement parameter.

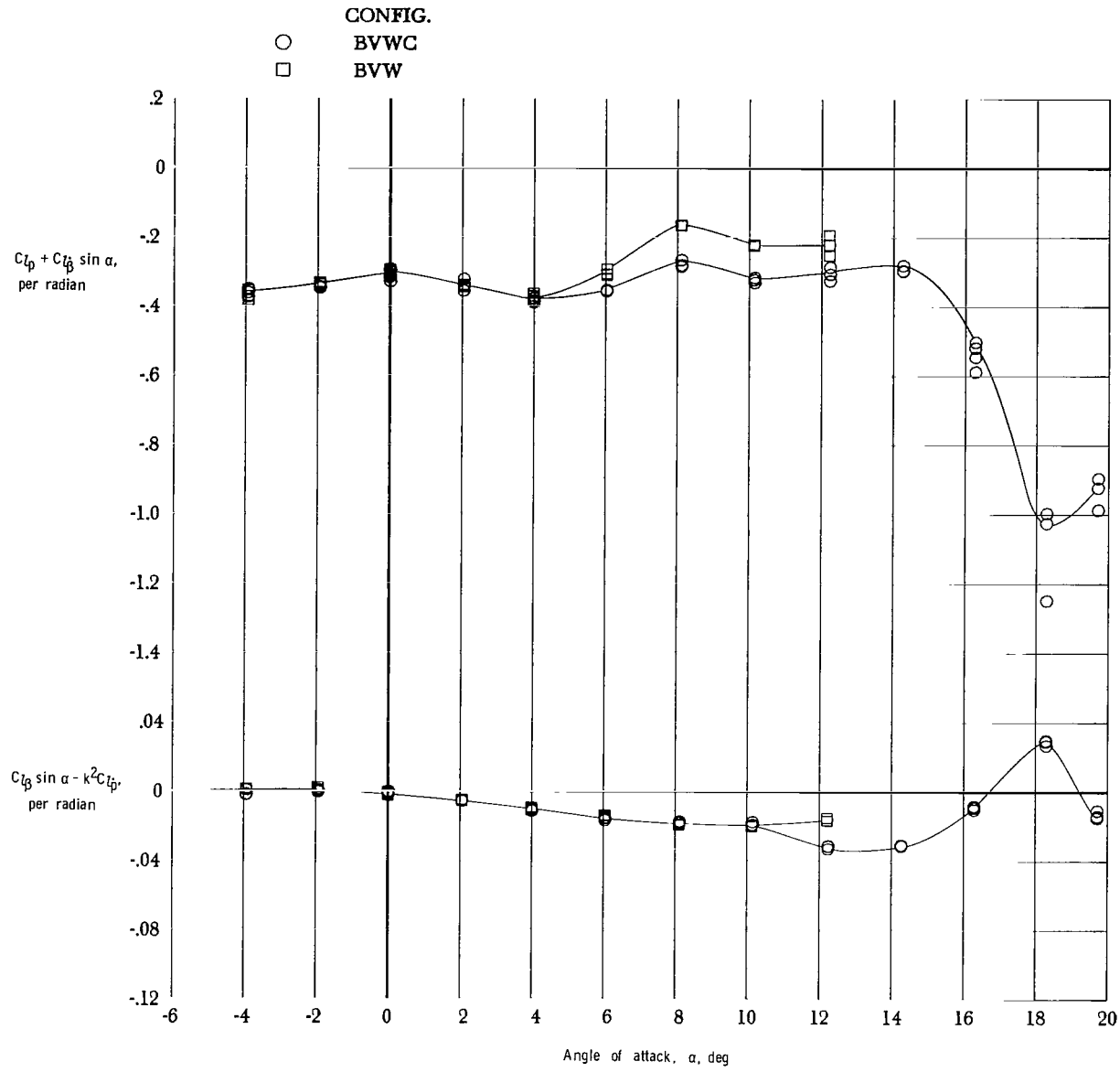

(b) M = 0.7.

Figure 24.- Concluded.

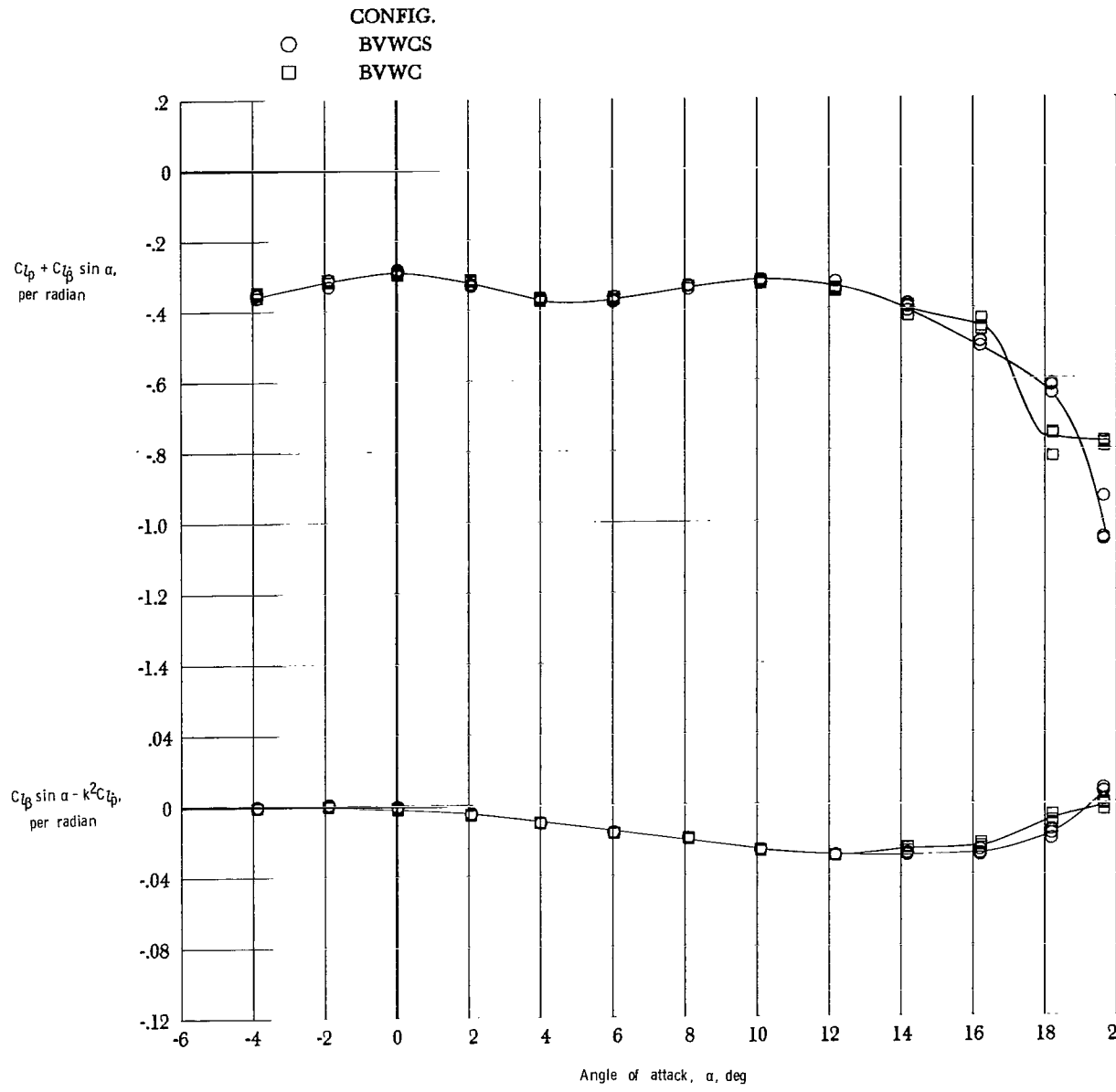

(a) M = 0.4.

Figure 25.- Effect of strake with 44° swept wing configuration on damping-in-roll parameter and on rolling moment due to roll displacement parameter.

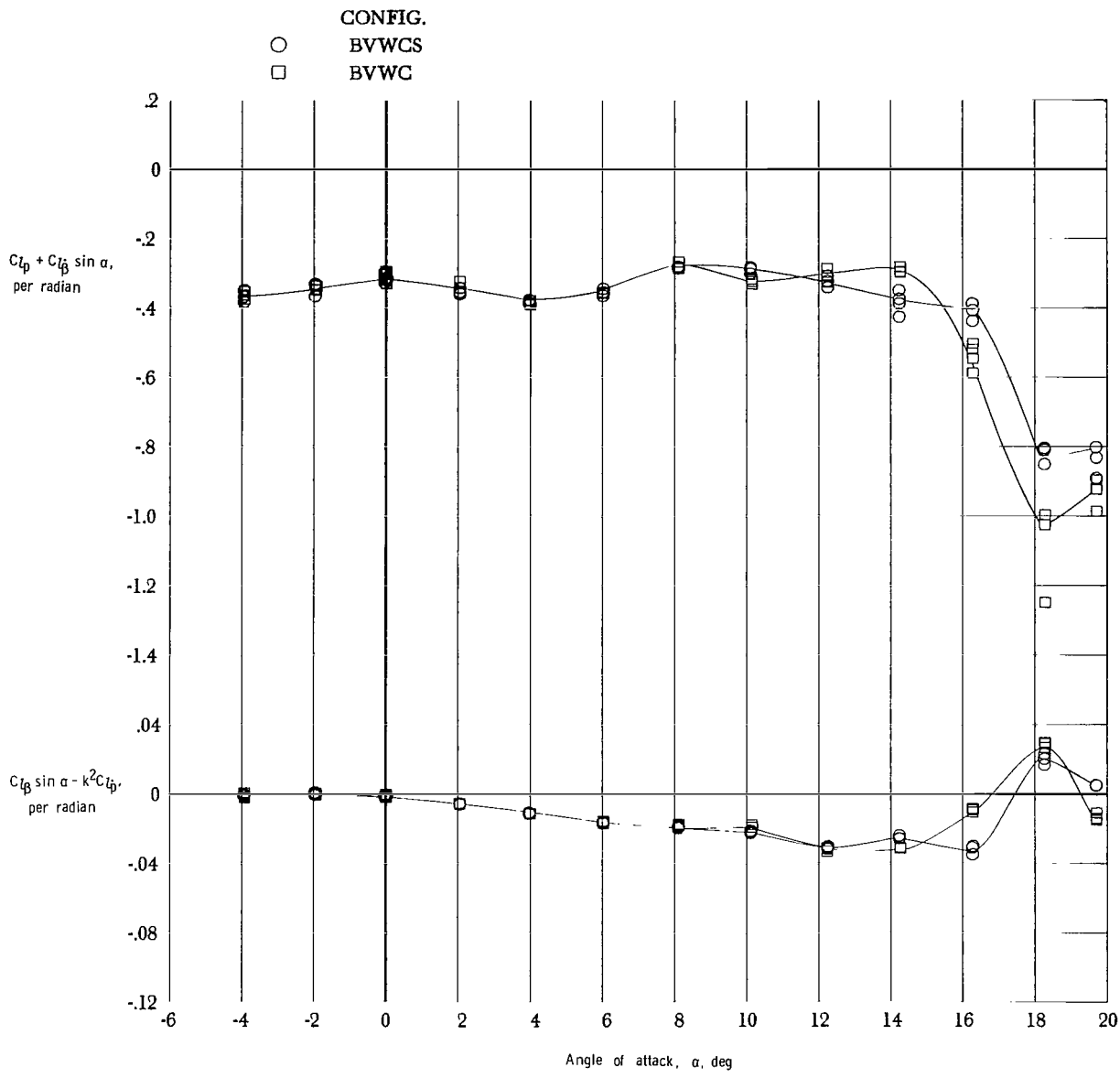

(b) M = 0.7.

Figure 25.- Concluded.

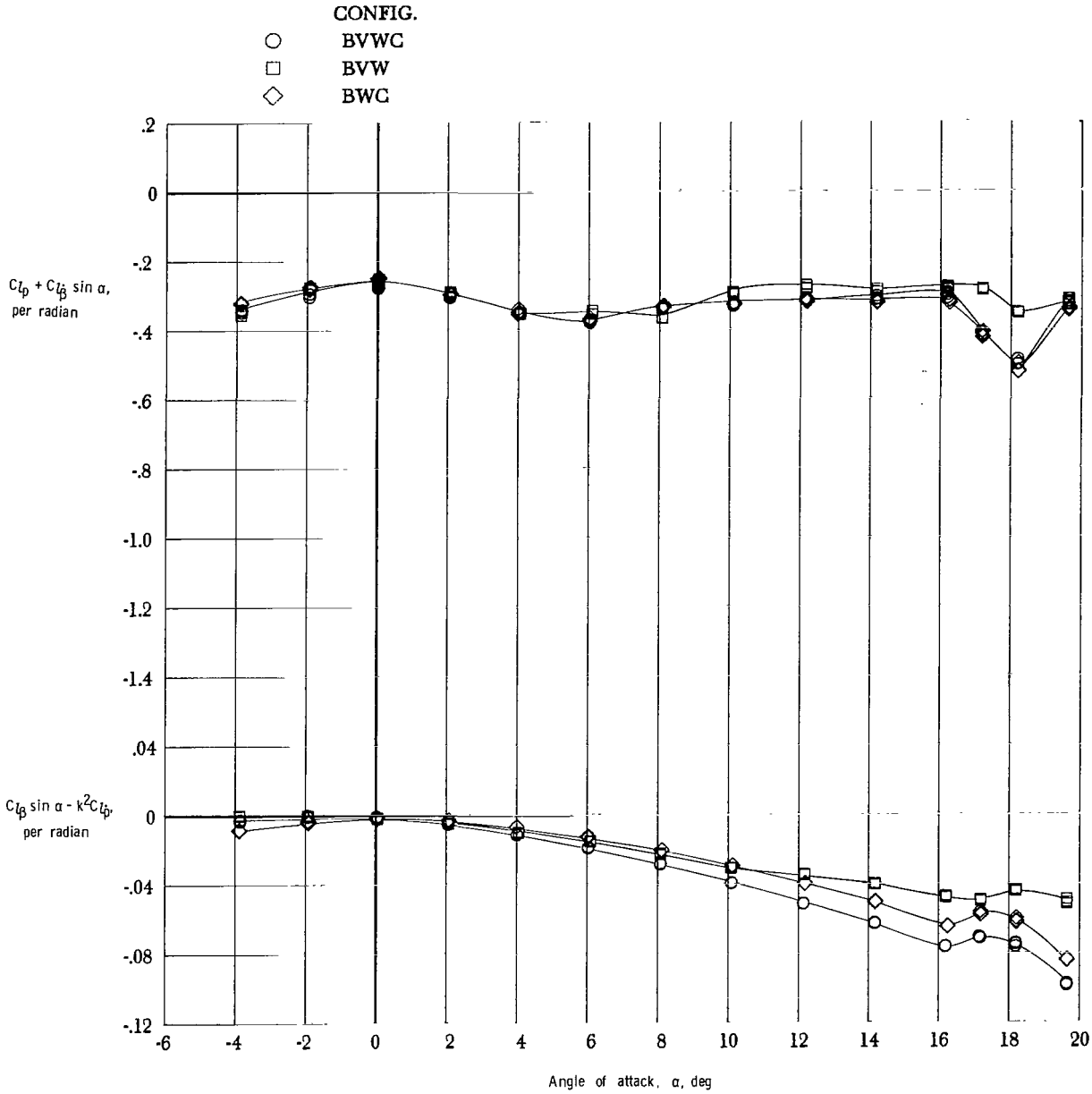

(a) M = 0.4.

Figure 26.- Effect of canard and vertical tail with 60° swept wing configuration on damping-in-roll parameter and on rolling moment due to roll displacement parameter.

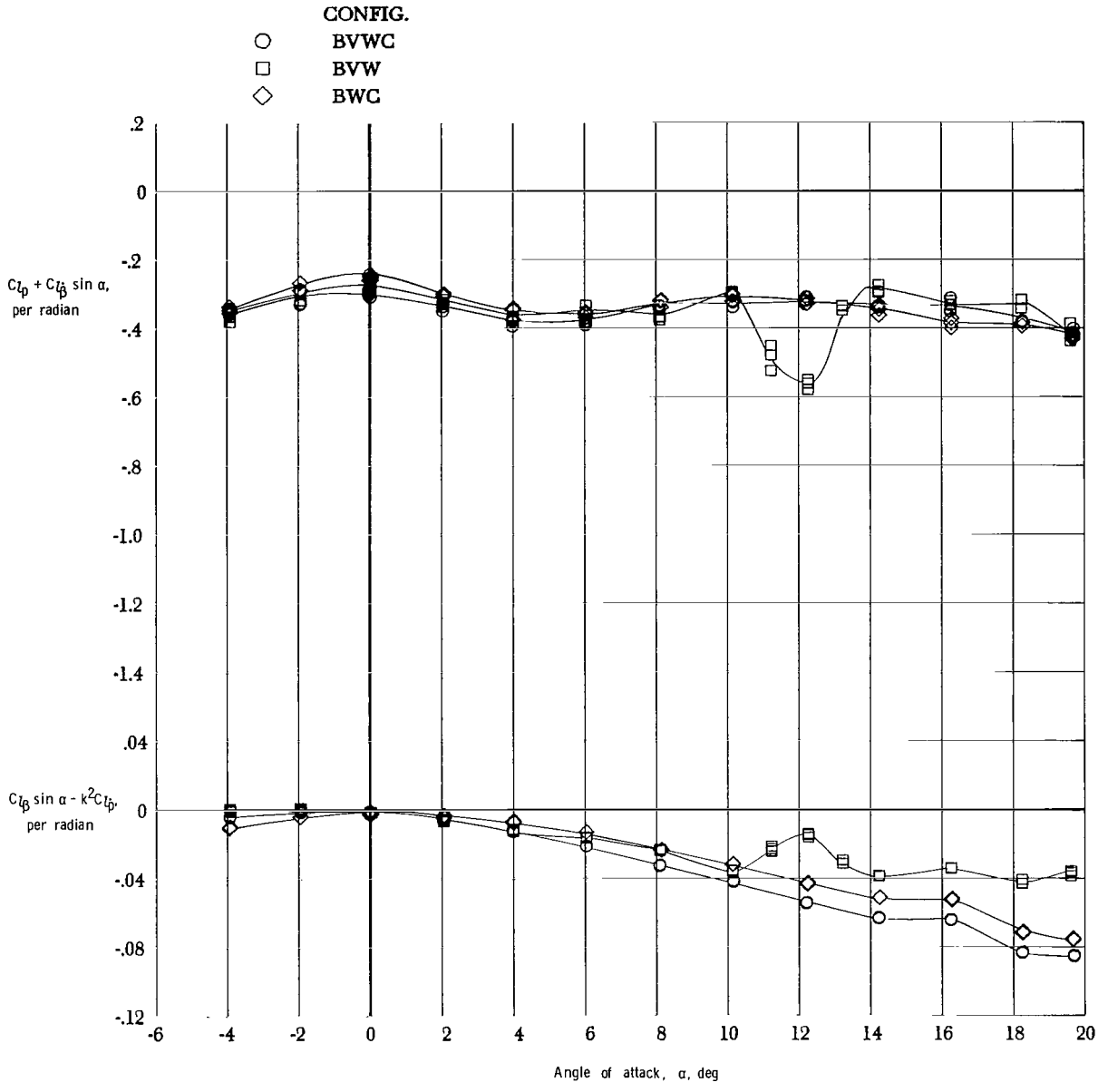

(b) M = 0.7.

Figure 26.- Concluded.

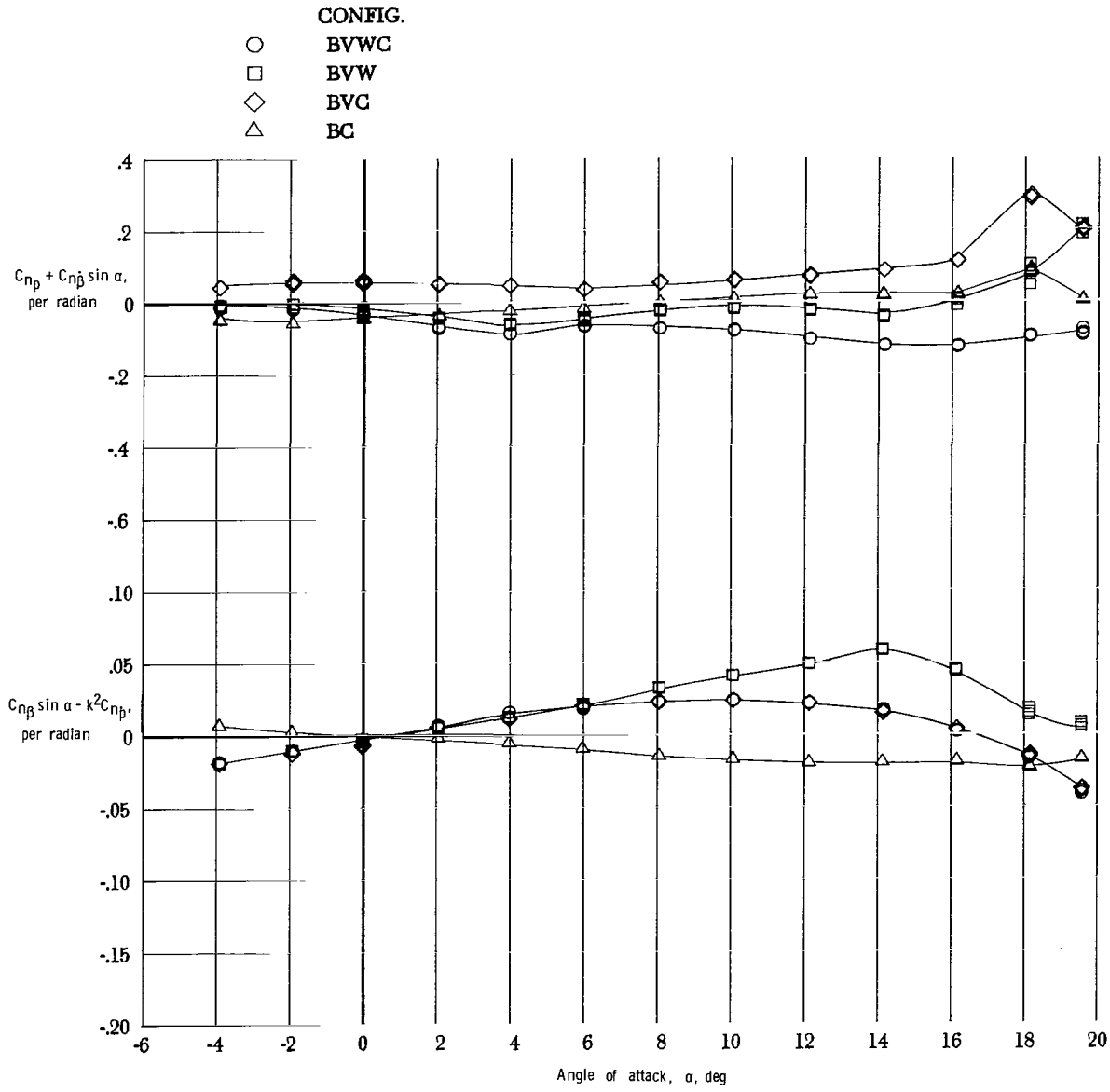

Figure 27.- Results for component breakdown of 44° swept wing configuration for yawing moment due to roll rate parameter and yawing moment due to roll displacement parameter. M = 0.3.

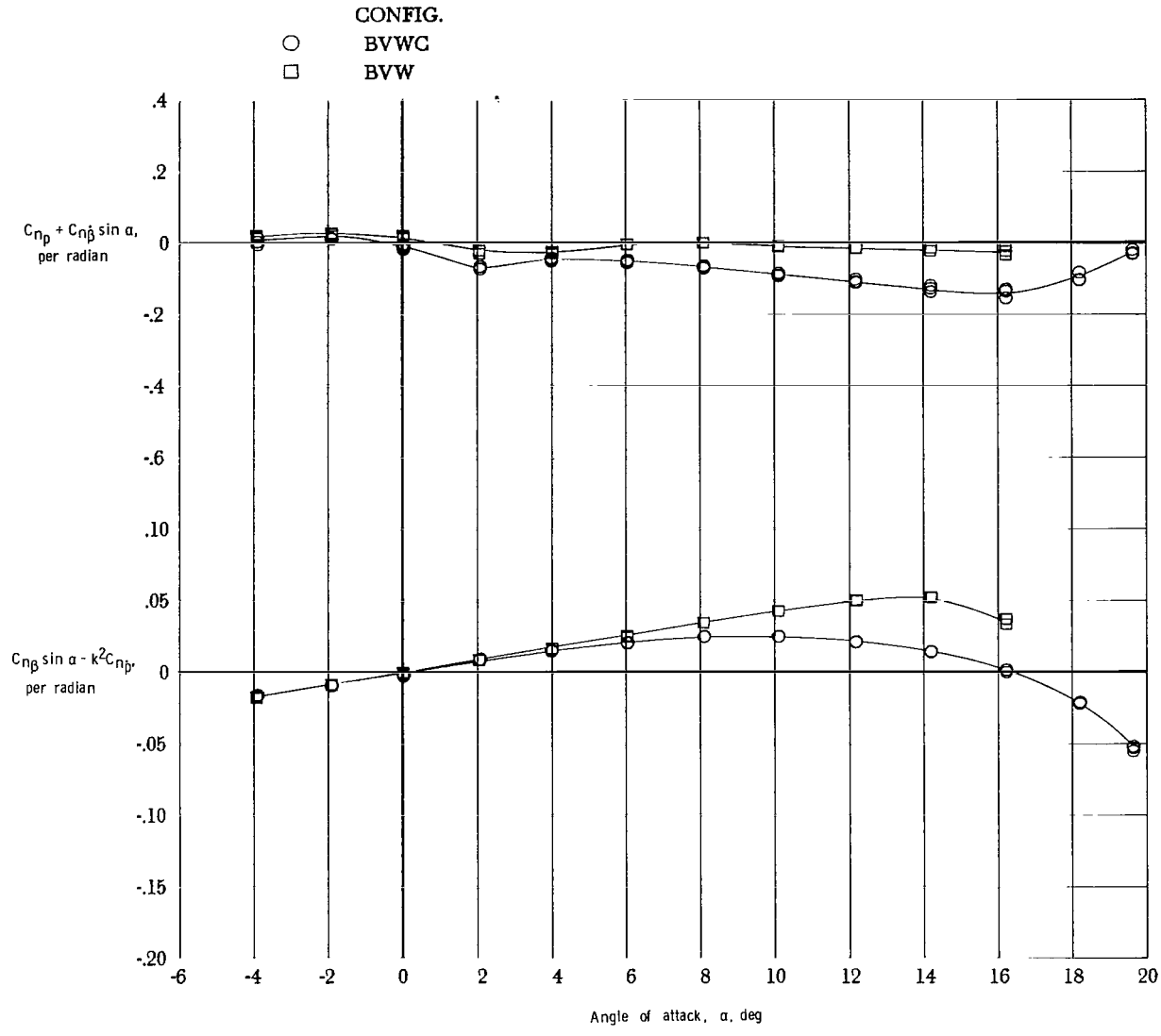

(a) M = 0.4.

Figure 28.- Effect of canard with 44° swept wing configuration on yawing moment due to roll rate parameter and on yawing moment due to roll displacement parameter.

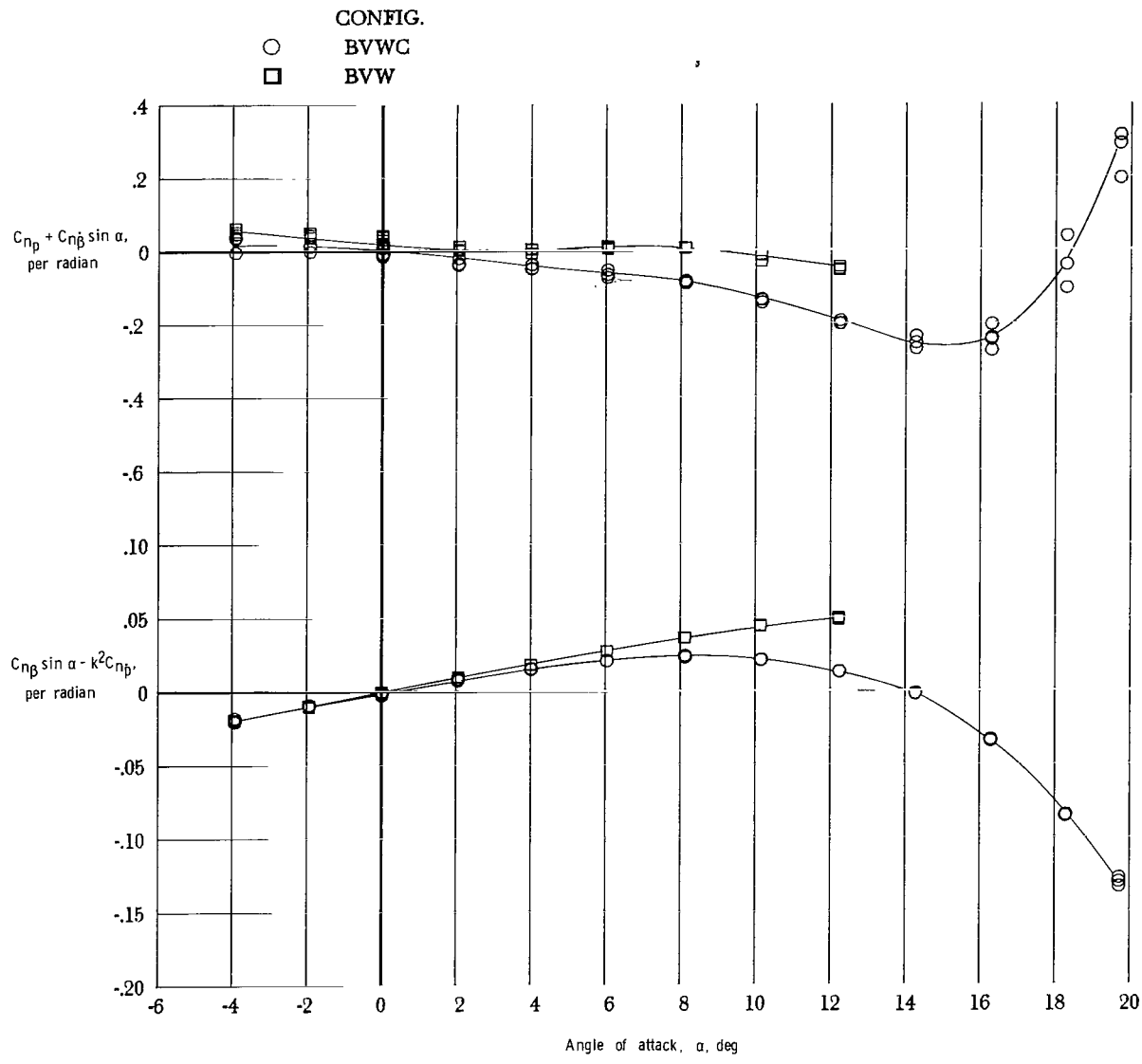

(b) M = 0.7.

Figure 28.- Concluded.

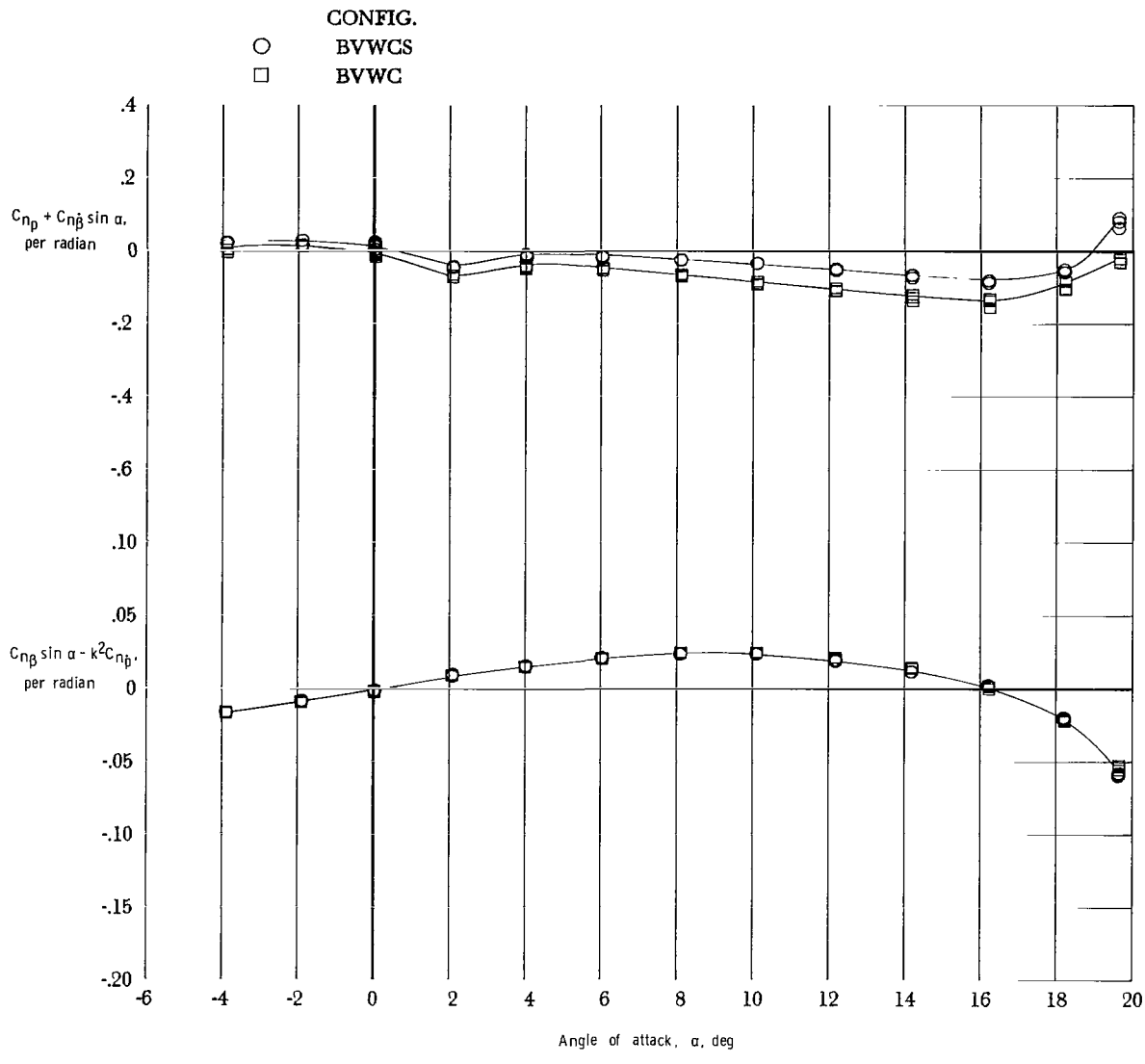

(a) M = 0.4.

Figure 29.- Effect of strake with 44° swept wing configuration on yawing moment due to roll rate parameter and on yawing moment due to roll displacement parameter.

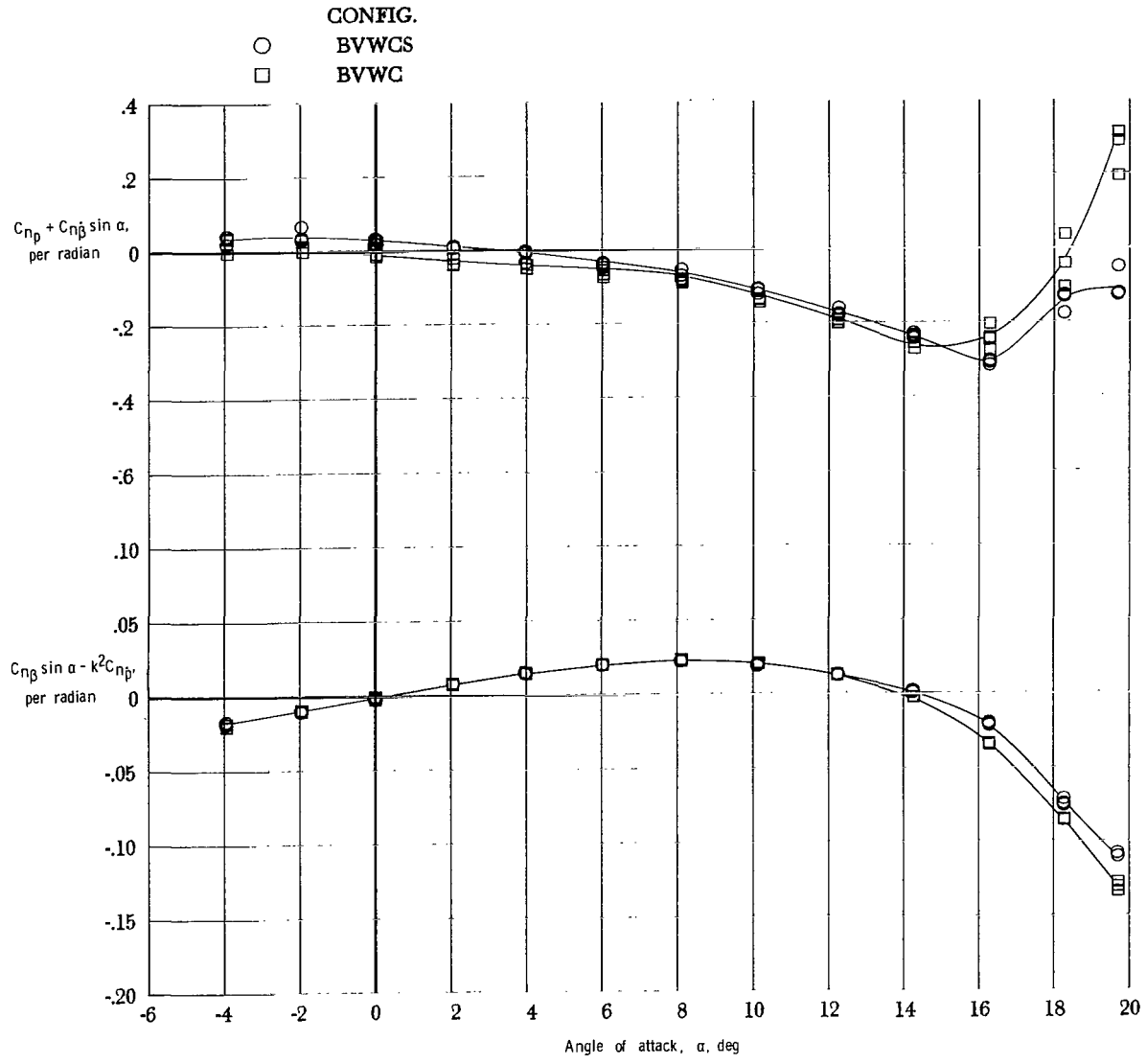

(b) M = 0.7.

Figure 29.- Concluded.

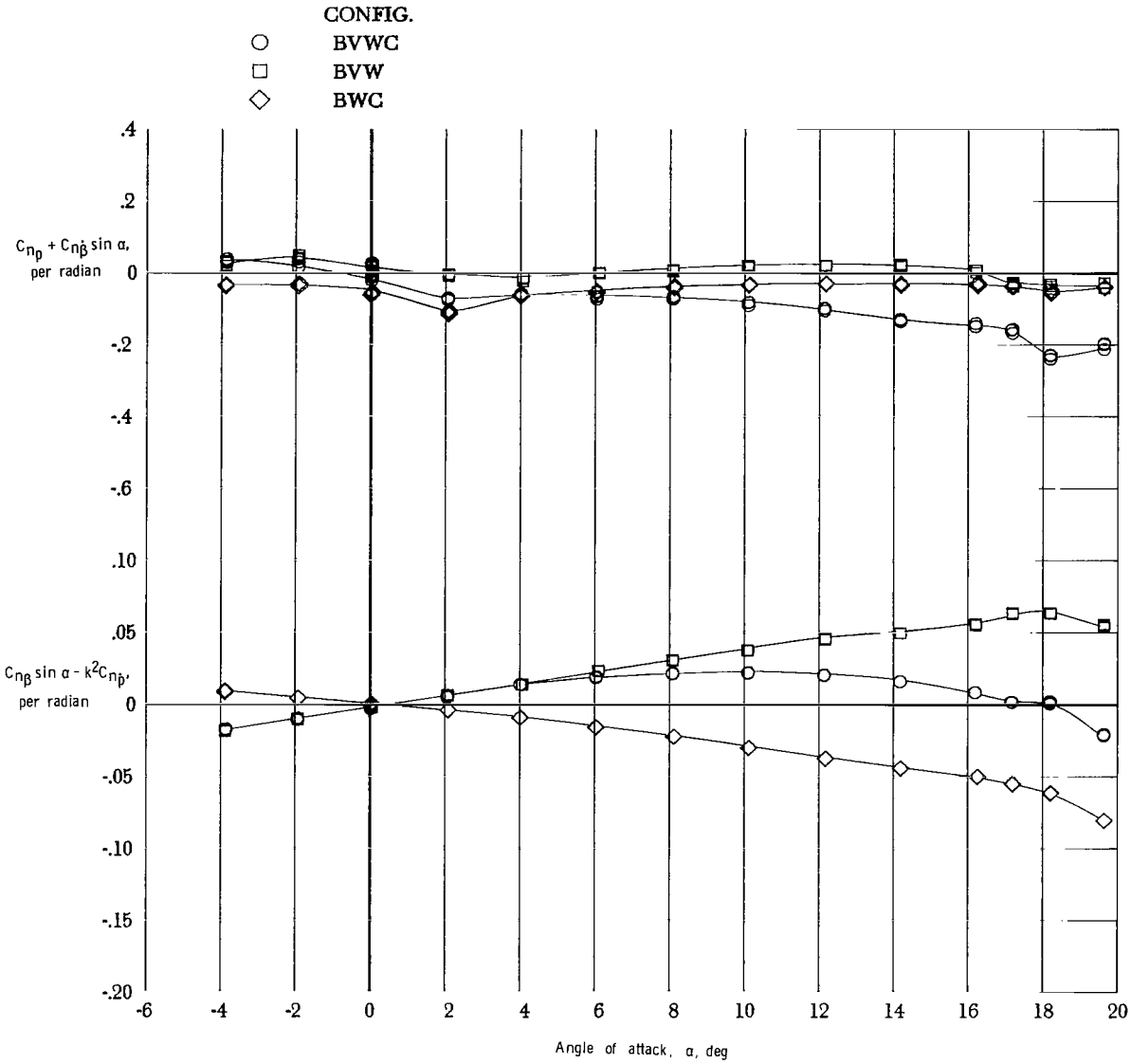

(a) M = 0.4.

Figure 30.- Effect of canard and vertical tail with 60° swept wing configuration on yawing moment due to roll rate parameter and on yawing moment due to roll displacement parameter.

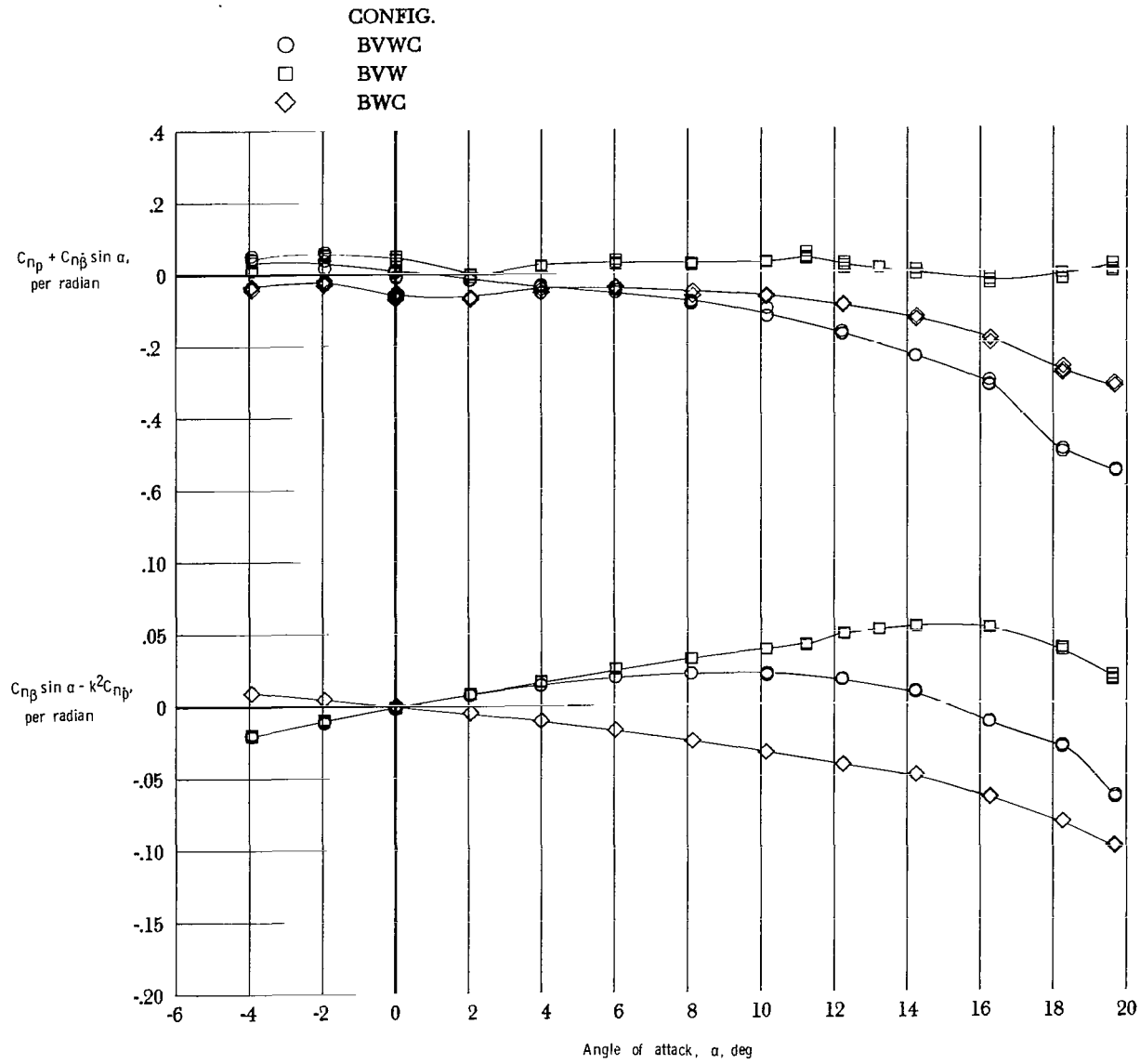

(b) M = 0.7.

Figure 30.- Concluded.

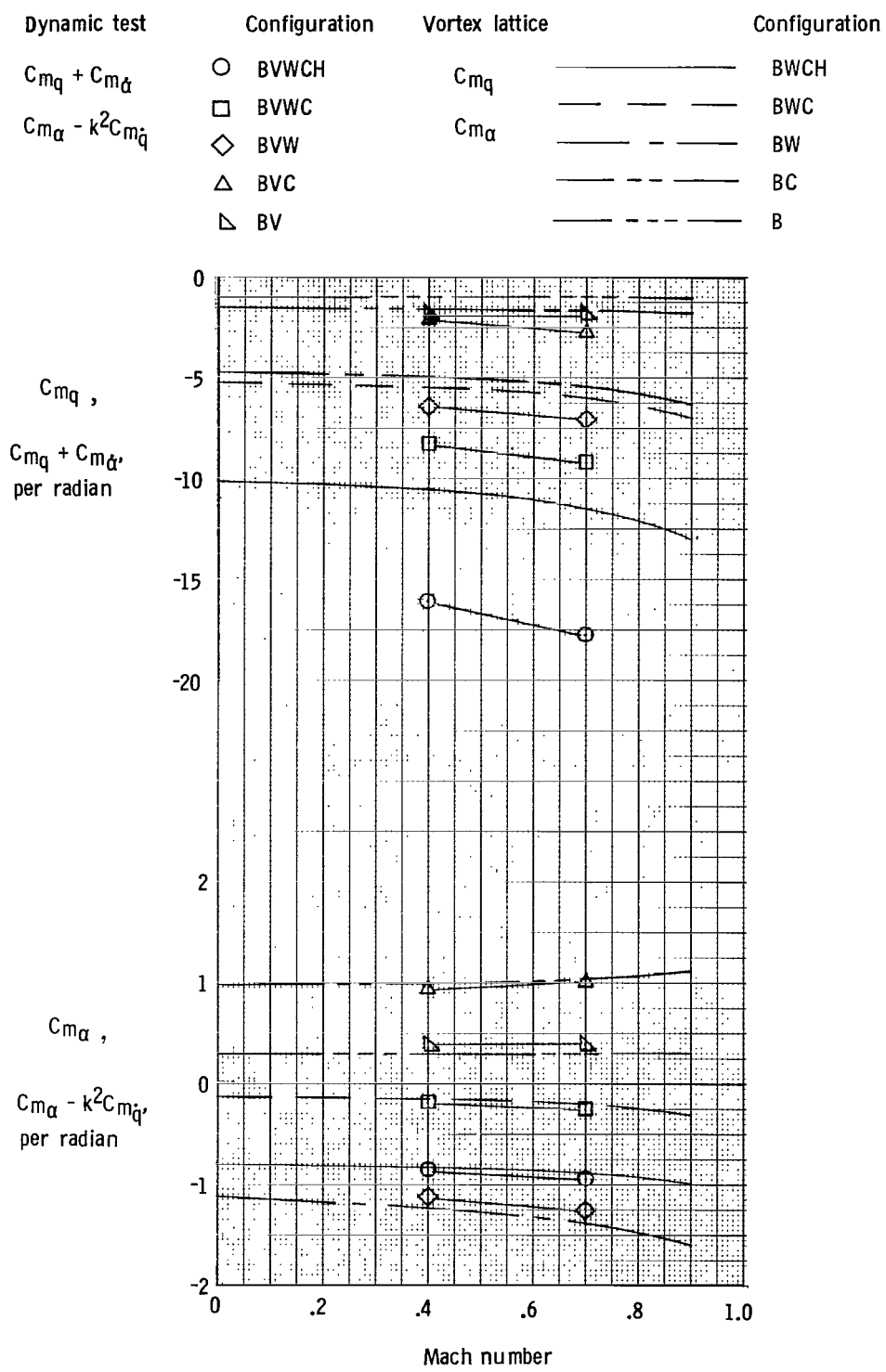

(a) Damping in pitch and oscillatory longitudinal stability.

Figure 31.- Comparison of dynamic test results with vortex-lattice theoretical estimates for 44° swept wing configurations. $\alpha = 0°$.

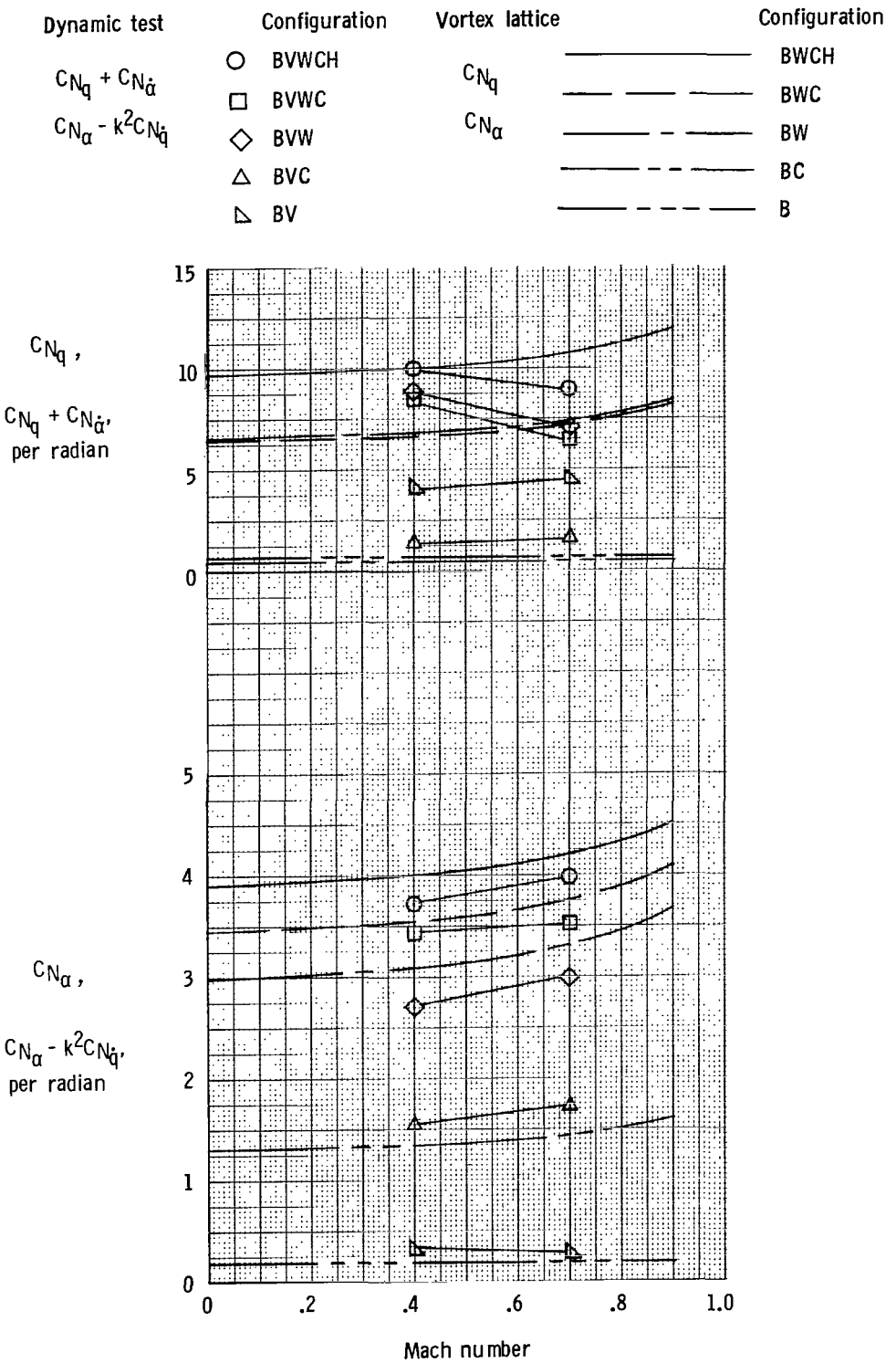

(b) Normal force due to pitch rate and normal force due to pitch displacement.

Figure 31.- Continued.

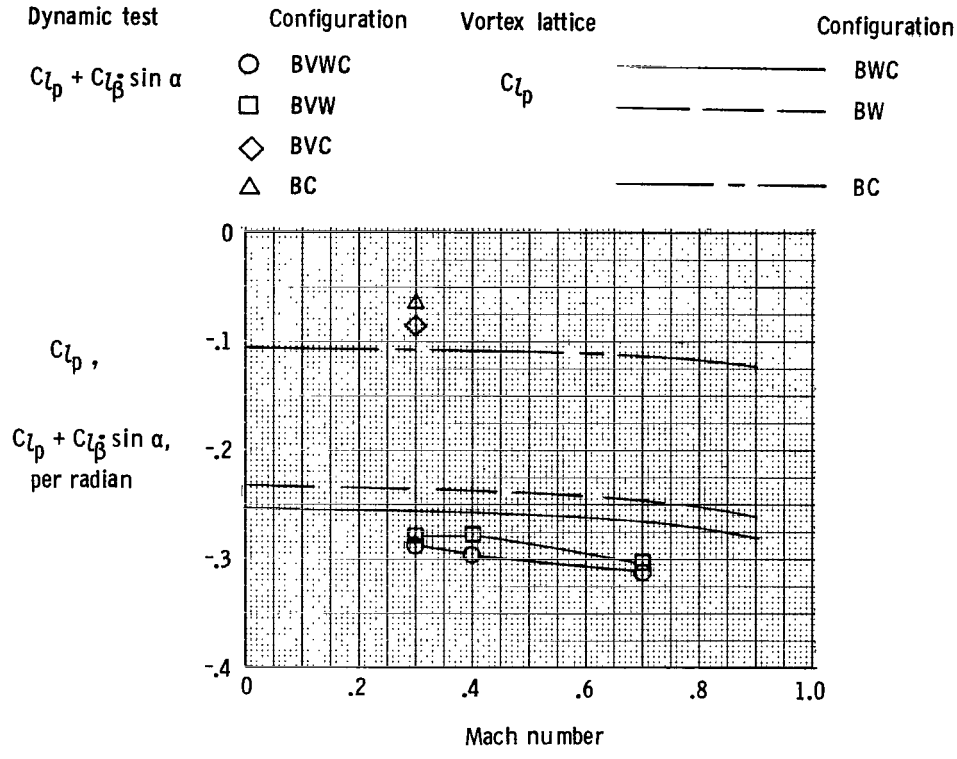

(c) Damping in roll.

Figure 31.- Concluded.

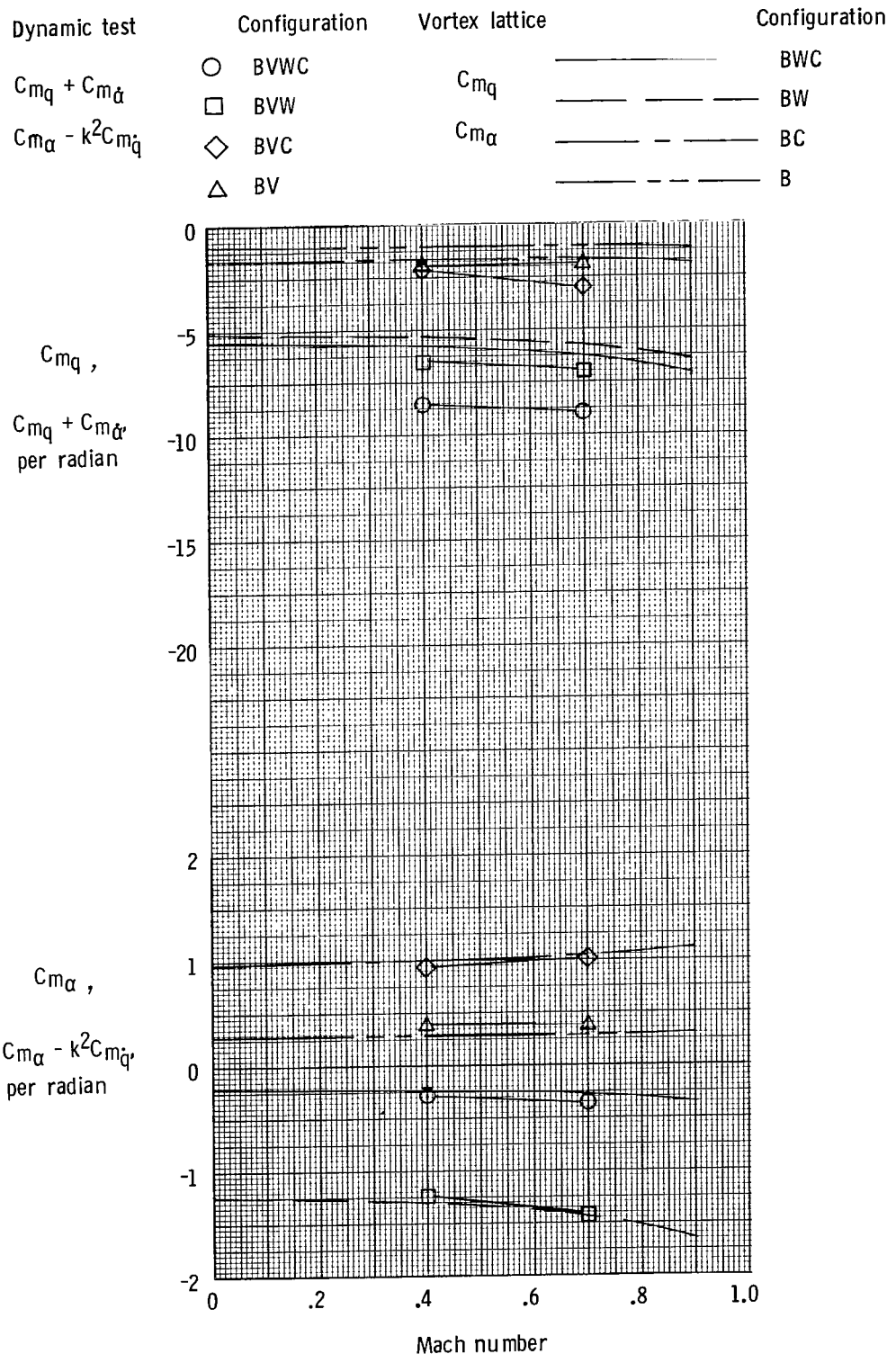

(a) Damping in pitch and oscillatory longitudinal stability.

Figure 32.- Comparison of dynamic test results with vortex-lattice theoretical estimates for 60° swept wing configurations. $\alpha = 0°$.

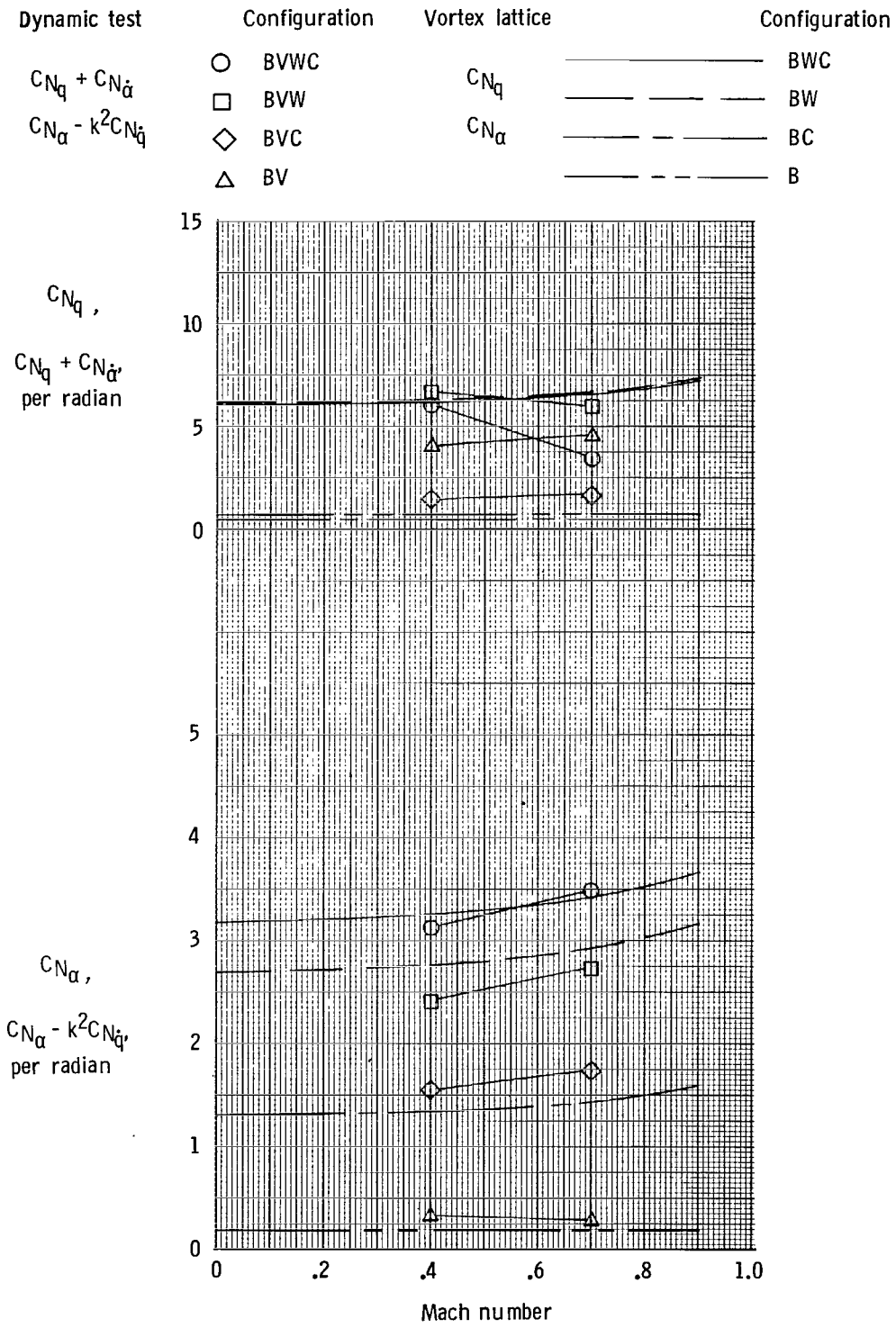

(b) Normal force due to pitch rate and normal force due to pitch displacement.

Figure 32.- Continued.

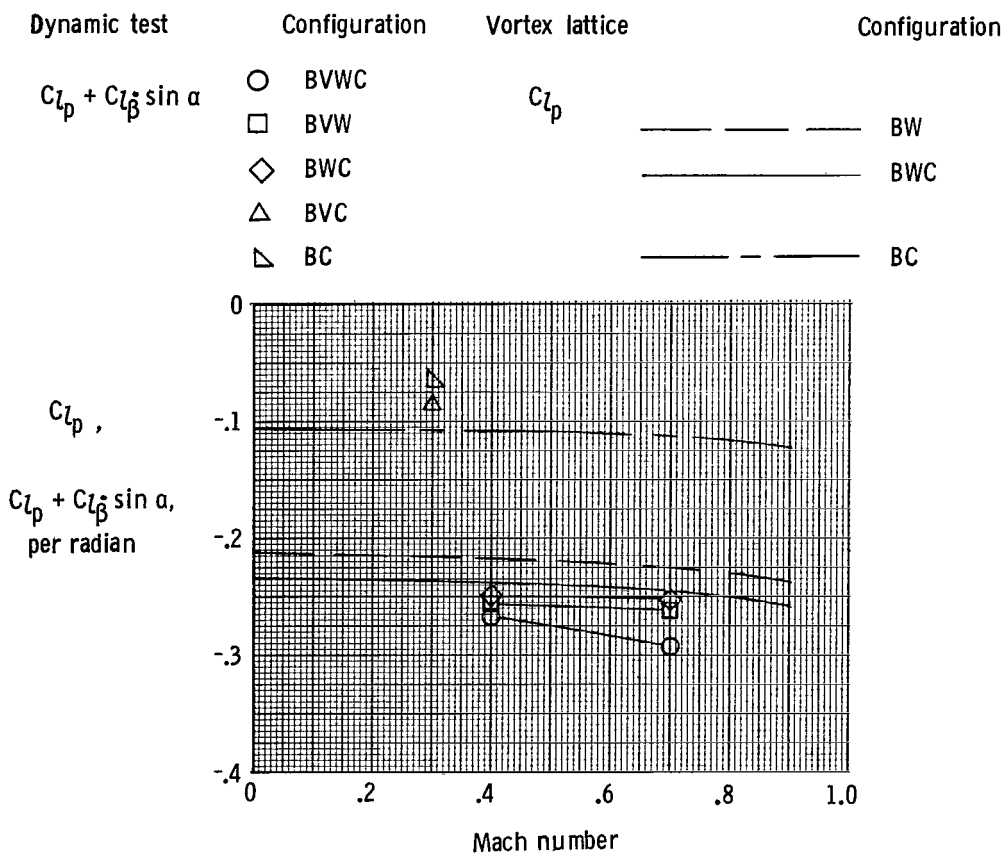

(c) Damping in roll.

Figure 32.- Concluded.

1. Report No.	2. Government Accession No.	3. Recipient's Catalog No.
NASA TP-1291		

4. Title and Subtitle	5. Report Date
SUBSONIC DYNAMIC STABILITY CHARACTERISTICS OF TWO CLOSE-COUPLED CANARD-WING CONFIGURATIONS	October 1978
	6. Performing Organization Code
7. Author(s)	8. Performing Organization Report No.
Richmond P. Boyden	L-12057
	10. Work Unit No.
9. Performing Organization Name and Address	505-11-23-13
NASA Langley Research Center Hampton, VA 23665	11. Contract or Grant No.
	13. Type of Report and Period Covered
12. Sponsoring Agency Name and Address	Technical Paper
National Aeronautics and Space Administration Washington, DC 20546	14. Sponsoring Agency Code

15. Supplementary Notes

16. Abstract

The pitch, yaw, and roll damping as well as the oscillatory stability in pitch and in yaw were measured for two canard-wing configurations with wing sweeps of 44° and 60°. Tests were made at free-stream Mach numbers of 0.3, 0.4, and 0.7 and for angles of attack from about -4° to 20°. The effects of various components such as the canard, nose strakes, wings, vertical tail, and horizontal tail were determined. The basic canard-wing vertical-tail configurations generally had positive damping in pitch, yaw, and roll. The effect of the canard was generally beneficial except for its tendency to decrease the oscillatory directional stability.

17. Key Words (Suggested by Author(s))	18. Distribution Statement
Aerodynamic damping Dynamic stability Canard	Unclassified - Unlimited Subject Category 02

19. Security Classif. (of this report)	20. Security Classif. (of this page)	21. No. of Pages	22. Price*
Unclassified	Unclassified	76	$6.00

* For sale by the National Technical Information Service, Springfield, Virginia 22161

NASA-Langley, 1978

5 1 1U,A, 092978 S00903DS
DEPT OF THE AIR FORCE
AF WEAPONS LABORATORY
ATTN: TECHNICAL LIBRARY (SUL)
KIRTLAND AFB NM 87117